ISSN : 0025-0422

JOURNAL
OF
THE MAHARAJA SAYAJIRAO UNIVERSITY OF BARODA: SCIENCE & TECHNOLOGY

VOL. 58
2024

सत्यं शिवं सुन्दरम्
Estd. 1949
Accredited Grade A+ by NAAC

Published by
The Maharaja Sayajirao University of Baroda
Vadodara, Gujarat, India

JOURNAL
OF
THE MAHARAJA SAYAJIRAO UNIVERSITY OF BARODA:
SCIENCE & TECHNOLOGY

Editorial Board

JOURNAL
OF
THE MAHARAJA SAYAJIRAO UNIVERSITY OF BARODA: SCIENCE & TECHNOLOGY

VOL. 58
2024

EDITOR
Prof. P. K. Jha

सत्यं शिवं सुन्दरम्
Estd. 1949
Accredited Grade A+ by NAAC

Published by
The Maharaja Sayajirao University of Baroda
Vadodara, Gujarat, India

ISSN : 0025-0422

Printed by Shri Jatin H. Somani, Manager, The Maharaja Sayajirao University of Baroda Press (Sadhana Press), Near Palace Gate, Palace Road, Vadodara, and Edited by **Prof. P. K. Jha,** Editor (Science & Technology) at the Maharaja Sayajirao University of Baroda, Vadodara - 390 002, (India), 2024.

CONTENTS

Journal of The Maharaja Sayajirao University of Baroda: Science & Technology

Vol. 58, 2024, pp. 1-8

Study of Arc and Flame Spray Thermal Spray Coating Corrosion Characterization for Upstream and Downstream Refineries Applications

Urvesh Vala[1], and I B Dave[2],

1 Research Scholer, Gujarat Technical University, Ahmedabad, Gujarat, India & L&T Energy Hydrocarbon Engineering Limited, L&T Knowledge City, Vadodara – 390019, urvesh.vala@larsentoubro.com

2 Metallurgy Engineering, Government Engineering College, Sector-28, Gandhinagar -382028, Gujarat, India, ibdave@gecg28.ac.in

Thermal spray coatings (TSC) have been widely adopted over the past decade for corrosion protection. The scope of thermal spray coatings and its application has been further explored as functional coating from conventional coating. Thermal spray coating is characterized as specialized industrial coating developed for corrosion protection having different wires and powders with their level of purity and coating application is developed with wide range of devices modified based on its application. TSC is developed extensively to withstand elevated process temperatures as compared to liquid coating to the best efficiency, cost effectiveness, erosion and corrosion resistant application. Thermal spray coatings have emerged as one of the best surface techniques to provide excellent resistance to corrosion. The process can be used to apply coatings to a wide range of materials and components, to provide resistance to wear, erosion, cavitation, corrosion, abrasion or heat. Thermal Spray process is an alternative coating testing to replace the Hot Dipped Galvanized coating at site due to limitation of hot dipped galvanizing [6]. Thermal spray coatings have been developed as one of the most effective surface coating techniques for achieving corrosion resistance as sacrificial cathodic protection application. TSC serve the purpose of cathodic protection as sacrificial coating to the base metal and provide high durability coating with intended design life of the structure to be protected by coating. TSC can be performed with pure zinc, pure aluminum or 85% zinc and 15% aluminum alloy based on corrosivity of environment and type of metal to be coated. In many corrosive environments, the zinc and aluminum coating application can be the proven solution to ensure an adequate service life based on coating thickness. Zn-15%Al provides the most effective corrosion protection to the steel in aggressive atmospheric conditions, such as marine humid environments, due to the microstructure of TSC coated automized particles placed over a metal surface in a such a way that it covers entire surface of metal due to its high surface spreading efficiency, which is composed of zinc, aluminum and its alloy having combination of zinc- rich and aluminum-rich phase to meet required corrosion protection against harsh environments. Zinc or Aluminum or its alloy was thermally applied using many application methods, however in this paper detail study of zinc sprayed arc and flame process were discussed. To improve efficiency and deposition rates of the TSC process, two consumable zinc wires are employed in the electric arc process commonly known as twin wire arc process in industry. By doing so, it can save time, cost and results in high productivity. The application of sealer coat (liquid coating) as a topcoat over TSC will enhance the coating life and further safeguard the un- insulated metal surface. The applicability of sealers will be determined based on the aggressiveness of environmental conditions. In general, a more aggressive corrosion environment needs hybrid coating for high durability purposes based on end users' specification requirements. This paper reveals a critical corrosion laboratory study observation on thermal spray coating based on the process parameters of the TSC by arc and flame spray processes. It also covers coating corrosion resistance and its characteristics in chloride environments. Based on study, arc spray shows better corrosion resistance as compared to flame spray at lower chloride concentrations. However, at higher chloride concentrations there is not much change with respect to corrosion resistance was observed and both processes show better corrosion resistance in chloride rich solutions.

Key words: Thermal Spray Coating, TSA, Arc Spray Coating, Flame Spray Coating, etc.

---

* Corresponding author.
Email: ibdave@gecg28.ac.in

INTRODUCTION

Thermal spraying is a method that enhances or rehabilitates the surface of a solid substance. The procedure may be used to apply coatings to various materials and components, resisting wear, erosion, cavitation, corrosion, abrasion, or heat. Thermal spray coating using Zinc as spraying material for barrier coating which includes sacrificial protection for the equipment, piping and associated structures. Zinc can be used with 100% Zn or can used Zinc Alloy for enhancing the coating life based on the environment. Surface finish is equally important like liquid coating for thermal spray coating to be high surface roughness and cleanliness to SA 3 surface finish which provide high quality adhesion to the metal substrate [3]. Metallizing is the process which is developed for corrosion protection as well as erosion corrosion applications in Oil and Gas Refinery applications. In the present situation thermal spray coating is the coating process with very high durability without any maintenance requirement for a minimum of 20 years of coating life. Thermal spray coatings have emerged as one of the best coating techniques for metal and non-metal surface to provide excellent resistance to corrosion and erosion.

TSC is a very old method of applying metallic coating (like zinc, aluminium and their alloys in various metal and power forms with its level of purity) and it developed in early 1900s and with respect to innovation in metallizing these techniques is wide sprayed in various industrial sectors and one of that is Oil and Gas Refineries [1]. TSC can replace the traditional hot dipped coating to a large extent due to its high merits and ease of application having no restriction to apply only in shop and can extend its use at site. Minimum coating required for any metallizing process is 100 micron or more, but very high coating thickness will not be advisable for longer durability with respect to adhesion property as recommended by many end users [3]. With the use of 100% Zn and Zn-15% Aluminium Alloy for corrosion study in various chloride concentrations there is very high durability of coating can be established in laboratory test conditions. Zinc coating can be well understood for its sacrificial action based on galvanic series for protecting the steel surface even if it applies without sealant coating considering a self-developed passive layer due to Zinc in atmospheric condition. In general, the use of zinc coating alone may provide enough durability based on study carryout in laboratory was proven and due to that thermal spray coating is more popular in the industry. The zinc 15% Aluminium thermal spray coating was developed in the late 1970s and is the greatest aluminium content in zinc that can be industrially produced as wire and tested for its durability with respect to highly corrosive environments. Thermal coating by Zn- 15%Al Coating having combination of both Zn and Al droplet in the coating where a higher percentage of Zn rich phases and lower percentage of Al rich phases can be revealed through Scanning Electron Microscope (SEM). As per literature Zn-15%Al Alloy is the most effective corrosion protection solution for steel under harsh atmospheric circumstances, including marine platforms and structures exposure to chloride containing environment with high and low tide situations.

Review of literature

Thermal spray technique is many, but Zinc is applied by either Arc Spray or Flame Spray method based on the application. In general arcs are not recommended in confined space due to electrical hazards. Multiple wires or twin wires can be used for enhancing the Zinc coating deposition efficiency as well as improving productivity. By adding twin wire method, cost of coating can be reduced to half the values and take advantage of higher productivity of coating at given time. The mechanism of zinc spray by electric arc process to align the gun position in proximity to sustain the established electrical arc resulting in the uniform coating having minimum porosity as well as un-melted zinc particle at the surface. By optimization of distance of thermal spray nozzle to the surface of metal will get the desire uniform coating with optimized coating thickness. With higher velocity of zinc bombardment due to very high- pressure capacity compressor air we get high quality sprade index of coating. During the combustion process, a solitary zinc wire is introduced into an oxy-fuel flame, resulting in the melting of the zinc wire and it will convert into small, atomized metal droplets and it can be controlled by high pressure gas used which can be controlled by compressor. The thickness of zinc and zinc alloy thermal sprayed coatings may be precisely regulated by controlling the machine variables and operators are qualified based on the optimized parameters to meet the uniform coating starting from 50 to 500 microns range depends on the type of equipment and operator skill. Coating thickness is directly corelate with atmospheric exposure and based on that the required protective thickness can be considered based on international standards based on environmentally corrosive category with exposure time as a factor for coating thickness calculation. The thicker the coating is the more severe the corrosivity of the environment.

In general, thermal coating limitations are in line with liquid coating with respect to its application for the corners and edge coating thickness requirement. It is advisable to have a curved surface in place of sharp edge to have proper coating thickness. In addition to those sealers or topcoats can be added depending on the environment (i.e. Under Insulation or atmospheric) exposure going to observed. Applying sealers and/or topcoats over a metalized coating enhances surface protection in harsh environments. It often extends the durability of the coating to a large extent. Environmental effect to the steel can govern the selection of coating and additional requirement of sealer coat often enhance the protection against the aggressive corrosion application.

Source journal

This paper will give a detailed insight into the applied simulation methodology and the assessment of the tested thermal spray coating material exposed to corrosive conditions via flame and arc spray methods.

With impressive corrosion resistance properties, zinc is commonly chosen as a protective coating on several components that must withstand harsh environmental conditions and not succumb to rust and corrosion.

There are several benefits of zinc thermal spray coatings as below [1, 5]:

1. Ideal for large or irregularly shaped components.
2. Zero risk of heat warping.
3. Thicker coatings mean components can withstand harsher environments.
4. Processes were faster and less expensive.
5. Zinc coatings were easy to apply and won't damage the substrate.

In some recent wire-arc developments, intermetallic compound coatings, metal and ceramic composite coatings were prepared by using pre-alloyed wires and cored wires, in which nonconductive materials are used as the core of a conductive wire.

Materials and Methods

The substrate was Carbon Steel sample with the chemical composition as shown in Table 1, having 6 cm length X 5 cm width and 10 mm thickness as shown in Figure 1.

Preparation for Substrates

Before coating, the substrate surfaces were blasted with Garnet 20/40 (nonmetallic material). The corundum used was irregular in shape and highly angular. This step provides enough room for anchorage of the splats and facilitates bonding through mechanical interlocking.

Before the substrate surface to be coated with TSC, the following conditions must be thoroughly verified [5]:

- The Surface cleanliness must be a minimum SA 2.5 based on ISO 8501-1 requirements. Surface cleanliness can be verified with the help of a comparator for its near white surface appearance through visual examination. Figure 2 shows the roughness of the blast surface and its roughness as well as its cleanliness by replica tape method.
- A Replica Tape method is necessary to measure a surface profile. To achieve better interlocking with single coat TSC minimum of 75-100 µ surface roughness is required as per standard/process. The replica tape is affixed to the substrate surface to get confirmation on surface profile verification due to blasting media used. After fixing replica tape it must be thoroughly rubbed with the help of circular- ended plastic tool available in the kit provided by quality department until a circular dark color is observed over the tape. Subsequently, the calibrated dial gauge employed to measure the roughness of replica tape to get required profile acceptance to start the TSC.
- The surface salt contamination must not exceed 50 mg/m2 as determined by the calibrated Elco-meter 138 in accordance with ISO 8502-6 requirements.
- The dust level must not exceed rating 1, using cellophane tape in accordance with ISO 8502-3 requirements.
- Abrasive blasting is prohibited when the air humidity exceeds 85% or the steel temperature was less than 30°C above the dew point of the ambient air. Figure 1 shows the humidity reading at the time of blasting

The quality of the surface coating may be impacted, potentially resulting in the deterioration of surface coating, if these conditions were not satisfied.

Arc spraying Process

Material that is used in this process is introduced into the process in the form of two electrically- conductive consumable wires. The wires commonly used in industry are usually made of electrically conductive materials, such as Aluminum, Zinc, Stainless Steel, and Copper. The gun geometry is designed such that the wire tips are separated by about a few tenths of a millimeter from one another.

An electric voltage of about 27 V, applied on the two wires, causes an arc in the gap between the wire tips. The arc heats the tips of the wires and produces a thin layer of molten material. A stream of atomizing gas strips the molten layer off the wire tips and propels it towards the substrate. The detached molten droplets will not only accelerate but also undergo further atomization and produce smaller droplets. The molten droplets are then deposited on the substrate one over another, where they solidify and form a coating layer.

Process and Variable Parameters of TSA Coating

As per present industrial requirement TSC to be applied to optimize the coating thickness based on approved process parameters provided by the thermal spray machine manufacturer. It should be recorded before application of coating based on NACE 12 standard to qualify the TSC operator. Approved process parameters need to be used during applications to standardize the coating thickness and its application for uniformity of coating application [4].

Thermal arc spray technology involves four main parts, namely as shown in Figure 3:

- Spray gun - used to receive the wire and shoot the melted material onto substrate
- Air Compressor with 4 to 6 Bar pressure – to accelerate melted material
- Blasting pot – for garnet space when blasting preparation is performed

TSC coating was performed with the approved operator qualification procedure based on the thermal spray machine standard parameters as listed in Table-2. Wire was automized at the tip of gun and with high pressure compressor gas, metallic particle spread over the metal surface uniformly by adjusting the velocity of the automized particle. The particles are spread over surface in different size to cover the entire metal surface get solidified without any porosity and discontinuity over the substrate. TSC process is like the welding principle from initiating the arc to metal spray over the substrate with electrically conductive media so that arc can be initiated, and wire can be melted at the tip of gun. In this paper, zinc, aluminum and zinc-aluminum alloy were used and it can be changed based on thorough study of environment and end user experience for their site condition [4].

Flame Spraying Process

The flame spray process consists of two steps, firstly, apply powder by thermal spraying with a gun, and secondly, fusing the deposit with a fusing torch as shown in Figure 4. The powder is fed into an oxy- acetylene or oxy-hydrogen gun by injection. It is projected towards the surface at high speed. The hot particles flatten upon impact and interlock both with the base material and each other thus forming a mechanical bond [2].

Figure 4: Flame spray system and thermal spray samples

This is followed by a fusion treatment to obtain a dense and well-bonded coating on the surface. The applied coating is heated to a temperature between the solidus and liquidus temperature around 1000°C. Typical shrinkage of 15 - 20% occurs during fusing when the melt fills the gaps between the particles and other parameters as per Table 3 followed for coating.

Results and Discussion

The electrochemical tests were performed using an EG&G Princeton Applied Research computer-controlled potentiate/galvanostatic (Model 273). A conventional electrochemical corrosion cell with three electrodes was used, a platinum plate counter-electrode, a saturated calomel reference electrode (SCE) and the sample as the working electrode.

To observe the effect of surface roughness on the electrochemical behavior, the coating surface was not polished. The sample was mounted in epoxy resin to create an active area of 1 cm2 (see Figure 5).

The corrosion behavior of the coatings was evaluated from open circuit potential (Eocp), potentiodynamic polarization curves and electrochemical impedance (EIS) measurements in 0.5 M NaCl solution. An EG&G (273A) potentiostat with Softcorr M352 was used. Before 0.5 An EG&G (273A) potentiostat with Softcorr M352 was used as shown in Figure 6.

Before each electrochemical measurement, the samples were immersed in the solution until the steady-state potential was reached, meaning the open circuit potential (OCP) was stable. The stabilization period was approximately 3 h for this configuration. The potentiodynamic polarizations were performed between 0.25V below OCP and +0.4V versus SCE at a scan rate of 0.2 mV/s.

Electrochemical impedance spectroscopy was carried out at frequencies ranging from 100 kHz to 10 Hz. The initial potential was fixed to that of the OCP, and a 10 mV AC amplitude was superimposed on top of the constant voltage. All electrochemical tests were carried out in an ambient atmosphere at 25 ◦C.

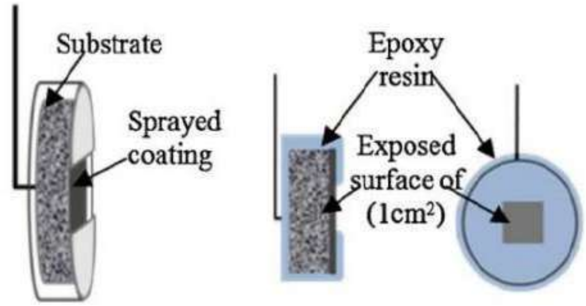

Figure 5: Schematic illustration of the working electrode

Potentiodynamic Testing studies were carried out to obtain potential (with respect to SCE) v/s log of current density plot which is known as polarization curve as shown in Figure 7 for arc spray coating and the actual values for arc spray coating reported in Table 4.

Similarly Figure 6 shows results for Potentiodynamic Testing studies for flame spray coating and Table 5 shows flame spray coating results.

Analysis of the Potentiodynamic curve can be carried out as per ASTM Standard G5, "Standard Reference Test Method for Making Potentiostatic and Potentiodynamic Anodic Polarization Measurements," contains useful information about potentiodynamic measurements techniques and can be consider as reference for the corrosion testing.

Table 1. Chemical composition of EN 24T substrate

.

C	Si	Mn	P	S	Mo	Cr	Ni
0.36-0.44	0.10-0.35	0.45-0.70	0.035 max	0.04 max	0.20-0.35	1.00-1.40	1.30-1.70

Figure 1: Carbon Steel surface preparation via blasting and humidity testing check

Figure 2: Surface Roughness check by Replica tape and comparing surface profile chart

Figure 3: Arc spray system, thermal spray gun and thermal spray samples

Table 2: Parameter for Thermal Spray Arc Process

Spray Parameter	Method of Application
Arc Voltage	Arc Wire Spray
	27 Volts
Air Pressure	80 psi
Steel Surface Cleanliness	NACE-1 White Metal
Steel Surface Profile	75 microns (minimum)
Arc Current	250-280A
Coating Thickness	225 Micron (Normal)
Coating Adhesion	> 1500 psi (total Coating)
Coating Porosity	Less than 8%
Spray Distance (spray gun work piece)	6-7”
Spray Pass Width	20mm

Table 3: Flame Spray Process Parameter

Spray Parameter	Method of Application
Air Pressure	Flame Wire Spray
	80 psi
Steel Surface Cleanliness	NACE-1 White Metal
Steel Surface Profile	75 microns (minimum)
Coating Thickness	225 Micron (Normal)
Coating Adhesion	> 1000 psi (total Coating)
Coating Porosity	Less than 8%
Spray Distance (spray gun work piece	6-7”
Spray Pass Width	20mm

Figure 6: Typical electrochemical corrosion test cell consisting of three electrodes for Potentiodynamic analysis

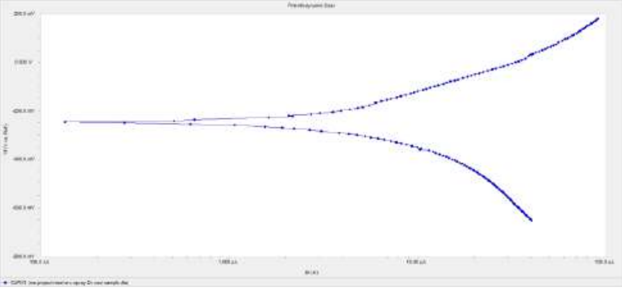

Potentiodynamic test of arc spray in 0.5% N NaCl

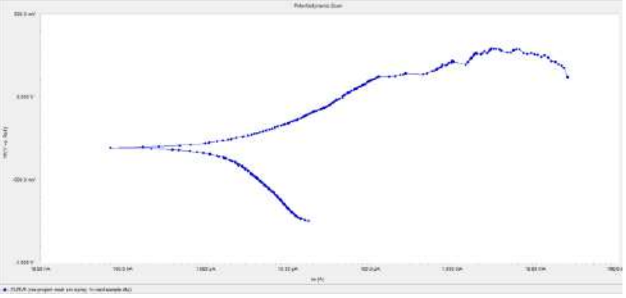

Potentiodynamic test of arc spray in 1% N NaCl

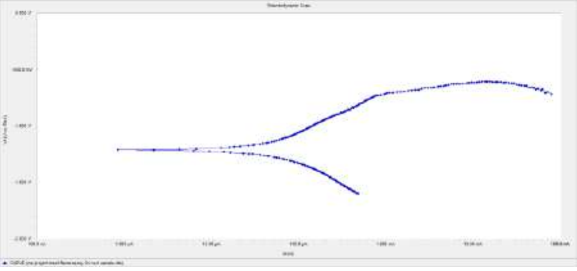

Potentiodynamic test of arc spray in 2% N NaCl

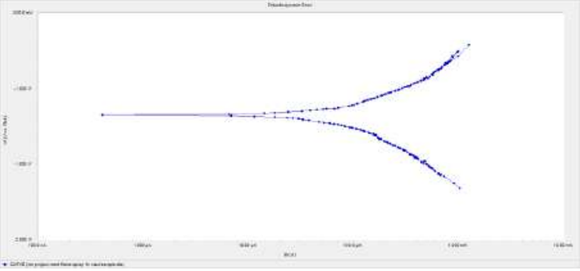

Potentiodynamic test of arc spray in 4% N NaCl

Figure 7: Potentiodynamic test of arc spray in 0.5%N, 1%N, 2%N and 4%N NaCl with Zn Coating at 225 microns Table 4: Electrochemical Parameters comparison for arc spray by Potentiodynamic Test

Sr. No.	Concentration	Icorr	Ecorr	Corrosion Rate
1	0.5% N NaCl	11.10 μA	-247.0 mV	16.67 mpy
2	1% N NaCl	104.0 μA	-1.10 V	157.6 mpy
3	2% N NaCl	95.20 μA	-1.210 V	143.0 mpy
4	4% N NaCl	122.0 μA	-1.180 V	183.3 mpy

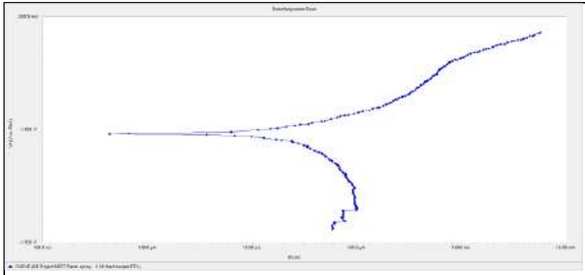

Potentiodynamic test of flam spray in 0.5%N NaCl

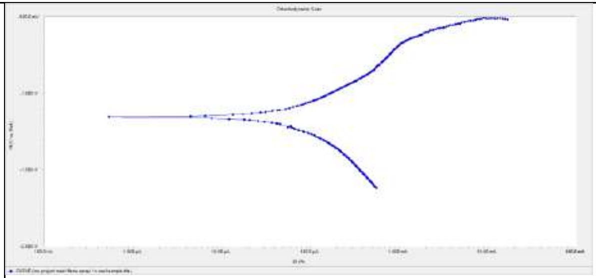

Potentiodynamic test of flam spray in 1% N NaCl

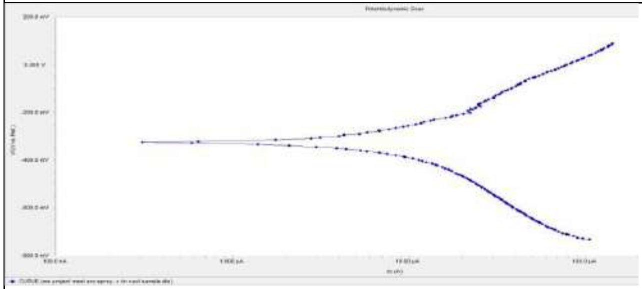

Potentiodynamic test of flam spray in 2% N NaCl

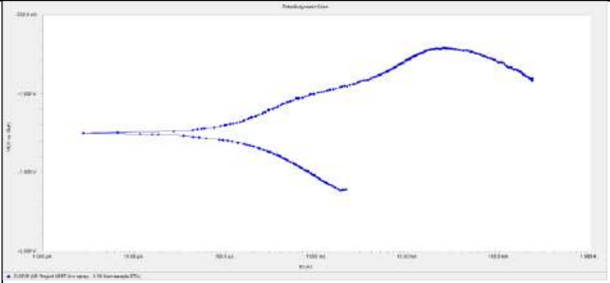

Potentiodynamic test of flam spray in 4% N NaCl

Figure 8: Potentiodynamic test of flame spray in 0.5%N, 1%N, 2%N and 4%N NaCl with Zn-Al Coating at 225 microns

Table 5: Electrochemical Parameters comparison for flame spray by Potentiodynamic

Sr. No.	Concentration	Icorr	Ecorr	Corrosion Rate
1	0.5% N NaCl	50.70 µA	-1.02 V	76.14 mpy
2	1% N NaCl	107.0 µA	-1.15 V	161.5 mpy
3	2% N NaCl	99.70 µA	-326.0 mV	149.7 mpy
4	4% N NaCl	152.0 µA	-1.25 V	228.0 mpy

The potential range was selected so the sample could be polarized both ways i.e. cathodically and anodically. It is used for Corrosion potential determination, Estimate corrosion current and Potential region for passivity.

Tafel Plot Corrosion Measurement by a wide DC potential spectrum (400 to 500 mV) provides more corrosion information than linear polarization. The Tafel plot corresponding to the anodic and cathodic half reactions for metal corrosion. Figure 8 shows potentiodynamic test results for flame spray process in 0.5%, 1%, 2% and 4% N NaCl solution.

Tafel plots are generalized in one of two ways, Polarization is begun at -200mV from OCP and increased until the potential reach at +200mV from OCP and the cathodic branch is generated by polarizing one of the test electrodes from OCP to -200mV from OCP. Potential changes are typically 2 mV per step for both methods and potential current data are graphed as applied potential verses log values of current density.

Based on study corrosion resistance of arc spray process shows 16.67 mpy corrosion rate as compared to flame spray process which shows 76.14 mpy corrosion rate at 0.5 % N NaCl solution which is 5000 ppm of chloride in water phase. With increasing chloride to 10,000 ppm chloride to 40,000 ppm chloride water, a solution does not show much change with respect to corrosion rate and shows similar behavior which indicates that increasing in chloride concentration has not much effect to thermal spray coating. However, coating may deteriorate due to localized pitting observed over surface but not reached to the base metal. Due to galvanic effect the base metal gets protected even though the pitting corrosion was observed on coating. During study it was observed that pitting potential & protection potential shifted towards the active direction shows that there is effect of corrosion over the coating surface, and it is further confirmed due to reduction in the potential passive range.

Conclusion

The major function of surface technology is to produce functionally useful surfaces. Coating improves the life of the parts and lowers the price of replacement. An extensive range of coatings can increase corrosion resistance, wear resistance and erosion resistance of materials. From the study it is found that thermal spray coating is the most important technique of surface modification. The result showed the more active corrosion reaction in presence of chloride ion results in pitting corrosion observed

the metal surface. Both the pitting potential & protection potential shifted towards the active direction as the potential range of passivity was shortened.

In 0.5% NaCl Concentration in arc spray and flame spray both showed the active corrosion reaction due to presence of a chloride. However, the arc spray process shows better results i.e. 16.67 mpy as compared to flame spray coating process i.e. 76.14 mpy and shows better corrosion resistance. This shows that the arc spray process is better than flame spray with respect to corrosion protection in chloride environment. 2%NaCl to each of the test medium concentration gave increased active corrosion reactions. The result shows that in lower chloride concentration the arc spray has lower corrosion rate while, in higher chloride concentration both processes show not much change with respect to corrosion rate and show almost similar corrosion protection. It shows that both processes are better for higher chloride concentrations and can be used for offshore and onshore refineries for high chloride environments applications.

REFERENCES

1. Sunil Kahar, Ashutosh Singh, Urvesh Vala, Aditya Desai1, Sumit Desai1, “Thermal Sprayed Coating using Zinc: A Review”, International Research Journal of Engineering and Technology (IRJET), Volume 07, Issue 06, June 2020 (Pg. Nos. ISSN: 2385-0072)

2. Vala Urvesh Inox India Pvt. Ltd. Kalol and Mihir Seth Sheth Corrosion & Coatings Vadodara, A case study on Blackening effect of Thermal Spray Aluminum Coating in the symposium Coatings and Linings, CORCON 2017 Mumbai, India, 17-20 September 2017 organized by NACE International.
3. https://thermalsprayzinc.zinc.org/about-thermal-spray
4. Urvesh Vala, “Comparing Thermal Spray Coating Characteristic using Al, Zn and Al-Zn Alloys by Arc and Flame Spray Process for Protecting Oil and Gas Offshore Platform” ASIA’S Largest Conference and Exhibition on CORROSION, CORCON 2023 at Mumbai, India Organized by AMPP India dated 25-28th October 2023

5. Sunil Kahar1, Ashutosh Singh1, Urvesh Vala2, Bhargav Navadiya1, Kaushik Pandya1 Suraj Dabhekar1, Metallurgy Department, M.S. University of Baroda1 and L&T Chiyoda Limited, Vadodara2, Thermal Sprayed Coating using Aluminium: A Review International Journal for Research in Applied Science & Engineering Technology (IJRASET), Volume 08, Issue VI, June 2020 (Pg. Nos. ISSN: 2321-9653) IC Value 45.98, SJ Impact Factor 7.429
6. Urvesh Vala, Head, L&T Chiyoda Limited “Thermal spray coating substitute for Hot Dipped Galvanized Steel” organized by Institute of Engineering & Ocean Technology, Oil and Natural Gas Corporation Limited, (ONGC), Panvel, Navi Mumbai on 2nd March 2022

Journal of the Maharaja Sayajirao University of Baroda: Science & Technology
Vol. 58, 2024, pp. 9-22

Comparing Thermal Spray Coating Characteristic Using Al, Zn and Al-Zn Alloy by Arc and Flame Spray Process to optimized the Coating Performance

Urvesh Vala[1], and I B Dave[2],
1 Gujarat Technical University, Ahmedabad, Gujarat, India & L&T Energy Hydrocarbon Engineering Limited, L&T Knowledge City, Vadodara – 390019, urvesh.vala@larsentoubro.com
2 Metallurgy Engineering, Government Engineering College, Sector-28, Gandhinagar -382028, Gujarat, India, ibdave@gecg28.ac.in

The objective of this research is to study the long-term performance of thermal-sprayed Aluminum, Zinc and Zn/Al coatings in tropical marine environments. Two different processes (electric arc and flame spray) were used with the application. Results showed that the optimized coating performance of thermal sprayed Zn/Al coating for corrosion protection requirements of highly corrosive structures. In service experience with TSA coatings demonstrated long-term corrosion protection and cost savings. Corrosion protection of structures in seawater is usually provided by cathodic protection. TSA coating has been proven to have a service life of more than 30 years with zero maintenance required. Offshore structure normally operates at ambient temperatures, and it is coated with thermal spray coating to enhance the design life of the structure by using aluminum, zinc or zinc-aluminum alloy as coating materials. By using metallic coating structures performance can be enhanced at high elevated temperatures for subsea application. Considering metallic coating in sea applications with coating breakdown shows better protection against deep sea structural application due to sacrificial action [4]. TSA has been shown to protect carbon steel in deep-sea environments even when damaged. The cyclic-temperature environment is a severe condition for coatings, and TSA has been proven to be an effective coating in such environments. TSA coating has merit in onshore and offshore under insulation, high temperature resistance as well as erosion corrosion resistance application in oil and gas refineries. This paper covers the spray patterns, adhesion quality, improved porosity and qualify bend test results based on optimized thermal spray coating considerations for corrosion resistance environments.

Key words: Thermal Spray Coating, Metallizing, Corrosion, Corrosion Under Insulation (CUI), Metallic Coating, Zinc Coating, etc.

INTRODUCTION

As we were aware that among all industries oil and gas refineries having higher global economic growth. Oil and Gas refineries products are used worldwide in many applications starting from aviation, automobile, defense to LPG gas used in house, where all individuals are getting affected with respect to quality and cost. In general, oil and gas refineries are operated at extreme process conditions like high pressure, high temperature, corrosive inhibitors injections, corrosive species handled, etc. Due to this there are corrosion, erosion, high temperature creep, fatigue, cracking damage mechanisms leading to operational loss, safety hazers, loss of process fluids, environmental loss due to toxic gas and liquids spillages leading to financial and human losses. Considering extremely corrosive service category, only thermal spray coating has merits considering severely heavy corrosion in marine environment worldwide with 25 years' design life assurance by many end users. Thermal spray coating involves atomizing molten aluminium, zinc, or aluminium-zinc alloys and spraying the particles onto the metal surface to create a dense, protective layer [1].

The coating will be supported by high velocity molten metal particles with variation in its size and type to be sprayed uniformly over the entire substrate surface. Coating may have melted, and un-melted metal particles mix with variation in porosity. This can be evaluated by Scanning Electron Microscope. If metal is spreads uniformly over the surface, then it can generate dense coating which is desired for high durability protective coating as compared to liquid coating. TSA coating having excellent corrosion resistance, erosion resistance, high temperature resistance. Coating variance are many like purity of metal wire or powder used, chemical composition of metal or alloy used, purity of metal used, thermal spray process or method used, surface preparation of substrate i.e. SA3 or equivalent surface cleanliness with 65 to 75 microns roughness, environmental conditions, corrosivity of processes, etc. Thermal spray coating having excellent resistance against corrosion under insulation applications as well as it is more corrosion resistance coating against cyclic temperature services observed by oil and gas refineries. With such industrial exposure TSA coating observed excellent adhesion strength and cohesive strength based on its surface preparation and type of coating method used. Moreover, detail examination of coating parameters to be study in laboratory environment to simulate the harsh industrial fluctuating cyclic service temperature requirements going to observed by oil and gas refineries [5].

---

* Corresponding author.
Email: ibdave@gecg28.ac.in

In recent years, extensive research on corrosion and erosion resistance properties of thermal spray coating is carryout with verity of coating parameters in immersion, under insulation, environmental climate changes, cyclic process temperature of upstream and downstream refineries application. Mechanical and chemical treatment provide additional coating protection characteristic to chemical and wear resistance against corrosion and erosion based on extensive research outcome published in present scenario.

There are many factors affecting coating characteristics like spray angle, power quality, power size, wire processing methods, chemical and mechanical properties of feeder material, gas flow rate for flame and arc spray, powder or wire feed rate, spray distance from gun to metal surface, etc.

Based on above parameters, trying to establish the optimum coating parameters for thermal spray coating to meet current industrial demand meeting desire design life of equipment and piping. This study covers silent features to develop thermal spray coating parameters as well as validate TSA machine capability and operator qualification to meet optimized coating thickness for most corrosive industrial environment-like offshore platforms, high temperature cyclic services, CUI, erosion corrosion, etc. for oil and gas refineries. Detailed thermal spray coating parameters including spray angle, spray distance, wire chemical and mechanical parameters, substrate surface preparation, environment temperature, substrate temperature, humidity, due point, etc. to be studied. Thermal spray coating is the only coating which can resist in upset process conditions as well as startup and shutdown of plant having fluctuating temperatures requirements.

Research Significance

Coating breakdown study needs extensive data for oil and gas plant operation in high temperature cyclic services for the equipment and piping as well as piping component like valves, pumps, strainers, etc. Out of all coating thermal spray coating is the only possible solution to have high durability and high service life of 25 years or more. Nevertheless, there exists an insufficiently defined set of optimal thermal spray coating parameters tailored to meet the demands of cyclic temperature service requirements within oil and gas refineries. Consequently, there is a compelling need to explore how thermal spray coating parameters, such as spray distance, spray angle, and spray rate, impact the performance of coatings subjected to cyclic temperature service conditions. Main objective of this study is to optimize thermal spray coating parameters for uniform coating application with optimized coating distance to improve the wastage of metal particles. Thermal Spray coating is critical, and its application plays a vital role in its durability as well as high temperature resistance requirements based on NACE MR 0175 standard requirements [3].

In present industrial demand, trying to establish the thermal spray variables by optimizing the spray pattern, spray distance, gas flow rate, gas mixture for flame spray coating and addition to that current and voltage parameter optimization for arc spray coating for most common industrial applications.

The silent features of thermal spray coating addressed in this study were listed below:

1. Thermal spray coating parameter establishment which includes spray pattern, spray distance, spray angle, gas flow rate, current and voltage to meet optimized coating thickness.
2. Verify adhesion strength of coating by Dolly Test Method, porosity check, Bend Test to check mechanical strength of coating.
3. Examine the impact of cyclic temperature service conditions on coating performance metrics such as adhesion strength, wear resistance, and corrosion resistance.
4. Compare the performance of the refined coatings with that of uncoated components and commercially available coatings when subjected to cyclic temperature service conditions.
5. Offer recommendations for selecting the optimal thermal spray coating parameters for cyclic temperature service requirements in oil and gas refineries based on the findings of this study.
6. In summary, the overarching objective of this research is to enhance the longevity and reliability of components used in oil and gas refineries by optimizing thermal spray coating parameters to meet the demands of cyclic temperature service conditions.

Materials And Methods [2]

Thermal spray coating refers to a collection of processes that utilize a concentrated heat source to melt materials that are propelled towards a prepared surface with kinetic energy from process jets. The molten particles, upon contact with the surface, quickly solidify, resulting in the build-up of a deposit. Thermal spray coating gun is the process unit and plays a vital role in establishing process temperature to bombard the metal particle over the metal substrate for achieving the uniform coating with high sprade angel. Gas plays an important role in thermal spray coating. Many gases can be used, which include combustion fuels like oxygen, air, LPG, etc. Compressors play an important role in accelerating the metal particles to the metal substrate. Gun alignment and nozzle size play an important role in accelerating the feedstock which is most commonly used wire than powder. Metallic coating as well as feedstock material to be verified for its purity with the help of chemical characterization in the laboratory. In this study the thermal spray setup shown in Fig.1 was used to establish optimized coating parameters as well as operator qualification based on the TSA machine used to characterize the coating strength and durability with respect to corrosive environment.

Carbon Steel substrate (150 mm X150 mm X3 mm plate size) was used to study the thermal spray coating characterization with respect to mechanical strength in this study. This costing can be further evaluated with respect to its corrosion resistance, hardness to check its erosion resistance to meet corrosion and high temperature thermal resistance to the process equipment and piping. Thermal spray is not going to alter the metal surface mechanical or thermal properties though it is high temperature coating application.

Flame spray zinc coating

Flame spraying zinc coating was considered for coating parameters establishment purpose. Also, operators are qualified based on NACE 12 standard as well as TSA machine manual to have a parameter optimization during coating application. As zinc is more active and acts as anode to the carbon steel and get protect the structure which is cathode as per galvanic series.

The initial stage in flame spraying zinc coating is surface preparation. Before initiating the coating process, it is imperative to thoroughly clean and ready the substrate. Blasting is commonly used to remove foreign particle on the metal surface as well as it creating profile for better interlocking of thermal spray coating. During blasting operation, blaster try to clean the surface to SA-3, nearly white metal surface.

Precise temperature control is crucial to prevent overheating or cooling of the substrate, with the ideal temperature range falling between 150°C to 400°C. Once the substrate reaches the necessary temperature, the zinc coating can be applied using a flame spray gun. The flame propels and deposits the molten zinc particles onto the substrate, creating a thin, uniform layer of molten zinc. As these zinc particles land on the substrate, they solidify and cool, forming a consistent coating.

The final stage in the flame spray zinc coating process pertains to post-processing. After the coating application, the substrate must be allowed to cool down to room temperature. Once cooled, the substrate undergoes inspection to confirm the uniformity and absence of defects in the coating. Any detected defects can be rectified by reapplying the coating to the affected areas.

In summation, the flame spray zinc coating process comprises several phases, including surface preparation, the application of a primer or bond coat, substrate heating, the spray application of molten zinc, and post-processing. This method is extensively used in the manufacture of steel structures, pipelines, and equipment necessitating protection against corrosion. Flame spray zinc coating represents a cost-effective and dependable coating technique that offers long-lasting safeguarding against corrosion.

Arc spraying zinc coating.

The first step in the arc spray zinc coating process is surface preparation. The substrate to be coated is cleaned and prepared to ensure proper adhesion of the coating. The next step is the selection of the appropriate zinc wire for spraying. The wire should be of high purity and have a uniform diameter to ensure a consistent coating thickness.

Figure 1: Thermal Spray Coating (Arc & Flame Spray)

Results And Discussion

The mechanical evaluation of thermal spray coatings encompasses the examination and measurement of a spectrum of mechanical attributes to gain insights into the behavior and functionality of the coating material. Thermal spray coatings are administered onto substrates with the aim of furnishing protective or utilitarian layers that enhance their characteristics, affording advantages like heightened performance, extended longevity, and fortification against wear, corrosion, and other types of deterioration.

The process of mechanical characterization comprises the execution of various tests and measurements designed to assess diverse mechanical properties inherent to the coating. These properties serve as indicators of how the coating will react to mechanical stresses, deformations, and loads, thereby offering valuable insights into its overarching mechanical performance.

Adhesion Test [2]

The evaluation of protective coating processes frequently relies on pull-off adhesion testing. This testing serves a dual purpose, to gauge the suitability of a coating for both new construction and the restoration of existing structures. The results of these tests hold significant sway in the acceptance or rejection of a coating process. Low adhesion values signal the potential for premature coating failure, often attributed to inadequate substrate surface preparation.

Various standards, including ASTM D4541 and BS EN ISO 4624, describe different testing equipment, but the fundamental approach remains consistent across these standards. It entails affixing a test dolly to the coated surface using adhesive and then applying a perpendicular force to the surface to attempt to detach both the dolly and the coating from the substrate. The force at which the coating fails and the type of failure observed furnish a measure of the coating's adhesion properties.

Numerous factors can influence test outcomes, including adhesive mixing, surface preparation of the coating and dolly, testing temperature, and whether the coating is incised or left unaltered. Additionally, the effects of manual versus automatic pull-off tester operation have undergone scrutiny. Each of these aspects has been evaluated, and the results analyzed to discern their potential impact on obtaining valid test results.

ISO 4624 provides guidance on the selection of suitable adhesives for the test. It underscores the necessity of adhesives with cohesive and bonding properties exceeding those of the coating being tested. Preliminary screening of adhesives is imperative to ascertain their appropriateness. Adhesives yielding higher adhesion values, signifying greater coating-substrate adhesive failure, are preferred.

ASTM D4541 clarifies that the adhesive is solely used for securing the fixture to the coating and does not influence the coating's properties.

Comparative tests were conducted to evaluate the relative strength of two frequently supplied adhesives from adhesion test kits. Ten dollies were affixed to an uncoated, unprepared steel substrate, with five employing Adhesive A and the remaining five using Adhesive B. After a 24-hour curing period, the dollies were extracted from the surface to assess their performance.

Pull-off adhesion testing is a widely employed methodology for scrutinizing the efficacy of coatings and ascertaining their suitability for diverse applications. Meticulous consideration of factors such as adhesive selection, surface preparation, testing conditions, and adherence to pertinent standards ensures accurate and meaningful test outcomes.

BEND TEST

The bend test is a cost-effective and uncomplicated qualitative evaluation used to appraise the flexibility and soundness of a material. It is frequently employed as a quality control procedure for coatings on base metals and butt- welded joints, offering the advantage of simplicity in terms of test specimens and equipment.

Figure 2 Adhesion Test

Figure 3: Bend Test

In the bend test, a specimen, often referred to as a coupon, is subjected to three-point bending, resulting in a specific degree of deformation. The outer part of the bend undergoes substantial plastic deformation, which serves to reveal any defects or embrittlement within the material through premature coupon failure.

Table 1: Flame Spray Sample

FLAME SPRAY ZINC			
Sr No	**FUEL GAS**	**SPRAY DISTANCE**	**SPRAY PATTERN**
1	15 (L) / 50 (O)	100 mm	—
2	15 (L) / 50 (O)	100 mm	○
3	15 (L) / 50 (O)	100 mm	⬭
4	15 (L) / 50 (O)	250 mm	—
5	15 (L) / 50 (O)	250 mm	○
6	15 (L) / 50 (O)	250 mm	⬭
7	15 (L) / 50 (O)	400 mm	—
8	15 (L) / 50 (O)	400 mm	○
9	15 (L) / 50 (O)	400 mm	⬭
10	20 (L) / 65 (O)	100 mm	—
11	20 (L) / 65 (O)	100 mm	○
12	20 (L) / 65 (O)	100 mm	⬭
13	20 (L) / 65 (O)	250 mm	—
14	20 (L) / 65 (O)	250 mm	○
15	20 (L) / 65 (O)	250 mm	⬭
16	20 (L) / 65 (O)	400 mm	—
17	20 (L) / 65 (O)	400 mm	○
18	20 (L) / 65 (O)	400 mm	⬭
19	25 (L) / 80 (O)	100 mm	—
20	25 (L) / 80 (O)	100 mm	○
21	25 (L) / 80 (O)	100 mm	⬭
22	25 (L) / 80 (O)	250 mm	—
23	25 (L) / 80 (O)	250 mm	○
24	25 (L) / 80 (O)	250 mm	⬭
25	25 (L) / 80 (O)	400 mm	—
26	25 (L) / 80 (O)	400 mm	○
27	25 (L) / 80 (O)	400 mm	⬭

Table 2: ARC Spray Sample

ARC SPRAY ZINC			
Sr No	**VOL / CURR**	**SPRAY DISTANCE**	**SPRAY PATTERN**
1	18 (V) / 245 (A)	100 mm	—
2	18 (V) / 245 (A)	100 mm	○
3	18 (V) / 245 (A)	100 mm	⬭
4	18 (V) / 245 (A)	250 mm	—
5	18 (V) / 245 (A)	250 mm	○
6	18 (V) / 245 (A)	250 mm	⬭
7	18 (V) / 245 (A)	400 mm	—
8	18 (V) / 245 (A)	400 mm	○
9	28 (V) / 335 (A)	400 mm	⬭
10	28 (V) / 335 (A)	100 mm	—
11	28 (V) / 335 (A)	100 mm	○

12	28 (V) / 335 (A)	100 mm	⬭
13	28 (V) / 335 (A)	250 mm	—
14	28 (V) / 335 (A)	250 mm	○
15	28 (V) / 335 (A)	250 mm	⬭
16	28 (V) / 335 (A)	400 mm	—
17	28 (V) / 335 (A)	400 mm	○
18	28 (V) / 335 (A)	400 mm	⬭
19	36 (V) / 400 (A)	100 mm	—
20	36 (V) / 400 (A)	100 mm	○
21	36 (V) / 400 (A)	100 mm	⬭
22	36 (V) / 400 (A)	250 mm	—
23	36 (V) / 400 (A)	250 mm	○
24	36 (V) / 400 (A)	250 mm	⬭
25	36 (V) / 400 (A)	400 mm	—
26	36 (V) / 400 (A)	400 mm	○
27	36 (V) / 400 (A)	400 mm	⬭

Table 3: Adhesion Test (Flame Spray)

Sr No	Description & Set	Required value (MPa)	Actual value (MPa)
1	Dolly no 1	5 MPa	3.22 MPa
2	Dolly no 2	5 MPa	3.69 MPa
3	Dolly no 3	5 MPa	3.88 MPa
4	Dolly no 4	5 MPa	5.82 MPa
5	Dolly no 5	5 MPa	6.33 MPa
6	Dolly no 6	5 MPa	6.74 MPa
7	Dolly no 7	5 MPa	2.11 MPa
8	Dolly no 8	5 MPa	2.88 MPa
9	Dolly no 9	5 MPa	3.05 MPa
10	Dolly no 10	5 MPa	4.19 MPa
11	Dolly no 11	5 MPa	4.53 MPa
12	Dolly no 12	5 MPa	4.92 MPa
13	Dolly no 13	5 MPa	12.66 MPa
14	Dolly no 14	5 MPa	15.57 MPa
15	Dolly no 15	5 MPa	17.89 MPa
16	Dolly no 16	5 MPa	3.44 MPa
17	Dolly no 17	5 MPa	3.91 MPa
18	Dolly no 18	5 MPa	4.23 MPa
19	Dolly no 19	5 MPa	3.36 MPa

20	Dolly no 20	5 MPa	3.81 MPa
21	Dolly no 21	5 MPa	4.51 MPa
22	Dolly no 22	5 MPa	7.52 MPa
23	Dolly no 23	5 MPa	8.21 MPa
24	Dolly no 24	5 MPa	8.97 MPa
25	Dolly no 25	5 MPa	4.03 MPa
26	Dolly no 26	5 MPa	4.38 MPa
27	Dolly no 27	5 MPa	4.74 MPa

Table 4: Adhesion Test (Arc Spray)

Sr No	**Description & Set**	**Required value (MPa)**	**Actual value (MPa)**
1	Dolly no 1	7 MPa	4.11 MPa
2	Dolly no 2	7 MPa	4.69 MPa
3	Dolly no 3	7 MPa	4.75 MPa
4	Dolly no 4	7 MPa	9.01 MPa
5	Dolly no 5	7 MPa	9.55 MPa
6	Dolly no 6	7 MPa	10.04 MPa
7	Dolly no 7	7 MPa	3.18 MPa
8	Dolly no 8	7 MPa	3.44 MPa
9	Dolly no 9	7 MPa	3.67 MPa
10	Dolly no 10	7 MPa	4.51 MPa
11	Dolly no 11	7 MPa	4.94 MPa
12	Dolly no 12	7 MPa	5.21 MPa
13	Dolly no 13	7 MPa	19.66 MPa
14	Dolly no 14	7 MPa	17.11 MPa
15	Dolly no 15	7 MPa	18.15 MPa
16	Dolly no 16	7 MPa	6.01 MPa
17	Dolly no 17	7 MPa	6.42 MPa
18	Dolly no 18	7 MPa	6.68 MPa
19	Dolly no 19	7 MPa	5.22 MPa
20	Dolly no 20	7 MPa	5.39 MPa
21	Dolly no 21	7 MPa	5.81 MPa
22	Dolly no 22	7 MPa	8.25 MPa
23	Dolly no 23	7 MPa	8.98 MPa
24	Dolly no 24	7 MPa	9.65 MPa
25	Dolly no 25	7 MPa	4.66 MPa
26	Dolly no 26	7 MPa	5.31 MPa
27	Dolly no 27	7 MPa	5.79 MPa

Graph 1: Adhesion Test (Flame Spray)

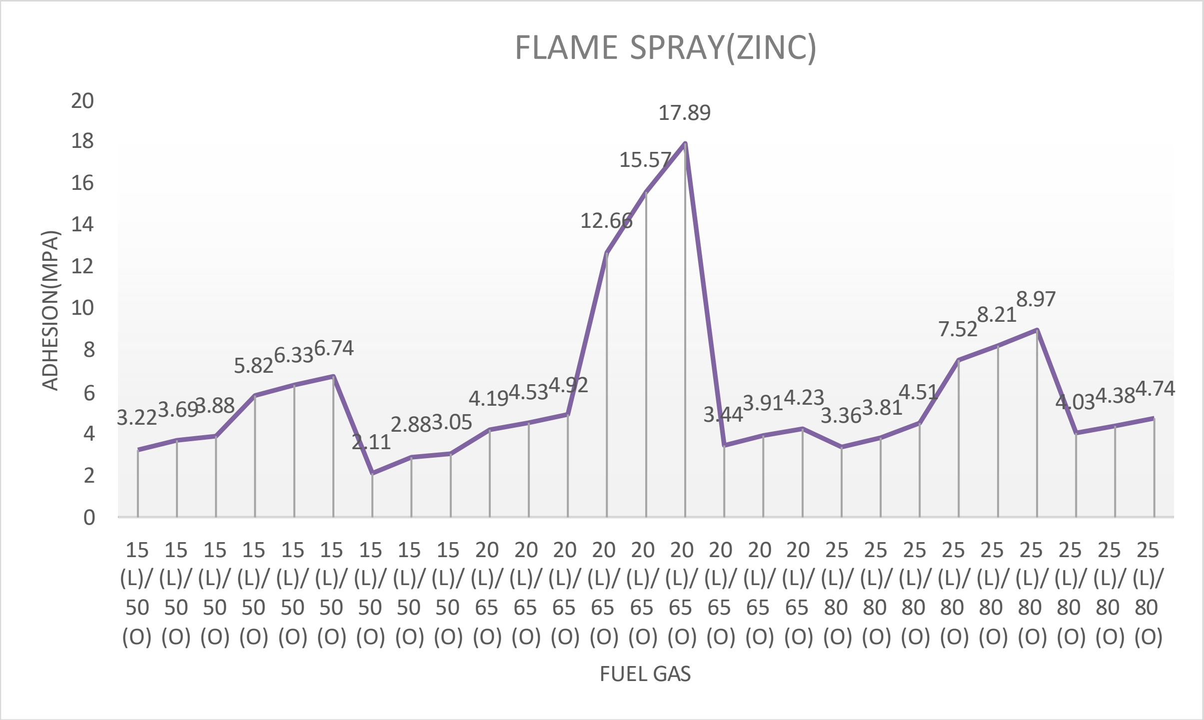

Graph 2: Adhesion Test (Arc Spray)

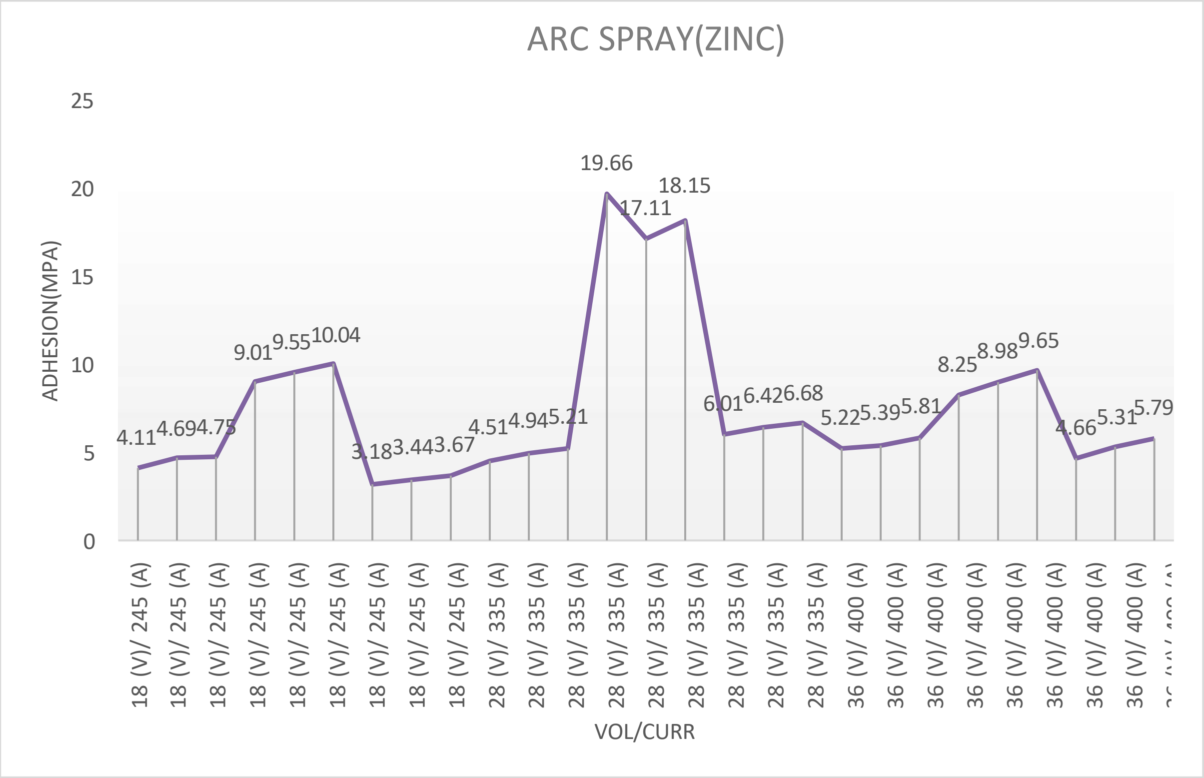

Table 5: Bend Test (Flame Spray)

Sr No	Description & Set	Results
1	Sample 1	Cracks with lifting from substrate
2	Sample 2	Cracks with lifting from substrate
3	Sample 3	Cracks with lifting from substrate
4	Sample 4	Minor Cracks with no lifting from substrate
5	Sample 5	Minor Cracks with no lifting from substrate
6	Sample 6	Minor Cracks with no lifting from substrate
7	Sample 7	Cracks with lifting from substrate
8	Sample 8	Cracks with lifting from substrate
9	Sample 9	Cracks with lifting from substrate
10	Sample 10	Cracks with lifting from substrate
11	Sample 11	Cracks with lifting from substrate
12	Sample 12	Cracks with lifting from substrate
13	Sample 13	No Cracks
14	Sample 14	No Cracks
15	Sample 15	No Cracks
16	Sample 16	Cracks with lifting from substrate
17	Sample 17	Cracks with lifting from substrate
18	Sample 18	Cracks with lifting from substrate
19	Sample 19	Cracks with lifting from substrate
20	Sample 20	Cracks with lifting from substrate
21	Sample 21	Cracks with lifting from substrate
22	Sample 22	Minor Cracks with no lifting from substrate
23	Sample 23	Minor Cracks with no lifting from substrate
24	Sample 24	Minor Cracks with no lifting from substrate
25	Sample 25	Cracks with lifting from substrate
26	Sample 26	Cracks with lifting from substrate
27	Sample 27	Cracks with lifting from substrate

Table 6: Bend Test (Arc Spray)

Sr No	Description & Set	Results
1	Sample 1	Cracks with lifting from substrate
2	Sample 2	Cracks with lifting from substrate
3	Sample 3	Cracks with lifting from substrate
4	Sample 4	Minor Cracks with no lifting from substrate
5	Sample 5	Minor Cracks with no lifting from substrate
6	Sample 6	Minor Cracks with no lifting from substrate
7	Sample 7	Cracks with lifting from substrate
8	Sample 8	Cracks with lifting from substrate
9	Sample 9	Cracks with lifting from substrate
10	Sample 10	Cracks with lifting from substrate
11	Sample 11	Cracks with lifting from substrate
12	Sample 12	Cracks with lifting from substrate
13	Sample 13	No Cracks
14	Sample 14	No Cracks
15	Sample 15	No Cracks
16	Sample 16	Cracks with lifting from substrate
17	Sample 17	Cracks with lifting from substrate
18	Sample 18	Cracks with lifting from substrate
19	Sample 19	Cracks with lifting from substrate
20	Sample 20	Cracks with lifting from substrate
21	Sample 21	Cracks with lifting from substrate
22	Sample 22	Minor Cracks with no lifting from substrate
23	Sample 23	Minor Cracks with no lifting from substrate
24	Sample 24	Minor Cracks with no lifting from substrate
25	Sample 25	Cracks with lifting from substrate
26	Sample 26	Cracks with lifting from substrate
27	Sample 27	Cracks with lifting from substrate

Table 7: Porosity Test (Flame Spray)

Sr No	Description & Set	Required Value (%)	Actual value (%)
1	Sample 1	8 %	11 %
2	Sample 2	8 %	13 %

3	Sample 3	8 %	14 %
4	Sample 4	8 %	7 %
5	Sample 5	8 %	9 %
6	Sample 6	8 %	15 %
7	Sample 7	8 %	18 %
8	Sample 8	8 %	21 %
9	Sample 9	8 %	23 %
10	Sample 10	8 %	12 %
11	Sample 11	8 %	14 %
12	Sample 12	8 %	15 %
13	Sample 13	8 %	5 %
14	Sample 14	8 %	7 %
15	Sample 15	8 %	8 %
16	Sample 16	8 %	20 %
17	Sample 17	8 %	23 %
18	Sample 18	8 %	27 %
19	Sample 19	8 %	24 %
20	Sample 20	8 %	26 %
21	Sample 21	8 %	31 %
22	Sample 22	8 %	6 %
23	Sample 23	8 %	7 %
24	Sample 24	8 %	17 %
25	Sample 25	8 %	32 %
26	Sample 26	8 %	35 %
27	Sample 27	8 %	39 %

Table 8: Porosity Test (Arc Spray)

Sr No	Description & Set	Required Value (%)	Actual Value (%)
1	Sample 1	8 %	10 %
2	Sample 2	8 %	11 %
3	Sample 3	8 %	14 %
4	Sample 4	8 %	5 %
5	Sample 5	8 %	10 %
6	Sample 6	8 %	12 %
7	Sample 7	8 %	15 %
8	Sample 8	8 %	18 %
9	Sample 9	8 %	25 %

10	Sample 10	8 %	13 %
11	Sample 11	8 %	15 %
12	Sample 12	8 %	17 %
13	Sample 13	8 %	6 %
14	Sample 14	8 %	8 %
15	Sample 15	8 %	9 %
16	Sample 16	8 %	22 %
17	Sample 17	8 %	25 %
18	Sample 18	8 %	30 %
19	Sample 19	8 %	22 %
20	Sample 20	8 %	25 %
21	Sample 21	8 %	34 %
22	Sample 22	8 %	7 %
23	Sample 23	8 %	8 %
24	Sample 24	8 %	22 %
25	Sample 25	8 %	36 %
26	Sample 26	8 %	39 %
27	Sample 27	8 %	44 %

Graph 3: Porosity Test (Flame Spray)

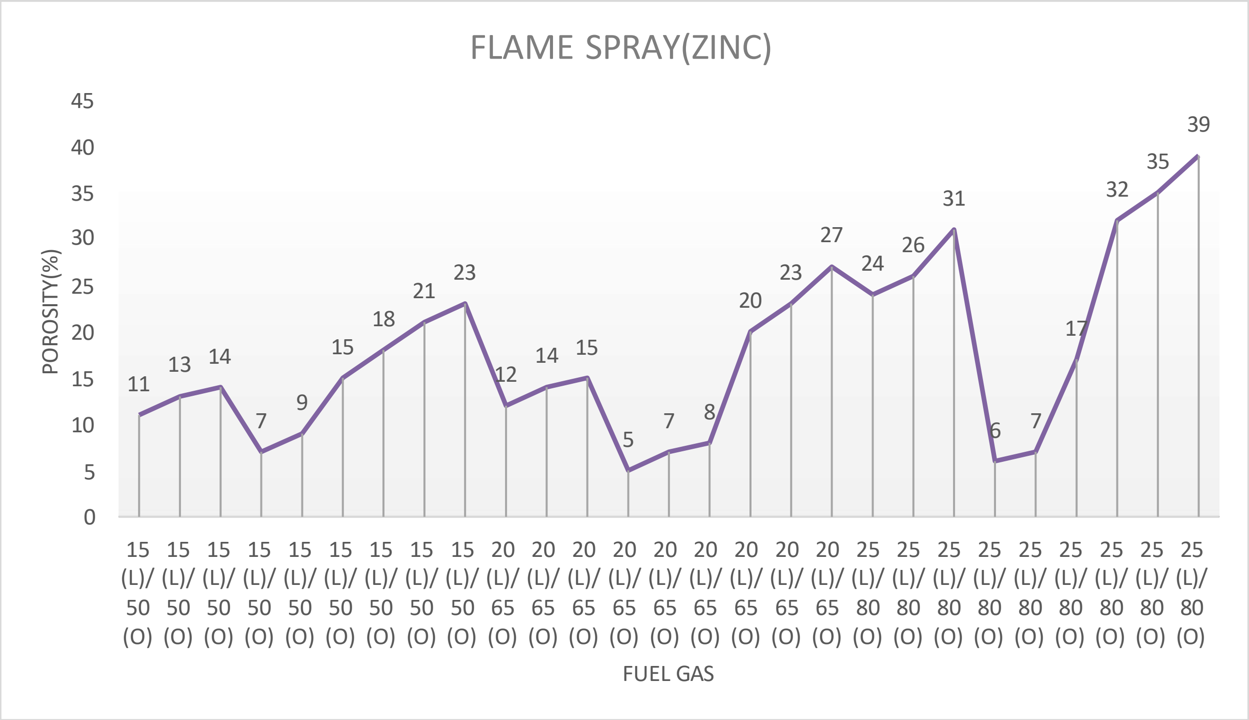

Graph 4: Porosity Test (Arc Spray)

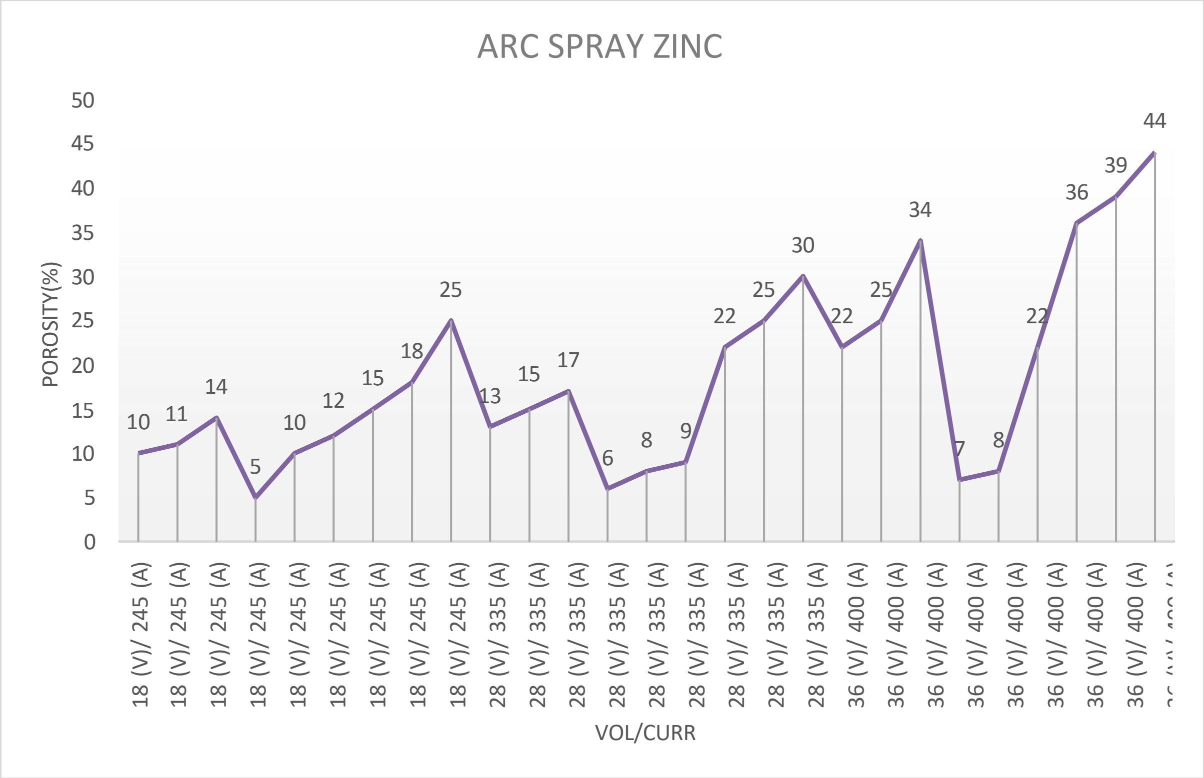

Porosity Test

Microscopy porosity testing is a technique employed for the evaluation of porosity within thermal spray coatings. This examination involves scrutinizing a cross-section of the coating under a microscope to visually assess the presence, dimensions, dispersion, and density of pores within the coating. The information obtained from this test is instrumental in ascertaining the quality and structural integrity of the coating.

To execute the microscopy porosity test, an appropriate sample representing the thermal spray coating must be procured. This sample should encompass both the coating layer and the underlying substrate.

The efficacy of the microscopy porosity test largely hinges on its capacity to accurately discern and characterize the pores within the coating. This assessment aids in evaluating the coating's structural integrity, adhesion, and its resistance to environmental influences. The results can be benchmarked against acceptance criteria or industry standards to gauge the quality of the thermal spray coating.

Standards such as ASTM E2109 (Standard Test Methods for Determining Area Percentage Porosity in Thermal Sprayed Coatings) and ISO 14956 (Thermal spraying - Determination of porosity) furnish comprehensive directives and specifications for conducting microscopy porosity testing on thermal spray coatings. These standards delineate the test procedures, sample preparation, equipment prerequisites, acceptance criteria, and reporting protocols, ensuring consistency and precision throughout the testing process.

Figure 4: Porosity Test

Conclusion

After conducting a comprehensive analysis of both the arc and flame spray processes, the following conclusions can be drawn:

1. When positioned at 100mm, the adhesion and bend tests produce satisfactory results, suggesting acceptable performance. However, the porosity tests indicate failure, signalling that the coating falls short of the required standards concerning porosity levels.

2. In contrast, when positioned at 400mm, all test

outcomes point to poor performance, with the porosity, adhesion, and bend tests all resulting in failure. This indicates a substantial compromise in the coating's quality and its adherence to standards at this distance.

3. The most promising results are consistently observed at a distance of 250mm, regardless of the specific parameter settings. At this distance, the coating passes both the adhesion and bend tests, indicating a strong bond and flexibility. However, in some cases, the porosity test may still fail with certain parameter combinations. This discrepancy can be attributed to unique properties of the adhesion values obtained, which may occasionally lead to inadequate filling of porosities as mandated by the standard requirements.

Taking into consideration both the arc and flame spray processes, it is evident that the most optimized results are consistently achieved at a spray distance of 250mm. Therefore, it is advisable to employ either the arc spray or flame spray process with the corresponding parameters, depending on the equipment used in the study. It is important to note that the outcomes mentioned above may vary depending on the manufacturer and specifications of the equipment utilized.

In summary, this study reveals that the best overall performance, as assessed through adhesion, porosity, and bend tests, is consistently achieved at the 250mm distance in both the arc and flame spray processes. These findings offer valuable guidance to practitioners in selecting the appropriate process and parameters to ensure the desired coating quality and adherence to established standards.

Future Work

Below are the proposed future tasks for the thermal spray project we have undertaken:

1. Extending the service life of the thermal spray coating in a corrosive environment by applying a sealer with a thickness ranging from 50 to 65 microns over the existing coating.

2. Carrying out electrochemical corrosion investigations, utilizing techniques such as potentiodynamic analysis, potentiogalvanic analysis, and AC impedance analysis to delve into the corrosion characteristics.

3. Utilizing scanning electron microscopy (SEM) to scrutinize the same samples under consistent parameters. This examination is intended to evaluate several aspects of the thermal spray coating, including: (a) Porosity (b) Un-melted and melted particles (c) The uniformity of the thermal spray coating across the substrate surface.

REFERENCES

1. Sunil Kahar, Ashutosh Singh, Urvesh Vala, Aditya Desai1, Sumit Desai1, "Thermal Sprayed Coating using Zinc: A Review", International Research Journal of Engineering and Technology (IRJET), Volume 07, Issue 06, June 2020 (Pg. Nos. ISSN: 2385-0072)
2. SSPC 2015, Pull-Off Adhesion Testing of Coatings – Improve Your Technique
3. Urvesh Vala, "Comparing Thermal Spray Coating Characteristic using Al, Zn and Al-Zn Alloys by Arc and Flame Spray Process for Protecting Oil and Gas Offshore Platform" ASIA'S Largest Conference and Exhibition on CORROSION, CORCON 2023 at Mumbai, India Organized by AMPP India dated 25-28th October 2023
4. Sunil Kahar1, Ashutosh Singh1, Urvesh Vala2, Bhargav Navadiya1, Kaushik Pandya1 Suraj Dabhekar1, Metallurgy Department, M.S. University of Baroda1 and L&T Chiyoda Limited, Vadodara2, Thermal Sprayed Coating using Aluminium: A Review International Journal for Research in Applied Science & Engineering Technology (IJRASET), Volume 08, Issue VI, June 2020 (Pg. Nos. ISSN: 2321-9653) IC Value 45.98, SJ Impact Factor 7.429
5. Urvesh Vala, Head, L&T Chiyoda Limited "Thermal spray coating substitute for Hot Dipped Galvanized Steel" organized by Institute of Engineering & Ocean Technology, Oil and Natural Gas Corporation Limited, (ONGC), Panvel, Navi Mumbai on 2nd March 2022

Journal of the Maharaja Sayajirao University of Baroda: Science & Technology
Vol. 58, 2024, pp. 23-34

Investigation of hydrogen-induced cracking (HIC) susceptibility in a steel pipe of grade API 5L X60 & API 5L X65

Sucheta Juneja*, Aditya Raj, Punit Dubey, Anil Arya

Jindal SAW Ltd., Nanakapaya, Mundra-370415, India.*sucheta.juneja@jindalsaw.com

Due to the growing global demand for oil and gas, major oil and gas producers are exploiting natural resources in challenging environments. Hydrogen-induced cracking (HIC) in the steel industry causes an enormous economic loss to the industry however, HIC behaviour is still an area of interest. Investigating hydrogen-induced cracking (HIC) susceptibility in sour service pipelines made of Grade API 5L X60 / X65 steels requires a comprehensive approach that combines experimental analysis, material characterization, and a thorough understanding of the operating conditions. Sour service conditions are categorized by the presence of hydrogen sulfide (H2S) in a gaseous environment poses a severe threat to carbon steel / low alloy steel. In the present work, three pipe samples produced from API 5L X60 & X65 Grades were studied and compared in terms of their HIC resistance. We have also investigated the HIC behaviour in pipeline steels and their correlation with microstructure, chemical composition, and mechanical properties. Steel plates are produced from a Thermo-Mechanically Controlled rolled process followed by accelerated cooling to impart good mechanical properties and low carbon equivalent to ensure good weldability. It is demonstrated that centreline segregation/microstructural bending and hard microstructure are the potential sites for the initiation of hydrogen-induced cracking in a steel which is relatively free from major inclusions. From the HIC test, we obtained useful information about the extent of cracks and their initiation. The micro-hardness test is carried out to obtain the correlation between the hardness of steel and the HIC susceptibility.

Keywords: Submerged Arc Longitudinal Welded pipe, hydrogen-induced cracking, Mechanical and chemical properties, Microstructure.

INTRODUCTION

In recent years, the need for pipeline transportation of gas and oil has grown significantly due to their widespread use in long-distance transmission of oil & gas [1]. Such pipeline steels must have high strength and fracture toughness to work in such challenging environments. [1]. The presence of hydrogen sulfide in oil and natural gas has led to a new interest in the pipeline industry. Due to its exceptional strength and safety, API 5L X60 & X65 steels are well-recognized in the industry for this kind of transportation. Annually, the useful lifetime of pipeline steels reduces due to hydrogen-induced cracking (HIC) & stress corrosion cracking (SCC). There have been several failures of pipelines due to the presence of a sour environment. Considering the consequences of the failure that occurred in the oil and gas industry, the investigation presents a view of the mechanisms of low-alloy pipe steel fracture in hydrogen sulfide-containing media. Wet H2S service (Sour Service) is the term commonly used for oil & gas transportation systems, containing liquid water and H2S (including other corrosives or contaminants). In carbon steel products, such as line pipes, sour service or moist H2S environments can cause hydrogen blistering, HIC / SWC (hydrogen-induced cracking / step-wise-cracking), SOHIC (stress oriented hydrogen induced cracking), and SSC (sulfide stress corrosion cracking). When hydrogen, which is found in natural gas and oil, diffuses and reaches a threshold quantity, cracks begin to form in the microstructure of steel. The initiation of cracks persists in the steel's thickness direction until the substance within the pipeline exudes excessive pressure. In particular, this damage is frequently seen in cold and severe conditions. It results in enormous financial losses for the replacement, upkeep, and repair of pipeline steels, it also pollutes/contaminates the environment due to the leakage of oil and gas through the areas where the pipeline passes, particularly agricultural areas.

The HIC phenomenon is a significant concern in sour environments because

---

* Corresponding author.
Email: sucheta.juneja@jindalsaw.com

hydrogen atoms are entered into the steel from hydrogen sulfide [2-4]. Aqueous H2S content significantly increases the corrosion rate. H2S in the presence of moisture dissociates itself into hydrogen ions (H+), thus increasing the Hydrogen content in the medium and reducing the pH causing the formation of an acidic medium. The detailed mechanism involved with reactions is discussed below:

$H_2S \rightarrow HS- + H+$ .... Eq. (1)

$HS- \rightarrow S_2- + H+$ .... Eq. (2)

This acidic medium in contact with the steel causes the following anodic reactions;

$Fe + H_2S + H_2O \rightarrow Fe(HS-) + H_3O+$ Eq…. (3)

$Fe(HS)- \rightarrow (FeHS)+ + 2e$ .... Eq.(4)

$(FeHS)+ + H_3O+ \rightarrow Fe_2+ + H_2S + H_2O$ Eq. (5)

Fe(HS)- acts as a catalyst and absorbs the metal surface causing the ionization of the Fe atom.
The following cathodic reaction takes place in the medium. H2S doesn't participate in the cathodic reaction but acts as a catalyst resulting in the formation of atomic hydrogen at the metal surface.

$Fe + HS- \rightarrow Fe(HS-)$ .... Eq. (6)

$Fe(HS-) + H3O+ \rightarrow Fe(H\text{-}S\text{-}H) + H2O$….Eq. (7)

$Fe(H\text{-}S\text{-}H) + e- \rightarrow Fe(HS)- + H$ (atomic) Eq. (8)

Atomic hydrogen can combine with another hydrogen atom and can result in the formation of a hydrogen (H_2) molecule, or it may absorb/penetrate in the metal. It is the presence of Fe (HS)- which hinders the recombination of the H atom and thus promotes the absorption of the Hydrogen atom into the metal. Hydrogen absorption also increases with the decrease in the pH and increase in the H_2S partial pressure, consequently increasing the tendency towards HIC and SSC Failures. The reason for this behaviour is the decrease in the availability of the hydrogen ion in the media with increasing pH. It has also been observed that HIC and SSC of failure of low-alloy steels increases with increasing H2S concentration. Mostly cracks appear in the rolling direction at the central part of pipe/plate thickness where centreline segregation of some elements such as manganese and carbon are present [5]. When cracks are not able to propagate further in the rolling direction blisters are form near the surface [5]. It is reported that HIC susceptibility increases with the increasing strength of the metal [6]. Several modifications of the process parameters, such as microalloying elements, control of sulfur, carbon, and nitrogen, the morphology of inclusions, etc., are to be analyzed to improve the microstructure and associated HIC performance [7]. However, the mechanism of HIC failure has yet not been fully understood by researchers [7].

There are several methods to evaluate HIC in pipeline steels. NACE TM 0284:2016. is considered to be an effective method [2]. However, this test method does not provide any information about HIC related to the microstructure of the pipe. The crack length ratio (CLR), crack thickness (CTR) and crack sensitivity ratio (CSR), respectively are the HIC parameters that show a standard for the level of HIC susceptibility. The larger the values of these parameters, the more the steel susceptibility towards HIC. The research aims to analyze the HIC susceptibility in the X60/X65 steel. HIC parameters were evaluated to determine the level of HIC susceptibility. The effects of different factors on HIC crack propagation such as hardness, chemical, mechanical, micro-texture, and type of grain boundaries were also discussed.

RESEARCH SIGNIFICANCE

The present Investigation establishes a relationship between the microstructure and hardness relationship with HIC failures. However, the mechanism of HIC failure has yet not been fully understood by researchers and is still an exciting and hotspot of a research area. However, a detailed study of the extent of chemical segregation and HIC susceptibility is not established due to the limited resources. The impact of the segregation of different elements in the vicinity of cracks needs to be considered further to establish the relationship between segregation and HIC Failure.

MATERIALS AND METHODS

The Segment of longitudinal submerged arc welded (LSAW) pipe with thicknesses of 14.3,17.5 & 20.6mm respectively was cut out for investigation of mechanical, chemical, and microstructure. The pipeline had originated from the micro-alloy steels designated X60 & X65 according to API 5L.

All experiments were performed on X60 & X65 pipeline steel. Three pipe samples were collected from different steel suppliers namely Indian Steel Mill, Korean Steel Mill, and Chinese Steel Mill were tested for HIC resistance, microstructure, and inclusion characterization. HIC test was carried out as per the requirements of NACE TM 0284:2016, Test Solution A is utilized as the test medium with the following acceptance criteria:

a) CLR ≤ 15%
b) CTR ≤ 5%
c) CSR ≤ 2%

Details of the pipe sizes are mentioned in Table 1. Steel was supplied in Thermomechanical Controlled Rolled Condition Micro-alloyed with Niobium (Nb) and Titanium (Ti).

The mechanical properties of the pipes were analyzed using a Shimadzu-made Universal testing machine (UTM) -200 Ton. The Chemical Composition of the samples was determined on a Shimadzu-made PDA-5500S spectrometer. Further, microhardness testing was carried out on the Zwick Roell Durascan 70G5 machine.

Sample details

Samples for HIC Testing are drawn from the pipe as per figure 1. The test specimens are cut from Longitudinally Welded Pipes. Three specimens are tested from one pipe. Three specimens are considered, one from 90° from the weld in Base Metal (in the longitudinal direction), another 180° from the weld from base metal (in the longitudinal direction), and one specimen across the weld as indicated and are shown in Figure 1.

The typical process of carrying out HIC Test was as per the requirement of NACE TM 0284. The NACE TM 0284 established the standard test method for evaluating pipeline and pressure vessel steels for resistance to hydrogen-induced cracking caused by hydrogen absorption resulting from corrosion in a wet H2S-containing medium.

In this test method, specimens are held in an H2S solution without applying external stress at ambient temperature and pressure and their post-exposure assessment is carried out. Test Solution A is used, which is a solution of 5% Sodium Chloride (NaCl) and 0.5% Acetic Acid (CH3COOH) in distilled or deionized water and is saturated with hydrogen sulfide. The dimensions of the specimens cut from workpieces for HIC are 100 ± 1 mm long X 20 ± 1 mm wide. The thickness of the specimen for testing the pipe body is equal to the total thickness of the pipe wall. A layer not more than 1 mm deep can be removed from each surface of the work pieces. The pieces for the test specimen from the pipes shall not be straightened.

After preparation, the specimens are put into a sealed vessel, where they are isolated from the vessel and other test specimens by glass or other non-metallic rods of at least 6 mm in diameter as shown in figure 2. Further, the vessel is filled with a test medium in such a way that the ratio of the solution volume to the total surface area of the specimen is at least 3 mL/cm2. The solution in the test vessel is purged with Nitrogen to remove any Oxygen present in the test solution.

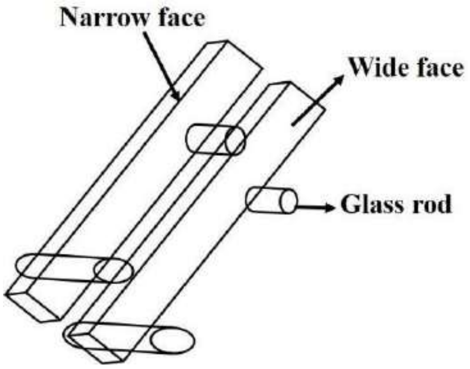

Figure 2. Represents the position of the specimen loaded in the test vessel

After purging, H2S is passed through the solution. The rate of hydrogen sulfide bubbling for the first 1 Hour shall be at least 200 cm3/min/Ltr of test solution. After an initial 1 hour of H2S bubbling concentration of H2S is checked by the Iodometric method. The typical test laboratory setup is as per figure 3.

Once the required concentration of H2S is achieved in the test solution, a decreased H2S gas flow is required to maintain the H2S saturation of the solution. The critical test parameters required for test solution A are:

- Initial pH of the Test Solution: 2.7±0.1
- pH at the start of the test (after H2S saturation): 2.7 to 3.3
- H2S Concentration after saturation: 2300 ppm minimum
- Test Duration: 96 Hrs
- Test Temperature: 25 ± 3°C
- pH at the end of the test: < 4
- H2S Concentration at the end of the test: 2300 ppm minimum

After completion of the test duration, the H2S feed is stopped, and the solution is purged with nitrogen to remove the hydrogen sulfide present in the test solution. The specimens are taken out and cleaned to remove scale and corrosion deposits. Thereafter, specimens are sectioned as represented in the figure. 1 and were polished for metallographic examination.

The formulae used for metallographic examination are mentioned in “Equation 9”.

$$CLR = \frac{\sum a}{W} * 100\% \; ; \; CTR = \frac{\sum b}{T} * 100\% \; ; \; CSR = \frac{\sum (a*b)}{(W*T)} * 100\% \text{ ....Eq. (9)}$$

After preparation of the surface, the cross sections of the specimens are inspected for cracks in a microscope. Based on measurements of crack geometric parameters for each cross-section, the following HIC parameters are calculated by formulas: the crack length ratio (CLR), the crack thickness ratio (CTR), and the crack sensitivity ratio (CSR) as per shown in figure 4(a). A light etching is applied to distinguish cracks from other discontinuities. In cases, where cracks are detected, they are measured for their sizes and relative positions as shown in figure 4(b). For each test specimen, the average value over three sections is determined.

RESULTS AND DISCUSSION

The specimens are taken from base metal as well as from weld metal of pipes as mentioned in Table 2 and are tested after pipe forming. The results are discussed in subsequent sections.

HIC test results and discussion

The HIC testing was performed on samples ID 1, 2, and 3 respectively as per NACE TM 0284:2016. The test specimens are evaluated and are results are presented in Table 2.

From the results, it has been found that the cracks were found in the base metal specimen (Specimen located at 180°) and there were no cracks observed in the weld metal.

The crack measurement on the HIC micro- sample must be taken carefully to obtain accurate results. Before evaluation, the key points should be considered, firstly each section shall be metallographically polished, and lightly etched only because a heavy etch may obscure small cracks) so the cracks can be distinguished from small inclusions, laminations, scratches, or other discontinuities. Moreover, all identifiable cracks visible at magnifications up to 100X should be included in the calculation except those that lie completely within 1.0 mm of the surface of the test specimen. In the evaluation of crack length and thickness, cracks separated by less than 0.5 mm shall be considered a single crack as shown in figure 4(b).

The mechanical and chemical test results are presented in Table.3 & Table 4. In addition, Inclusion analysis, microstructural analysis, and Micro Hardness Test were made particularly on the failed specimen to understand the material properties.

Mechanical and Chemical Test Analysis

The Mechanical Properties of the pipes are as per Table 3. Tests were carried out on Shimadzu UH-200 Ton. Tensile testing is the most fundamental type of mechanical test, mechanical properties such as yield strength, ultimate tensile strength, and strain can be obtained. The yield strength of the test material is a key measure of the material's ability to resist high solicitations in the elastic region.

The microstructure of sample 1 as shown in Table 6 below indicates the presence of a small amount of Martensitic Austenite, which is also indicated by the high hardness obtained in the specimen. The microstructure of the sample 3 is indicated in Table 6 below. Segregation Bands in the central region of the plates resulted in the hardness variation along with the peak Hardness of 268 HV in the area of high carbon / Bainite. It can be concluded that when the steel is free from significant inclusions, the predominant site for the nucleation and growth of HIC are the areas of the maximum segregation as indicated in Image N of Table 6. Base metal not having structural heterogeneity is typically free from any HIC as indicated by the results of sample-2, Image H, I of Table 6. To prevent microstructural banding in the steel and has low carbon and manganese content and has been treated with effective accelerated cooling. The results of metallurgical properties were summarised as follows. Olympus BX 53 MRF -S metallurgical microscope was utilized for the analysis of samples.

4.4 Inclusion Analysis & Microstructural Analysis

As shown in Table 6, the microstructure has been composed of the ferrite phase which is accepted as the softest phase in pipelines. However, this phase has more HIC susceptibility due to its low strength which does not meet the standard requirements for API steels. Therefore, other elements such as carbon and manganese, are also added to create other phases or structures such as pearlite.

Table 1. Details about different pipe sizes

Sample ID	Pipe Diameter (mm)	Pipe Thickness (mm)	Pipe Grade	Steel Source
Sample-1	610	14.3	API 5L X60 PSL2	Indian Steel Mill
Sample-2	914	17.5	API 5L X 60 PSL2	Korean Steel Mill
Sample-3	610	20.6	API 5L X65 PSL2	Chinese Steel Mill

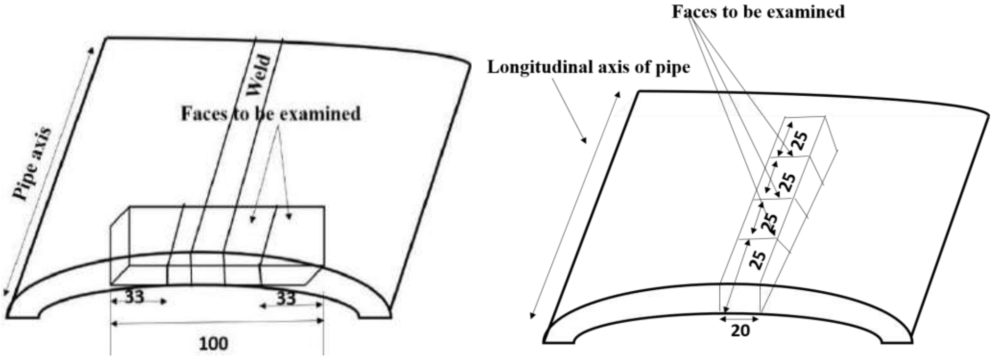

Figure 1. represents the location in which specimens were drawn for HIC**.**

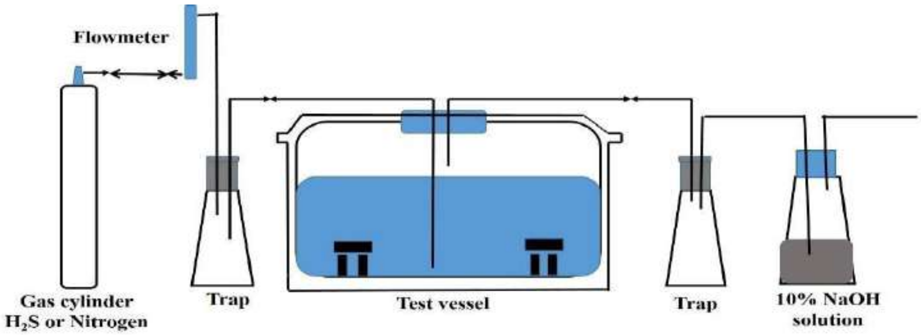

Figure 3.

Illustrates the typical test laboratory setup

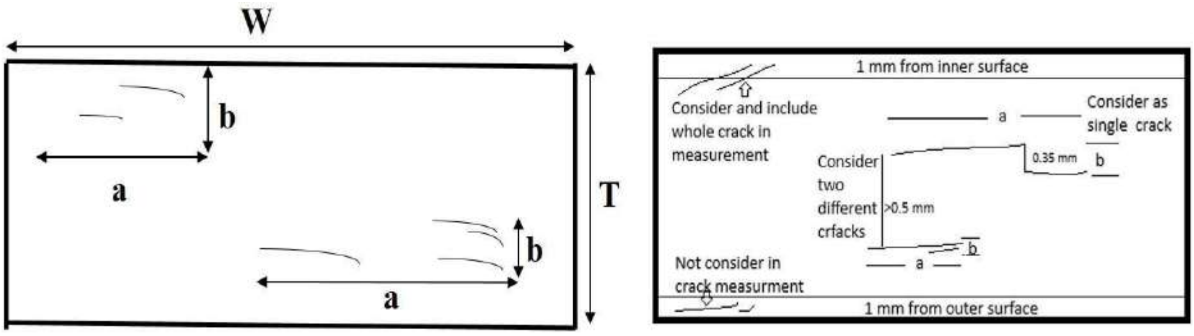

Figure 4 (a): shows the sectioning of specimens and Figure 4(b): evaluation of cracks for metallographic examination

Table 2: Parameter evaluation for HIC testing

Sample ID	**(90° from weld)**			**(180° from weld)**			**(Weld)**		
	%CLR	**%CTR**	**%CSR**	**% CLR**	**%CTR**	**%CSR**	**%CLR**	**%CTR**	**%CSR**
Sample-1	0	0	0	11.8	1.3	0.45	0	0	0
Sample-2	0	0	0	0	0	0	0	0	0
Sample-3	0	0	0	28.7	3.2	2.7	0	0	0

Table 3: Mechanical results of samples

Sample ID	**YS (MPa)**	**UTS (MPa)**	**Elongation (%)**	**Hardness (HV10)**
Sample-1	494	612	40	177-191
Sample-2	504	602	39	176-207
Sample-3	515	600	48	197-204

Table 4: Chemical results of samples

Sample ID	**C%**	**Si%**	**P%**	**S%**	**Cu%**	**Ti%**	**Mn%**	**Ni%**	**Cr%**	**Al%**
Sample-1	0.05	0.25	0.011	0.0009	0.01	0.01	0.89	0.01	0.17	0.037
Sample-2	0.04	0.25	0.007	0.0004	0.03	0.01	1.20	0.15	0.20	0.043
Sample-3	0.04	0.18	0.009	0.0009	0.18	0.01	1.17	0.15	0.25	0.035

Mo%	**V%**	**Nb%**	**B%**	**Ca%**	**N%**	**CE (IIW)**	**CE (PCM)**
0.07	0.00	0.05	0.0002	0.002	0.004	0.25	0.12
0.07	0.00	0.04	0.0001	0.002	0.006	0.31	0.13
0.07	0.00	0.05	0.0002	0.001	0.004	0.32	0.13

Table 5 Indicates hardness values under different zones

Sample ID	**Hardness (HV0.05) Under surface at 1 mm Distance**	**Hardness (HV0.05) at Mid Thickness**
Sample-1	211, 201, 214, 200, 220, 199 206, 211, 212, 214, 212, 210	205, 236, **290,** 242**, 258**, 214, 250, 214, **272**, 221-------- **Δ 85 HV0.05**
Sample-2	229, 227, 235, 208, 217, 217 208, 213, 207, 212, 208, 229	199, 208, 202, 225, 208, 201, 217, 210, 215, 195--------- **Δ 26 HV0.05**
Sample-3	201, 187, 196, 192, 181, 208 222, 229, 210, 230, 223, 227	**263**, 215, **257, 268**, 234, **266**, 231, 208, **260,** 215-------- **Δ 60 HV0.05**

Table 6. shows the microstructural analysis

Sample Number	**Image**	**Results & discussions**
Sample-1 /Image A		Un-etched Microstructure at 100 X Magnification, showing the HIC Crack.
Sample-1/Image B		Microstructure at 100 X Magnification, showing the HIC Crack. HIC Crack originates in the mid-thickness of the section
Sample-1 /Image C	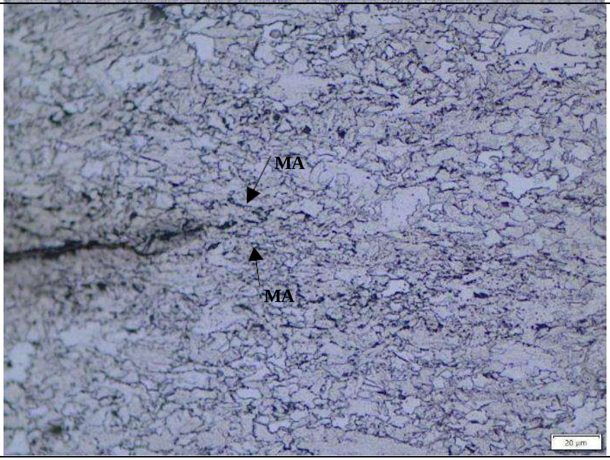	Microstructure at 500 X Magnification, showing the HIC Crack. HIC Crack is originated presence of some martensitic austenite (MA) is also evident near the crack end point. Presence of high Hardness (up to 290 HV confirms the presence of Hard constituents in the steel)

Sample-1 /Image D	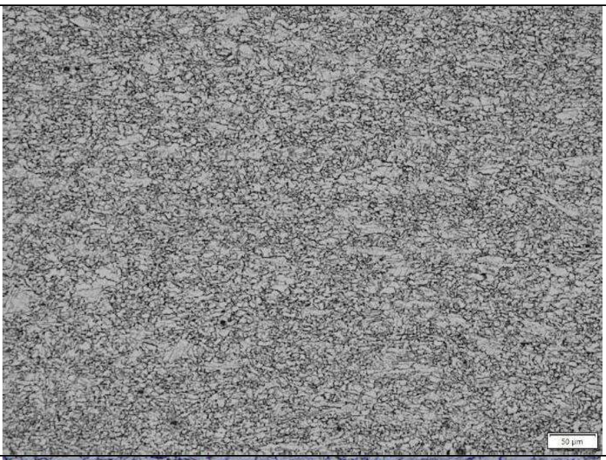	Microstructure at 200 X Magnification at plate / pipe mid thickness. No Microstructural banding observed. Grain size Finer than 10
Sample-1 /Image E	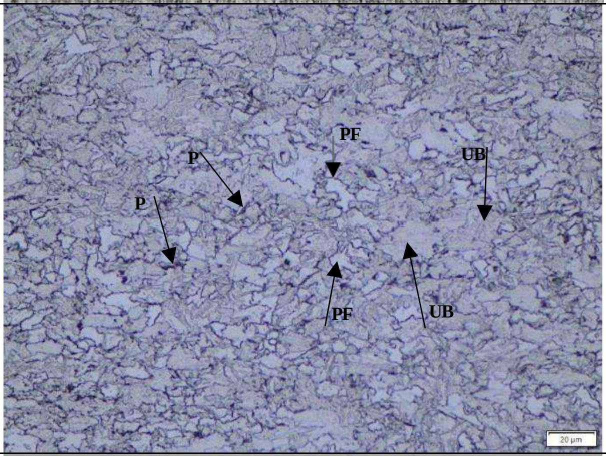	Microstructure at 500 X Magnification at plate / pipe mid thickness. Predominantly consist of Polygonal ferrite (PF), Upper Bainite (UB), and a small quantity of grain boundary pearlite (P).
Sample-1/Image F		Inclusion at 500 X Magnification. No elongated sulfide inclusion was observed. A small quantity of Alumina and Globular inclusion was observed along with some complex-shaped inclusion (Probably hard inclusion broken into the pieces during rolling).
Sample-1/Image G		Inclusion at 500 X Magnification. No elongated sulfide inclusion was observed. Some complex-shaped inclusion was observed (Probably hard inclusion broken into the pieces during rolling).

Sample-2/Image H	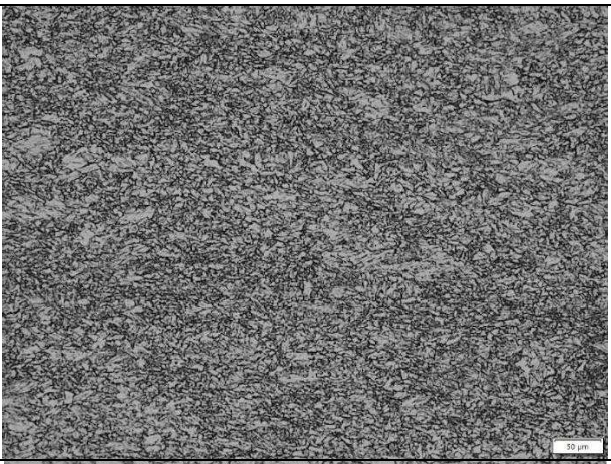	Microstructure at 200X at plate / pipe mid thickness. No sign of Banding / segregation of microstructure. Fine microstructure with grain size finer than 10 (evaluated at 100X)
Sample-2/Image I	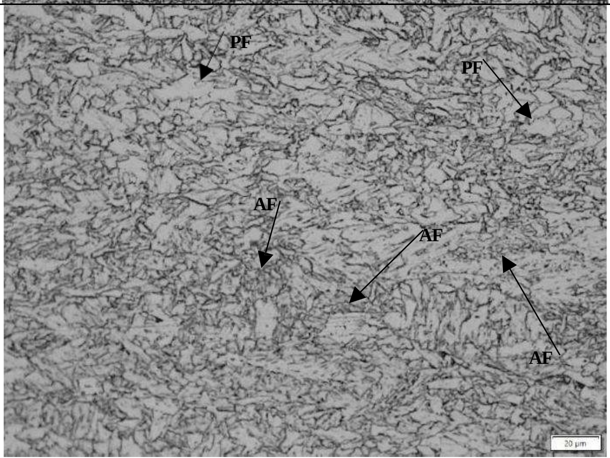	Microstructure at 500X at plate / pipe mid-thickness: consists of Predominantly Polygonal ferrite and acicular Ferrite.
Sample-2/Image J		The un-etched specimen at 500 X. Clean steel, No significant presence of Inclusions.
Sample-3/Image K	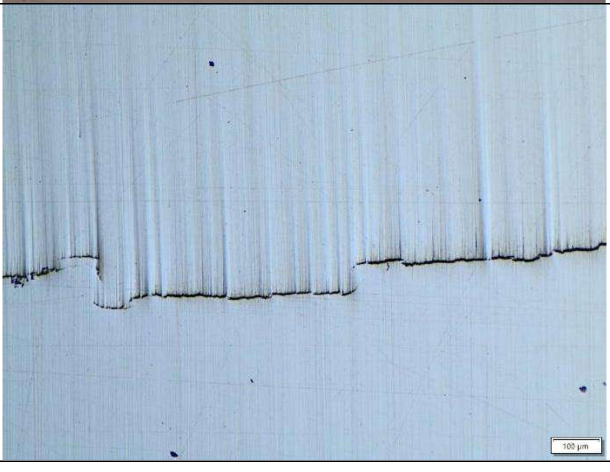	Sample without etching at 100 X Magnification, showing the HIC Crack.

Sample-3/Image L	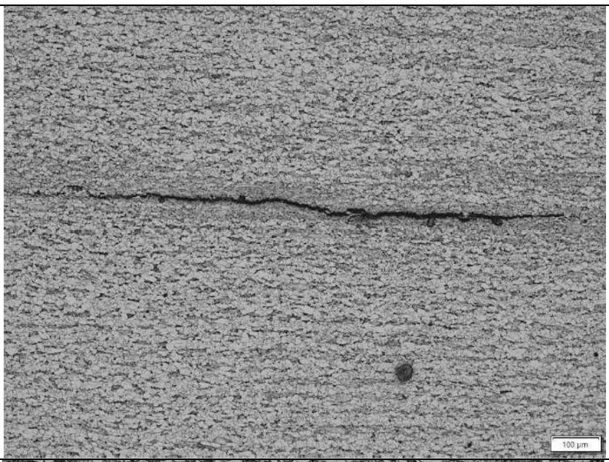	Microstructure at 100 X Magnification, showing the HIC Crack. Crack is entirely lying in the Banded center region of the pipe thickness.
Sample-3/Image M	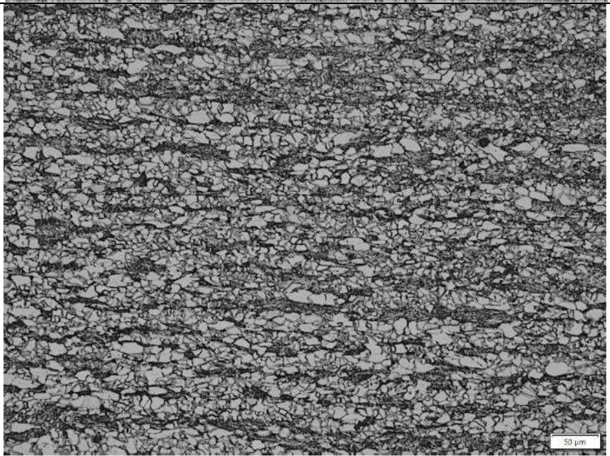	Microstructure at 200 X Magnification at plate / pipe mid thickness. Heavily banded Microstructure/ heavy segregation of microstructure Grain size Finer 9.0 to 9.5
Sample-3/Image N	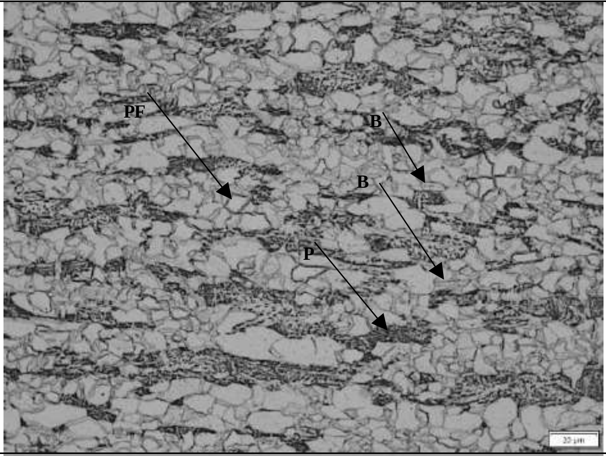	Microstructure at 500 X Magnification at plate/pipe mid-thickness. Predominantly consist of Polygonal ferrite, Pearlite Upper Bainite.
Sample-3/Image O	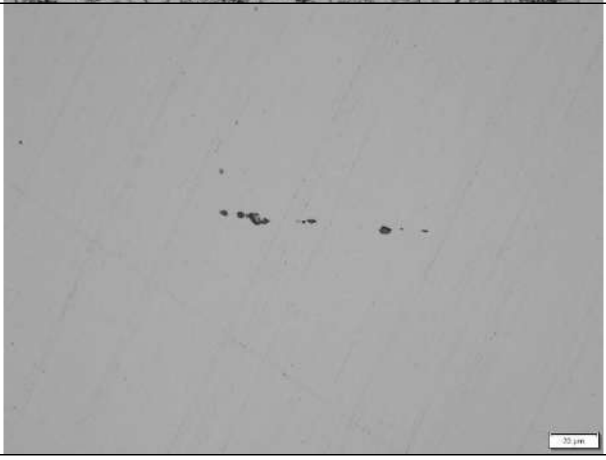	No elongated sulfide inclusion was observed.

Sample-3/Image P	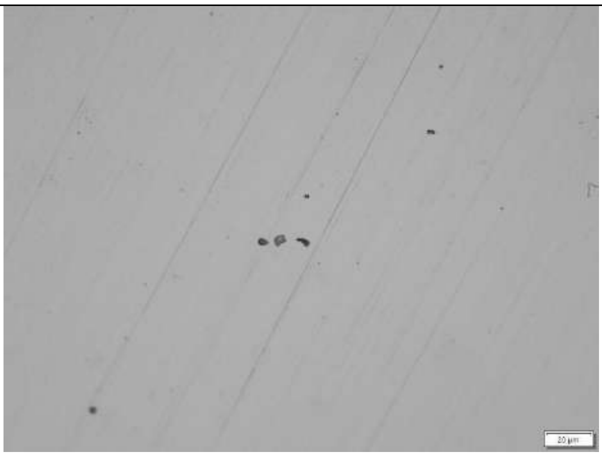	No elongated sulfide inclusion observed.

Interphase in between the Inclusions and parent steel matrix is the potential site where the atomic Hydrogen diffuses and recombines to produce a Hydrogen Molecule, which can lead to high internal pressure and tensile stresses causing the HIC. MnS inclusion is particularly very harmful as it gets elongated with sharp ends during hot rolling, which turns into a potential site for HIC crack initiation.

Martensitic Austenite with Ferrite is the potential site for the embrittlement, which is indicated by the analysis of sample 1. High hardness also observed in Sample 1 is the predominant cause of HIC failure in this case. It can also be concluded from the results obtained from Sample 3, that segregation bands of high hardness in the center region of the specimen are the predominant site for Hydrogen Cracks. Ferrite – Pearlite microstructure is particularly very sensitive to HIC [8]. The Pearlite boundary and interface in between Ferrite and cementite in pearlite is the trap site for Hydrogen. In bainitic microstructure, thin plates of cementite act as a barrier to the hydrogen diffusion

1 CONCLUSIONS

Due to the inherent characteristics of the solidification of slabs in continuous casting, most of the impurities, harmful inclusions, and alloy elements have more concentration in the central axis of the slab. Careful attention is required during the continuous casting process of HIC-resistant steel to improve cleanliness and reduction in centreline segregation. Excessive centreline segregation results in the banded microstructure during the subsequent rolling of steel into the flat products causing the microstructural variation, undesirable microstructure, and excessive hard zone in the centreline axis of the plate which is a cause of HIC failure in steel-free from excessive inclusions in the present study. A great precaution is needed during the steel making and preventive measures such as electromagnetic stirring and dynamic soft reduction shall be applied during the continuous casting of steel slabs. A quantifiable criterion shall be applied for chemical composition heterogeneity for the acceptance of slabs for sour service. Hardness Control is an essential tool in controlling the resistance of steel plates for hydrogen-induced cracking. Hardness requirements as indicated in API Specification 5L (i.e. 250 HV10) may not be the only criteria for the steel acceptance, Maximum Hardness along the center axis of the steel plates need to be controlled on Micro Vickers level, a typical Micro hardness of 225 HV0.05 Max found to produce satisfactory HIC Resistance. Sample 2 indicates base metal free from structural heterogeneity with relatively uniform hardness across the thickness and doesn’t show the tendency of Hydrogen Cracking. Acicular ferrite can be considered as the most resistant microstructure for the prevention of HIC.

2 ACKNOWLEDGMENTS

The authors would like to acknowledge Jindal SAW Limited, Nanakapaya, Gujarat for providing their continuous support and motivation.

3 REFERENCES

1. Ghosh, G., Rostron, P., Garg, R., & Panday, A. (2018). Hydrogen induced cracking of pipeline and pressure vessel steels: A review. *Engineering Fracture Mechanics, 199,* 609-618.
2. TM0284, N. A. C. E. (2016). Test Method “Evaluation of Pipeline and Pressure Vessel Steels for Resistance to Hydrogen-Induced Cracking”(2016). *Houston, TX, United States*.
3. Mohtadi-Bonab, M. A., & Eskandari, M. (2017). A focus on different factors affecting hydrogen-induced cracking in oil and natural gas pipeline steel. *Engineering Failure Analysis*, *79*, 351-360.
4. Kane, R. D., & Cayard, M. S. (1998). Roles of H2S in the behavior of engineering alloys: a review of

literature and experience. *NACE CORROSION*, NACE-98274.

5. Mohtadi-Bonab, M. A., Szpunar, J. A., Collins, L., & Stankievech, R. (2014). Evaluation of hydrogen- induced cracking behavior of API X70 pipeline steel at different heat treatments. *International journal of hydrogen energy*, *39*(11), 6076-6088.
6. Zhang, P., Laleh, M., Hughes, A. E., Marceau, R. K., Hilditch, T., & Tan, M. Y. (2024). Effect of microstructure on hydrogen embrittlement and hydrogen-induced cracking behaviour of a high- strength pipeline steel weldment. *Corrosion Science*, *227*, 111764.
7. Anijdan, S. M., Arab, G., Sabzi, M., Sadeghi, M., Eivani, A. R., & Jafarian, H. R. (2021). Sensitivity to hydrogen induced cracking, and corrosion performance of an API X65 pipeline steel in H2S containing environment: Influence of heat treatment and its subsequent microstructural changes. *Journal of Materials Research and Technology*, *15*, 1-16.
8. Li, J., Gao, X., Du, L., & Liu, Z. (2017). Relationship between microstructure and hydrogen induced cracking behavior in a low alloy pipeline steel. *Journal of Materials Science & Technology*, *33*(12), 1504- 1512.

Journal of The Maharaja Sayajirao University of Baroda: Science & Technology

Vol. 58, 2024, pp. 35-43

Study The Electrochemical Behaviour of al-mg-si Alloy - A Review

Tushal K. Kyada[1,2], Indravadan B. Dave[3*], Sonam M. Patel[2]

[1] Research Scholar, Gujarat Technological University, Ahmedabad, India

[2] Metallurgy Department, Dr. S. & S. S. Ghandhy College of Engineering & Technology, Surat- 395001, Gujarat, India, tushalkyada21@gmail.com & smp22789@gmail.com

[3*] Metallurgy Engineering, Government Engineering College, Sector-28, Gandhinagar -382028, Gujarat, India, ibdave@gecg28.ac.in

This review comprehensively analyzes the electrochemical behavior of Al-Mg-Si alloys as sacrificial anodes, focusing on factors like microstructure, alloying elements, and second- phase particles. Alloying elements' presence can impede surface film formation on aluminum. Microstructure, grain size distribution, precipitate volume fraction, and crystallographic orientation affect aluminum alloy properties. The paper describes the Al- Mg-Si phase diagram, emphasizing Mg and Si solubility with the Mg2Si phase presence. Mg and Si addition shifts anodic polarization curves, impacting electrochemical behavior and Mg2Si morphology. Corrosion mechanisms consider varying Mg and Si content effects on mechanical properties and microstructure. Furthermore, the paper explores heat treatment effects, addressing precipitation sequence, aging time, cooling rate, and their influence on intergranular corrosion (IGC) susceptibility.

Keywords: *Al-Mg-Si alloy, 6XXX, electrochemical behavior,* Mg_2Si*, sacrificial anode*

INTRODUCTION

Aluminum can serve as a corrosion-resistant material or as an activated sacrificial anode in a cathodic protection system, depending on the appropriate alloying system. Aluminium as sacrificial anode has attained considerable merit as the basis for a galvanic anode mainly due to its low density, large electrochemical equivalent, availability, thermal and electrical conductivity, high current capacity, low specific weight, and reasonable cost.

However, if aluminum is utilized as a sacrificial anode, its passive film must be modified to undergo active dissolution. The continuity of the film is affected by the microstructure of the metal, presence of alloying element and volume fraction of second phase particles. The alloying element that hinder or prevent the formation of surface film on aluminum are Zn, Mg, Sn, Bi, Ti, In and Ga.
[1] In order to improve the efficiency of aluminum anodes they are typically alloyed with other elements to encourage depassivation (breakdown of the oxide film) and/or shift the operating potential of the metal to a more electronegative direction. The alloying elements used to accomplish this are referred to as depassivators and modifiers. Modifiers that have been used include zinc (Zn), magnesium (Mg), barium (Ba), and cadmium (Cd). In this work, Zn and Mg are employed. The depassivators commonly used are indium (In), mercury (Hg), and tin (Sn) and also rarely used are gallium (Ga), titanium (Ti) and thallium (Tl). [2] To overcome the passivity of aluminum, magnesium, which is one of the most active metals in the galvanic series, can be added. [3]

6XXX ALLOY (AL-MG-SI ALLOY) SYSTEM

Composition of 6xxx series aluminum alloys plays an important role in determining its mechanical as well as electrochemical properties. Properties of aluminium alloys also depend on its microstructure, average grain size and its distribution, volume fraction of precipitate and the crystallographic orientation. [4]
6XXX series alloy mainly alloyed with Mg and Si and they are heat-treatable alloys. The maximum solid solubility of Mg in an aluminum matrix is around 16.26 atomic weight percentage when the temperature is around 450°C. [5] Similarly, Si has maximum solid solubility in an aluminum matrix, which is 1.59

---

* Corresponding author.
Email: ibdave@gecg28.ac.in

atomic weight percentages when the temperature is around 1080°C. [6] In the presence of Mg, Mg_2Si particles are formed, which are uniformly distributed at the grain boundary. [7]

A phase diagram of Al-Mg-Si alloys showing the solubility of Mg and Si as a function of temperature represented by the Mg_2Si phase are shown in figure 1. The maximum solubility of Mg_2Si in aluminium is 1.85%, and this decreases with temperature. [4]

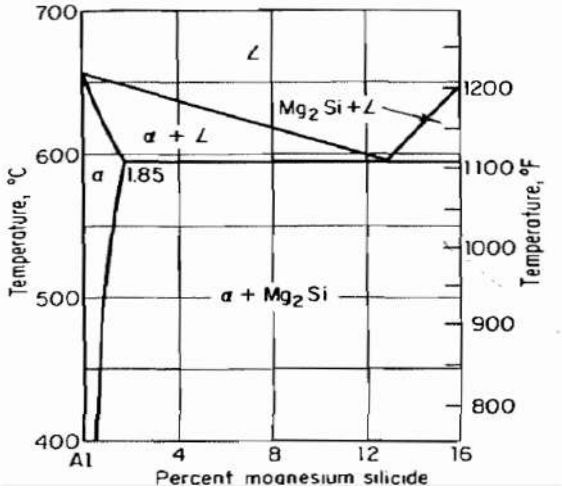

Figure 1. Aluminium- Magnesium Silicide Phase Diagram [4]

Increasing the content of Mg in the Al-Mg alloy from 5 to 10 mass% can enhance sacrificial protection, as suggested in [8]. As the content of both Mg and Si increase, the anodic polarization curve shifts to a more negative value of potential and higher current. This shift in potential is believed to be due to the amount of Mg2Si phase present, and the amount of sacrificial protection provided increases as the content of Mg and Si increase. [9] Mg has a very low solubility for Si, and the majority of Si atoms react with Mg atoms to create a precipitation of the intermetallic compound Mg2Si. This is due to reaction (Eq. 1), where Mg_2Si is formed by the diffusion of magnesium and silicon atoms. [10]

$$2Mg + Si \; \square \; Mg_2Si \qquad \text{Eq. (1)}$$

The Mg_2Si phase, which contains 63.2% Mg and 36.8% Si, has a cubic structure with a lattice parameter of a = 0.635-0.640 nm. This low solubility Mg2Si phase has a density of 1.88 g/cm3 and a melting point of 1087°C. [4]

ELECTROCHEMICAL BEHAVIOR OF MG_2SI PHASES

The Potentiodynamic scanning curves and associated corrosion parameters of individual α(Al), Mg_2Si, and Si are presented in Fig. 2 and Table 1, respectively. From these results, the corrosion potential of Mg_2Si is the most negative, while that of Si is the most positive. Additionally, the corrosion current density of Mg_2Si is much greater than that of α(Al) or Si, indicating that Mg_2Si particles are more susceptible to corrosion than α(Al) or Si particles at the beginning of the corrosion process. [11]

Similar results were observed by Buchheit et al. [8][9] during Potentiodynamic polarization tests that Potential of Mg_2Si is much lower. The Volta potential of Mg_2Si particles, as measured by scanning Kelvin probe force microscopy (SKPFM), is approximately 100-180 mV lower than that of the aluminum matrix. [12] These findings suggest that the Mg_2Si particle is initially anodic in relation to the aluminum matrix. [13]

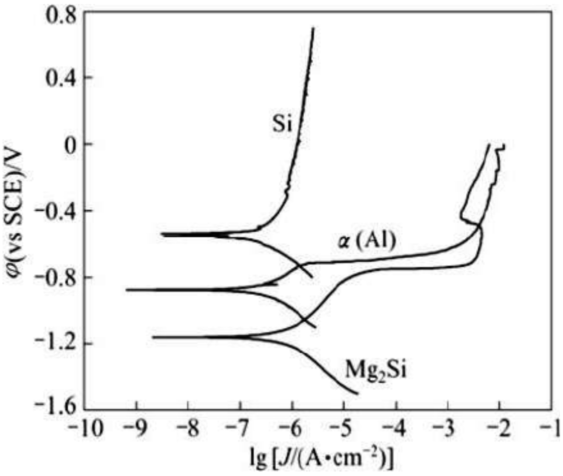

Figure 2. Potentiodynamic scanning curves of individual α(Al), Si and Mg2Si in 3.5% NaCl solution at the beginning [11]

Overall, the potential of the 6xxx series Al alloy matrix ranges from about -0.72 V to -0.75 V (vs SCE), and the potential of Mg_2Si is considerably lower. Birbilis et al [14] observed a similar trend in their experiments where the corrosion potential of Mg_2Si particles was much more negative than that of the aluminum alloy matrix when tested in a 0.1 mol/L NaCl solution.

Table 1: Corrosion parameters of α(Al), Mg2Si and Si in 3.5% NaCl Solution at the beginning [12]

Phase	SCE (V)
α(Al)	-0.8761
Mg_2Si	-1.1598
Si	-0.5470

In areas containing a large number of Mg_2Si particles, the values of OCP (Open Circuit Potential) shift to a less negative value. This shift in potential can be attributed to the selective dissolution of Mg from Mg_2Si in chloride solutions, which leads to the formation of SiO_2. This preferential dissolution of Mg leads to an enrichment of Si in the remaining Mg_2Si particles, which makes them more noble and thus shifts the OCP to a less negative value.[12]

CORROSION MECHANISM OF Al-Mg-Si ALLOYS

For Al−Mg−Si alloys, aging precipitates and grain boundaries are seen as the main anodic corrosion initiation sites, and most precipitates enhance the corrosion rate due to their cathodic activity. [15]

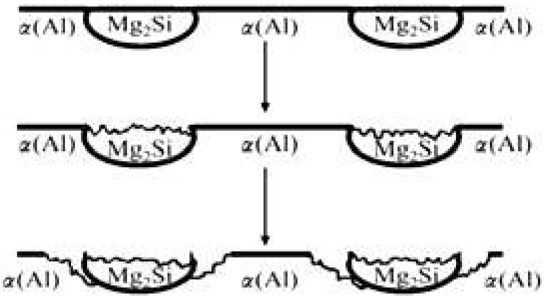

Figure 3. Schematic diagram of corrosion mechanism of Mg_2Si precipitate in Al-Mg-Si alloy [11]

At the beginning, the precipitate of Mg_2Si is anodic than the alloy base or PFZ (precipitate free zone), leading to the formation of a galvanic cell between the Mg2Si and the alloy matrix. This galvanic cell accelerates the corrosion rate of the aluminum matrix and can lead to localized corrosion at the interface between the Mg2Si precipitate and the aluminum matrix as shown in fig 3. However, the potential of the corroded Mg_2Si phase becomes more noble than the alloy base or PFZ over time, due to the preferential dissolution of Mg and the enrichment of Si in the Mg_2Si precipitate. As the Mg2Si phase continues to corrode, it eventually becomes cathodic to the PFZ at the grain boundary which was confirmed by potentiodynamic of alloy after 312 hr immersion in corrosive environment as shown in fig 4.

This leads to the anodic dissolution and corrosion of the PFZ at its adjacent periphery, resulting in corrosion that develops along the PFZ at the adjacent periphery of the Mg_2Si precipitate. It is important to be aware of this behavior when designing and using Al-Mg-Si alloys in applications that may be exposed to corrosion, as it can impact the overall corrosion resistance and durability of the alloy. When an Al alloy contains only Mg_2Si particles, corrosion happens primarily on the surface of the Mg_2Si particles and then spreads to the surrounding Al base. In comparison, the corrosion level of the Al base at the Si adjacent periphery is significantly higher than that at the Mg_2Si adjacent periphery, as shown in Fig.5. [11]

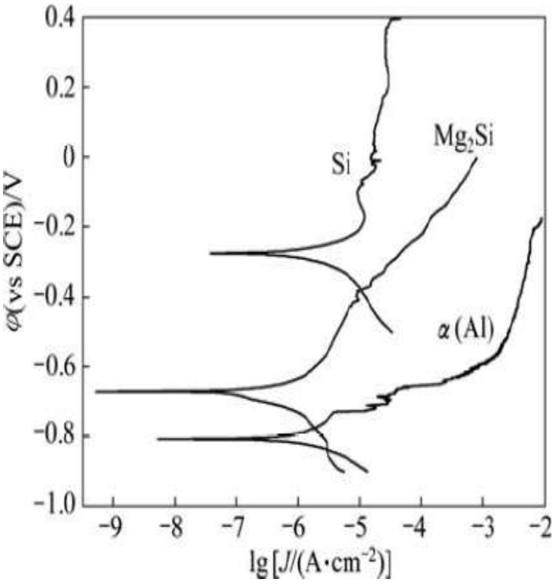

Figure 4. Potentiodynamic scanning curves of individual α(Al), Si and Mg_2Si in 3.5% NaCl solution after 312 h in NaCl solution [11]

Effect of varying Mg & Si in Al-Mg-Si alloy

Effect on Mechanical properties

The mechanical properties of Al–Mg–Si alloys are influenced by the levels of Mg and Si. Higher Mg content improves yield strength but decreases elongation. The ultimate tensile strength initially increased when the Mg level reached at certain level but showed a subsequent decrease when the Mg level was further increased. This decrease in ultimate tensile strength was attributed to the formation of primary Mg_2Si as shown in fig 6a, while higher Si content enhances yield and ultimate strength but reduces elongation as shown in fig 6b. [16]

Effect on Microstructure

The microstructural inhomogeneity and eutectic Mg2Si morphology of Al-Mg-Si alloys can be modified by varying the levels of Mg and Si. According to Fig 7, increasing Mg or Si levels can remarkably decrease the liquidus temperature of Al–Mg–Si alloys. Hence for the alloys with a higher Mg or Si level, the nucleation of a1 grains is late and the following growth time of a1 grains is short.

In addition, higher levels of Mg or Si can cause the α1 grains to become smaller in size while maintaining their initial spherical morphology as shown in Fig 8. However, increasing Mg or Si levels also leads to a decrease in the solid fraction of primary α-Al phase, resulting in a lower volume fraction of primary α-Al and a higher volume fraction of Al-Mg_2Si eutectic. [16]

MORPHOLOGY OF Mg_2Si

The eutectic Mg_2Si in as-cast Al–Mg–Si alloys have a variety of morphologies as shown in fig 9. Various researchers reported typical morphologies such as lamellar, rod, crossed and rooftop-like, flake and curved. [17–20] Fig 9, (a1) shows rod-like and intergranular lamellar Mg_2Si, (b1) shows lamellar Mg_2Si, (a2) shows flake like Mg_2Si while (b2) shows rod like Mg_2Si morphology.

The increasing Mg level transformed eutectic Mg2Si from rod or lamellae to curved flake with larger eutectic spacing fig 10(a1-e1), while the increasing Si level promoted the formation of rod-like or lamellar eutectic Mg2Si with smaller eutectic spacing as shown in fig 10(a2-e2). [11]

The morphologies of Mg_2Si transforms from lamellar to rod like when solidification rate is higher.[18] Li [21] and Shimosaka [22] found that increasing the cooling rate could transform eutectic Mg_2Si from lamellae to rod. The literatures also reported that alloying elements could induce morphological change of eutectic Mg_2Si phase. Tebib [23] and Farahany [24] reported that Sr, Bi altered the eutectic Mg_2Si morphology from flake-like (or described as ‘Chinese script-like’ flake-like) to fibrous. Li [20] also reported that the flake-like eutectic Mg_2Si transforms into rods with the increase in Ni content. Mischmetal changed eutectic Mg_2Si from a fibrous morphology to a flake-like morphology. [17] Nordin [25] also found Sb increased the irregularity of flake-like eutectic Mg2Si and resulting in an obvious divorced eutectic microstructure.

HEAT TREATMENT OF Al-Mg-Si ALLOY

Al-Mg-Si alloy are heat treatable which mostly undergoes precipitation hardening, also called age hardening, to alter the mechanical properties. Precipitation hardening relies on changes in solid solubility with temperature to produce fine particles of an impurity phase, which impede the movement of dislocations, or defects in a crystal's lattice. This alloys must be kept at elevated temperature for hours to allow precipitation to take place. This time delay is called aging. In case of age-hardenable Al-alloys, room or elevated temperature ageing treatment generates various precipitates in the matrix that contribute to the strengthening. [26, 27] However, the formation of these secondary phases as well as the presence of inclusions develops microstructural heterogeneity. Such heterogeneity creates a large difference in the corrosion potential between the matrix and intermetallic phases which allows the flow of electrons promoting the anodic dissolution in the presence of an electrolyte. [16] The corrosion levels in age-hardenable Al-alloys vary from extremely localized to highly uniform with the progress of ageing for all types of corrosions such as pitting, crevice, intergranular and exfoliation.[28]

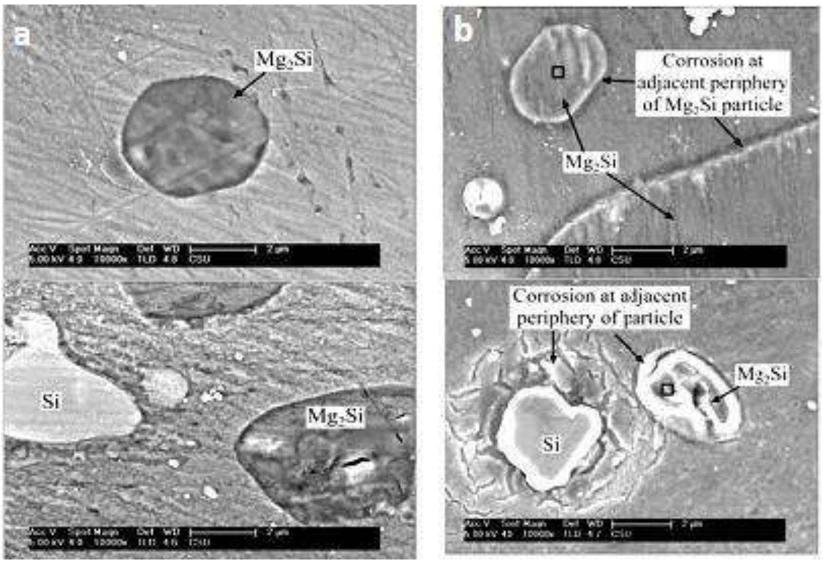

Figure 5. Corrosion morphologies of Al-Mg-Si alloy containing Mg_2si particle immersed in 3.5% NaCl solution for a) 0.5 h, b) 2h [11]

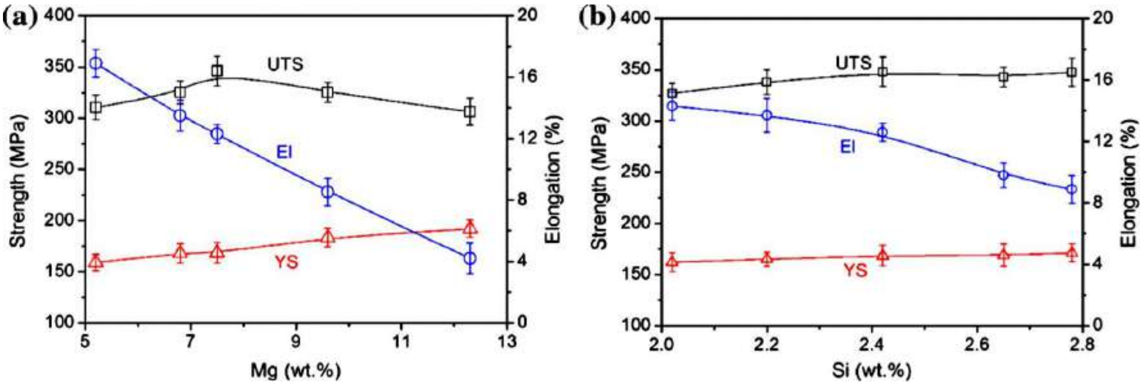

Figure 6. Effect of(a) Mg and (b) Si levels on the mechanical properties of die-cast Al– xMg–2.4Si and Al–7.5Mg–xSi alloys [11]

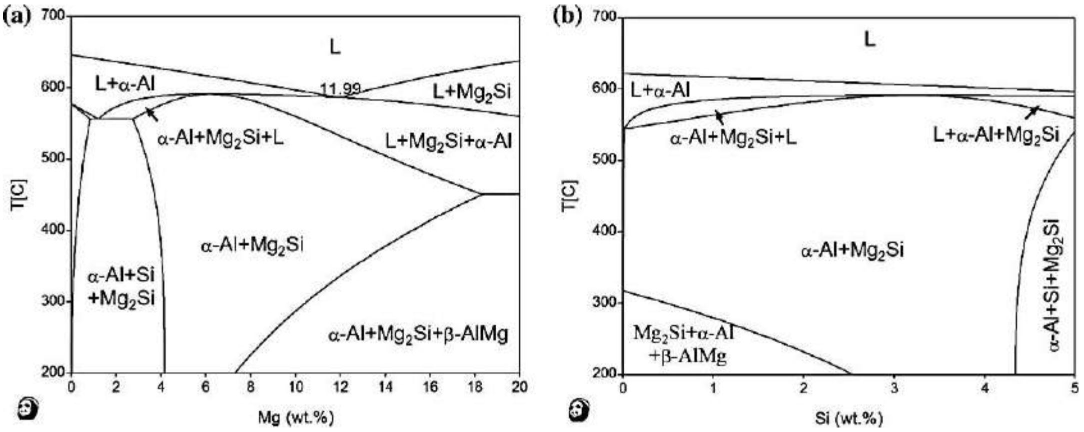

Figure 7. Calculated equilibrium phase diagram of Al-Mg-Si Alloys a) Al–xMg–2.4Si alloy, b) Al–7.5Mg– xSi alloy [11]

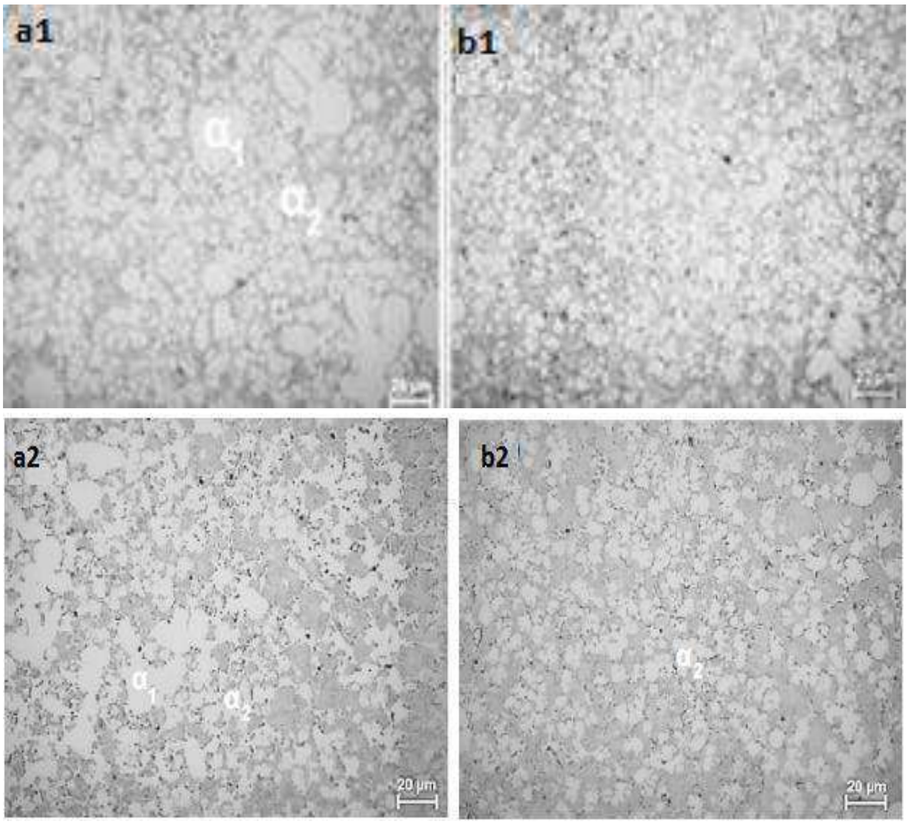

Figure 8. Optical micrographs showing the microstructures of a1) Al–5.2Mg–2.4Si alloys b1) Al–5.2Mg–2.4Si alloys a2) Al–7.5 Mg–2.4Si alloys b2) Al–7.5Mg–2.8Si alloys [16]

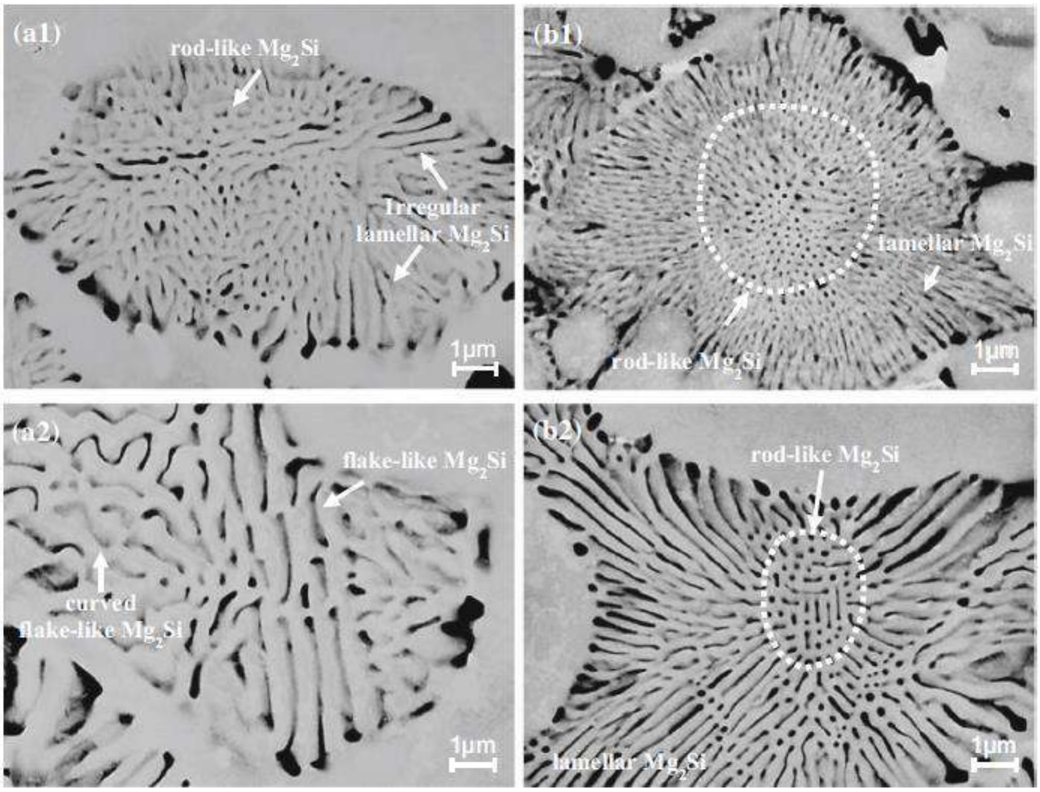

Figure 9. SEM image of difference morphology of Mg_2Si phase [11]

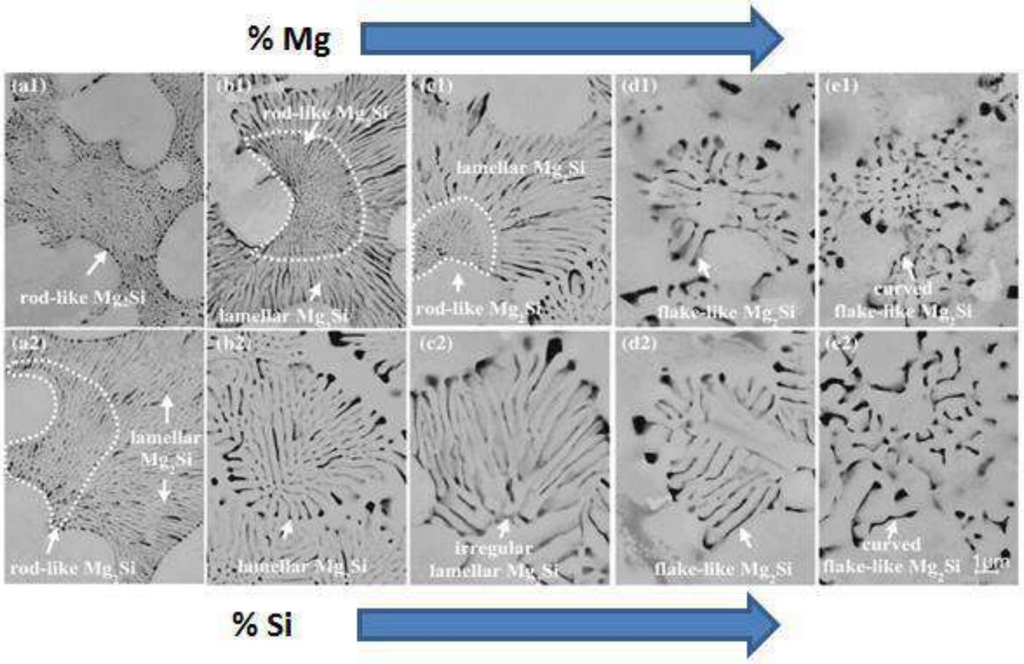

Figure 10. Effect of Mg and Si on Morphology of Mg_2Si [11]

Table 2: Overview of precipitate phases in the Al-Mg-Si system

Precipitation Sequences	Composition	Morphology	Crystal structure	Ref.
SSSS	Unknown	Point Defect	FCC	[33]
GP zone	$MgxAl_5\text{-}xSi_6$	Spherical Primarily	monoclinic	[34]
β″	Mg_5Si_6	Needles	Body cantered monoclinic	[35]
β′	$Mg_{1.8}Si$	Rods	Hexagonal	[36]
β	Mg_2Si	Plates or cubes	FCC	[34]

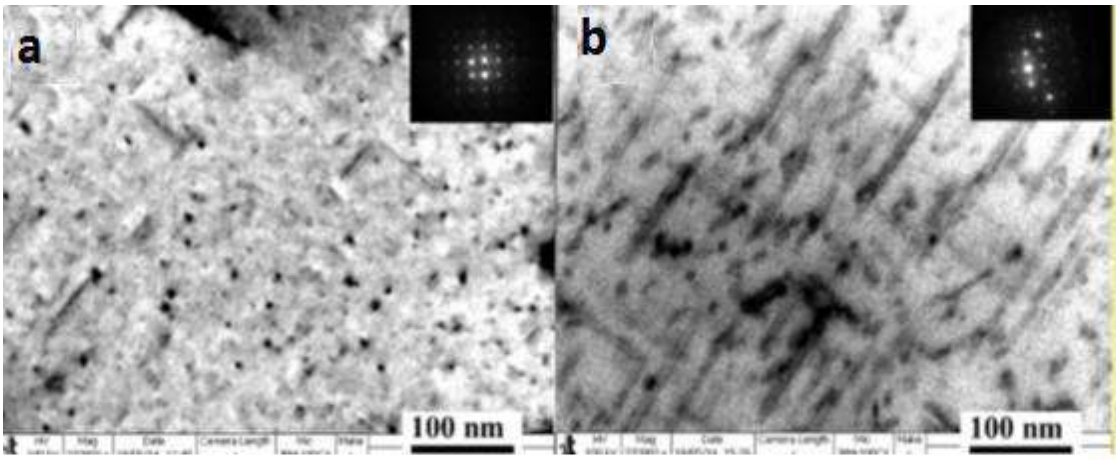

Figure 11: Bright field TEM of selected Al-Mg-Si alloys with (a) aged for 6 hr (b) aged for 22 hr and [44]

Precipitation Sequence During Aging of Al- Mg-Si Alloy

During aging treatment of this alloy, the precipitation of metastable precursors of the equilibrium β (Mg_2Si) phase occurs in one or more sequences which are quite complex. Generally the precipitation sequence for 6xxx Al alloy which is generally accepted in the literature which is:

SSSS(α) – GP zones -β''- β'- β (stable)

Where SSSS (α) represents supersaturated solid solution, GP-zones are Guinier Preston zones, metastable phases β″ (Mg_5Si_6), β′ (Mg_9Si_5)and and equilibrium) β (Mg2Si). [16, 29–32] All phases possesses different chemical composition, morphology and crystal structure as mentioned in table 2. This often changes the local chemistry and continuously assists in attacking the grain boundary. The susceptibility of Al–Mg–Si alloy to IGC in the peak-aged condition is found to increase with Si content due to the increase in the precipitation at the intergranular regions. It has been suggested that a high potential difference among the MgSi, Si particles, PFZ's and solute depleted zones is the primary reason for the initiation of the corrosion. [28]

It has been claimed that the susceptibility to IGC increases during aging, and it is highest at the peak hardness. [4, 8, 9, 12] IGC susceptibility is caused by grain boundary precipitates formed during aging. If the corrosion potential of these particles are different from that of the matrix, the grain boundaries will be decorated with microgalvanic cells, and susceptibility to IGC is expected. [37] Slow quenching after solution heat treatment, which increases the probability of grain boundary precipitation, [10] may also introduce IGC. [15] Overaging may be beneficial; it can reduce, or remove, IGC susceptibility at the expense of introducing pitting. It was found that the precipitates grow and coarsened as the aging time increases as shown in fig 11. [38]

Cooling rate after solution heat treatment had a strong influence on the corrosion performance. Slow cooling in air rendered the model AlMgSi (Cu) alloy susceptible to IGC, whereas water quenching gave resistance against IGC. [37]

CONCLUSIONS

1 Aluminum alloying with elements like magnesium and silicon boosts anode efficiency by promoting depassivation and shifting potential. However, Mg_2Si particles, though prone to corrosion, enhance overall corrosion resistance.
2 The mechanical properties of Al-Mg-Si alloys vary with Mg and Si levels. Higher Mg content improves yield strength but decreases elongation, while higher Si content enhances yield and ultimate strength but lowers elongation.
3 Eutectic Mg_2Si morphology is sensitive to processing conditions and alloy composition, altering from lamellar to rod- like, flake-like to fibrous, or irregular structures.
4 During aging, the precipitation sequence in Al-Mg-Si alloys involves stages from supersaturated solid solution to GP zones, metastable phases like β″ and β′, and ultimately the stable β (Mg_2Si) phase. The precipitation at grain boundaries increases the susceptibility to intergranular corrosion, especially with higher Si content. The presence of different phases and microgalvanic cells at grain boundaries intensify intergranular corrosion (IGC) susceptibility.
5 Overaging reduces intergranular corrosion susceptibility but may induce pitting. Precipitate growth and coarsening during aging affect corrosion behavior. Cooling rate after solution heat treatment significantly impacts corrosion performance; slow cooling in air makes the alloy prone to intergranular corrosion, while water quenching enhances resistance.

REFERENCES

1. Muazu A, Yaro (2011) Effects of Zinc Addition on the Performance of Aluminium as Sacrificial Anode in Seawater
2. Umoru LE, Ige OO (2007) Effects of Tin on Aluminum-Zinc-Magnesium Alloy as Sacrificial Anode in Seawater
3. Hariyanti, El-Mahdy GA, Nishikata A, Tsuru T (2012) Effect of scratching of coating surface on the electrochemical behavior of PVD Al-Mg-Si coated steel. Electrochemistry 80:214–217. https://doi.org/10.5796/electrochemistry.80.214
4. Baruah M, Borah A (2020) Processing and precipitation strengthening of 6xxx series aluminium alloys: A review. Int J Mater Sci 1:40–48.https://doi.org/10.22271/27078221.2020.v1.i1 a.10

5. Avner SH, Guatemala B, Lisbon H, et al INTRODUCTION TO PHYSICAL METALLURGY Second Edition

6. Davis JR, Pdf Jrd Asm Specialty Handbook: Aluminum And Aluminum Alloys Download Ebook : Asm Specialty Handbook: Aluminum And Aluminum Alloys

7. Larsen MH, Walmsley JC, Lunder O, et al (2008) Intergranular Corrosion of Copper-Containing AA6xxx AlMgSi Aluminum Alloys. J Electrochem Soc 155:C550. https://doi.org/10.1149/1.2976774

8. Hariyanti, Yadav AP, Nishikata A, Tsuru T (2012) Effect of corrosion product on the electrochemical behavior of Zn, Zn-Al and Al-Mg-Si alloy coated steel. Electrochemistry 80:218–221. https://doi.org/10.5796/electrochemistry.80.218

9. Enokida M, Kyo Y, El-Mahdy GA, et al Effect of Mg and Si Content on the Electrochemical Behavior of Al-Mg-Si Alloy

10. Seth PP, Parkash O, Kumar D (2021) Mechanical and electrochemical behavior of Mg-Al-Si alloys fabricated with formation of fine Mg2Si phase. Proc Inst Mech Eng Part C J Mech Eng Sci 235:4129–4142. https://doi.org/10.1177/0954406220967686

11. Zeng FL, Wei ZL, Li JF, et al (2011) Corrosion mechanism associated with Mg 2Si and Si particles in Al-Mg-Si alloys. Trans Nonferrous Met Soc China (English Ed 21:2559–2567. https://doi.org/10.1016/S1003-6326(11)61092-3

12. Kruehong C, EL-Mahdy GA, Nishikata A, Tsuru T (2010) Influence of second phases on the electrochemical behavior of hot dipped Al-Mg-Si coated steel. Corros Sci 52:2379–2386. https://doi.org/10.1016/j.corsci.2010.04.013

13. Li LL, Zhang B, Tian B, et al (2017) SVET Study of Galvanic Corrosion of Al/Mg 2 Si Couple in Aqueous Solutions at Different pH . J Electrochem Soc 164:C240–C249. https://doi.org/10.1149/2.0671706jes

14. Birbilis N, Buchheit RG (2005) Electrochemical Characteristics of Intermetallic Phases in Aluminum Alloys. J Electrochem Soc 152:B140. https://doi.org/10.1149/1.1869984

15. Eckermann F, Suter T, Uggowitzer PJ, et al (2008) The influence of MgSi particle reactivity and dissolution processes on corrosion in Al-Mg- Si alloys. Electrochim Acta 54:844–855. https://doi.org/10.1016/j.electacta.2008.05.078

16. Zhu X, Yang H, Dong X, Ji S (2019) The effects of varying Mg and Si levels on the microstructural inhomogeneity and eutectic Mg2Si morphology in die-cast Al–Mg–Si alloys. J Mater Sci 54:5773– 5787. https://doi.org/10.1007/s10853-018-03198-6

17. Zhang J, Fan Z, Wang YQ, Zhou BL (2000) Microstructural development of Al-15wt.%Mg 2 Si in situ composite with mischmetal addition

18. Zhang J, Fan Z, Wang YQ, Zhou BL Equilibrium pseudobinary Al ± Mg 2 Si phase diagram

19. Li S-P, Zhao S-X, Pan M-X, et al Eutectic reaction and microstructural characteristics of Al (Li)-Mg 2 Si alloys

20. Li C, Wu Y, Li H, et al (2010) Effect of Ni on eutectic structural evolution in hypereutectic Al- Mg2Si cast alloys. Mater Sci Eng A 528:573–577. https://doi.org/10.1016/j.msea.2010.09.056

21. Shunpu Li, Shengxu Zhao, Mingxiang Pan, Deqian Zhao, Xichen Chen, O. M. Barabash RIB (1997) Solidification and Structural Characteristics of α(Al)–Mg2Si Eutectic. Mater Trans 38:553–559

22. Shimosaka D, Kumai S, Casarotto F, Watanabe S (2011) Effect of cooling rates during solidification of Al-5.5%Mg-2.3%Si-0.6%Mn and Al-13%Mg2Si pseudo-binary alloys on their secondary-particle morphology and tear toughness. In: Materials Transactions. pp 920– 927

23. Tebib M, Samuel AM, Ajersch F, Chen XG (2014) Effect of P and Sr additions on the microstructure of hypereutectic Al-15Si-14Mg-4Cu alloy. Mater Charact 89:112–123. https://doi.org/10.1016/j.matchar.2014.01.005

24. Farahany S, Ghandvar H, Nordin NA, et al (2016) Effect of Primary and Eutectic Mg2Si Crystal Modifications on the Mechanical Properties and Sliding Wear Behaviour of an Al–20Mg2Si–2Cu– xBi Composite. J Mater Sci Technol 32:1083– 1097. https://doi.org/10.1016/j.jmst.2016.01.014

25. Nordin NA, Farahany S, Ourdjini A, et al (2013) Refinement of Mg2Si reinforcement in a commercial Al-20%Mg 2Si in-situ composite with bismuth, antimony and strontium. Mater Charact 86:97–107. https://doi.org/10.1016/j.matchar.2013.10.007

26. Wang Z, Li H, Miao F, et al (2014) Improving the intergranular corrosion resistance of Al-Mg-Si-Cu alloys without strength loss by a two-step aging treatment. Mater Sci Eng A 590:267–273. https://doi.org/10.1016/j.msea.2013.10.001

27. Kairy SK, Rometsch PA, Diao K, et al (2016) Exploring the electrochemistry of 6xxx series aluminium alloys as a function of Si to Mg ratio, Cu content, ageing conditions and microstructure. Electrochim Acta 190:92–103. https://doi.org/10.1016/j.electacta.2015.12.098

28. Sekhar AP, Samaddar A, Mandal AB, Das D (2021) Influence of Ageing on the Intergranular Corrosion of an Al–Mg–Si Alloy. Met Mater Int 27:5059–5073. https://doi.org/10.1007/s12540-020-00843-1

29. Kairy SK, Rometsch PA, Davies CHJ, Birbilis N The influence of copper additions and ageing on the microstructure and metastable pitting of Al- Mg-Si alloy

30. Bhattamishra AK, Lal K (1997) Microstructural studies on the effect of Si and Cr on the intergranular corrosion in AI-Mg-Si alloys. Elsevier Science Ltd

31. Li W, Chen X, Chen B (2018) Effect of aging on the corrosion behavior of 6005 Al alloys in 3.5 wt% NaCl aqueous solution. J Mater Res 33:1830–1838. https://doi.org/10.1557/jmr.2018.86

32. Cevik E, Sun Y, Ahlatci H (2012) Effect of peak- aged heat treatment on corrosion behavior of the AA6063 alloy containing Al 3Ti. Arch Metall Mater 57:469–477. https://doi.org/10.2478/v10172-012-0048-x

33. Edwards GA, Stiller K, Dunlop GL, Couper MJ THE PRECIPITATION SEQUENCE IN Al±Mg±Si ALLOYS

34. Marioara CD, Andersen SJ, Jansen J, Zandbergen HW (2001) Atomic model for GP- zones in a 6082 Al-Mg-Si system. Acta Mater 49:321–328. https://doi.org/10.1016/S1359-6454(00)00302-5

35. Andersen SJ, Zandbergen HW, Jansen J, et al THE CRYSTAL STRUCTURE OF THE b0 PHASE IN Al±Mg±Si ALLOYS

36. Vissers R, van Huis MA, Jansen J, et al (2007) The crystal structure of the β′ phase in Al-Mg-Si alloys. Acta Mater 55:3815–3823. https://doi.org/10.1016/j.actamat.2007.02.032

37. Svenningsen G, Larsen MH, Nordlien JH, Nisancioglu K (2006) Effect of high temperature heat treatment on intergranular corrosion of AlMgSi(Cu) model alloy. Corros Sci 48:258–272. https://doi.org/10.1016/j.corsci.2004.12.003

38. Chang C-I, Tseng T-Y, Chang J-P, et al Influence of Si/Mg, Cu Content and Aging Condition on the Electrochemical Behaviors of Al-Mg-Si Alloy

Journal of the Maharaja Sayajirao University of Baroda: Science & Technology
Vol. 58, 2024, pp. 44-48

Microstructure and Corrosion Behavior of Al, Al-Mg, and Al-Mg-Si Alloy as a Sacrificial Anode

Tushal K. Kyada[1,2], Indravadan B. Dave[3*], Sonam M. Patel[2]

[1] Research Scholar, Gujarat Technological University, Ahmedabad, India

[2] Metallurgy Department, Dr. S. & S. S. Ghandhy College of Engineering & Technology, Surat-395001, Gujarat, India, tushalkyada21@gmail.com & smp22789@gmail.com

[3*] Metallurgy Engineering, Government Engineering College, Sector-28, Gandhinagar -382028, Gujarat, India, ibdave@gecg28.ac.in

Aluminium, alloyed with elements such as magnesium and silicon, is the preferred sacrificial anode for protecting carbon steel, demonstrating heightened efficiency in depassivation and shifting the operating potential in a more electronegative direction. Consequently, this study focuses on a comparative examination of the microstructure, hardness, and corrosion behavior of Al, Al-Mg, and Al-Mg-Si alloys. Microstructural analysis of the developed alloys was conducted using an optical microscope, revealing that the grain structure of pure aluminum is refined in the presence of Mg and Si. The study assesses hardness test results to provide insights into the mechanical characteristics of the materials, with hardness values increasing due to the presence of Mg and Si. Subsequently, the developed alloys were immersed in a 3.5 wt.% NaCl solution, and their corrosion behavior was scrutinized using the weight loss method. The findings enhance our understanding of Al, Al-Mg, and Al-Mg-Si sacrificial anode materials, emphasizing their potential for corrosion protection applications.

Keywords: *Al, Al-Mg, Al-Mg-Si, sacrificial anode materials, microstructure, corrosion, weight loss method, hardness test*

INTRODUCTION

Nowadays, the most common metals used as sacrificial anodes in cathodic protection systems, especially in oil and gas environments, are aluminum (Al) alloys, magnesium (Mg), and zinc (Zn). [1] Due to its many beneficial qualities, including its low density, significant electrochemical equivalent, accessibility, high current-carrying capacity, high electrical and thermal conductivity, low specific weight, and affordable price, aluminum has become increasingly well-known. [2] However, because γ-Al_2O_3 forms a thin, continuous, adherent, and passive layer on the surface of pure and unalloyed aluminum, it cannot be used as a sacrificial anode. The quick polarization that happens when aluminum is exposed to a corrosion load in a cathodic protection circuit is caused by this γ-Al_2O_3 compound. [3]

If aluminum is utilized as a sacrificial anode, its passive film must be modified to undergo active dissolution. The continuity of the film is affected by the microstructure of the metal, presence of alloying element and volume fraction of second phase particles. To enhance the effectiveness of aluminum anodes, they are often alloyed with other elements to promote the depassivation process, which involves breaking down the oxide film, and to shift the operating potential of the metal towards a more electronegative direction. [3–5]

Aluminum, alloyed with elements such as magnesium (Mg) and silicon (Si), has gained significant attention as a sacrificial anode for protecting carbon steel due to its superior depassivation efficiency and ability to shift the operating potential in a more electronegative direction. Mg has maximum solid solubility in an aluminium matrix which is 16.26 atomic weight percentage around 450°C and Si has maximum solid solubility in an aluminium matrix which is 1.59 atomic weight percentage around 1080°C. [6] Mg, having more negative potential than pure aluminum, are added, the corrosion potential typically increases to more noble values. For example, pure aluminum has a corrosion potential of -920 mV, which decreases to a more

---

* Corresponding author.
Email: ibdave@gecg28.ac.in

negative value of -1120 mV after adding magnesium. This is due to the formation of Al_3Mg_2 particles at the grain boundary, which can lead to grain boundary corrosion or dealloying. [7]

In the presence of magnesium, silicon will combine to form Mg_2Si particles, which are uniformly distributed along the grain boundaries. Initially, these Mg and Si second-phase particles act as anodes during corrosion, but later transition to cathodic behavior, turning the aluminum matrix into the anode. As the magnesium and silicon content increases, the anodic polarization curve shifts towards a more negative potential and higher current. This change in potential is attributed to the quantity of Mg_2Si phase present. [8, 9]

Muazu A. et al. discovered that the inclusion of zinc in aluminum enhances the efficiency of the aluminum anode, with the highest efficiency observed at a zinc content of 6%. This addition results in the formation of the β-phase, which aids in the breakdown of the passive film, consequently improving the efficiency of the aluminum anode. [10] Zheng Y. et al. investigated the precipitation hardening behavior and intergranular corrosion (IGC) of Al- 2Mg-Si alloy. They found that increased Si content in Al-Mg-Si alloys enhances age- hardening response and hardness by promoting the β″ phase. Additionally, IGC susceptibility is attributed to electrochemical potential differences between MgSi particles and solute- depleted zones, with corrosion initiated at grain boundaries and around MgSi precipitates, ultimately leading to continuous corrosion pathways. [11] Nevertheless, the impact of increased levels of magnesium and 1.5 wt.% silicon on microstructure, hardness, and corrosion behavior has not been previously explored. Therefore, our objective is to address this gap by examining these properties and evaluating the potential of the alloy for use as a sacrificial anode.

MATERIALS AND METHODS

Commercially pure aluminum (99.7% wt%), silicon (99.9%), and magnesium (99.8%) were utilized to develop Al–Mg and Al-Mg-Si alloys with compositions of Al–6.5%Mg and Al– 6.5%Mg-1.5%Si. The process began with heating the pure aluminum to 850°C in an electrical resistance furnace. Subsequently, dross was removed from the molten aluminum, and pure magnesium and silicon were added to the melt. To ensure complete dissolution, the melt was held at this temperature for 30 minutes before being poured into a preheated metallic mold after thorough degassing. Both alloys underwent the same casting process.

Chemical analysis of the developed alloy was conducted using the Bruker Q4 TASMAN advanced CCD-based optical emission spectroscopy, following ASTM E1251:2017 standards. [12] The chemical composition of the cast aluminum, aluminum with 6.5% magnesium, and aluminum with 6.5% magnesium and 1.6% silicon was detailed in Table 1.

Table 1. Chemical composition of develop alloy

Element %	**Mg**	**Si**	**Fe**	**Cu**	**Mn**	**Zn**	**Al Balance**
Al	0.002	0.25	0.68	0.11	0.08	0.04	98.7
Al+ 6.5% Mg	6.5	0.25	0.47	0.11	0.06	0.04	92.4
B (Al-6.5%Mg-1.5%Si)	6.6	1.61	0.47	0.10	0.05	0.04	90.8

Metallographic specimens were prepared by cutting and abrading the working surfaces with emery papers, followed by polishing with alumina powders. The specimens were then cleaned in alcohol and rinsed in deionized water before being etched with Keller's etchant solution (2.5 ml HNO_3, + 2.5 ml HCl + 2 ml HF and 95 ml water) [13] for microstructure analysis using a Radical microscope.

For hardness testing, samples were cut and polished with emery paper before undergoing Brinell hardness tests using a 31.25 kg load with a 2.5 mm steel ball indenter. Brinell hardness measurements were taken at five different locations on each sample.

Corrosion testing was conducted by immersing samples in a 3.5 wt.% NaCl solution, and the results were assessed through weight loss measurements following ASTM G31 standards.

[14] All samples were ground with SiC papers and then cleansed in ethanol before exposure to the 3.5 wt.% NaCl solution for one to seven weeks for weight loss measurement analysis. After every week a test samples are taken out from the corrosion media and rinsed with water, cleaned with acetone and air-dried after that final weight is measured and calculates corrosion rate by using the mpy formula.

$$Corrosion\ Rate\ (mpy) = \frac{534\ W}{D\ A\ T}$$

where, W = Weight loss (mg),

D = Density of sample (gm/cc),

A = Area of specimen exposed to corrosion ($inch^2$),
T = Time of exposure (hours)

RESULTS AND DISCUSSION

Microstructure Analysis

Figures 1(a,b) and (c,d) illustrate the optical microstructures of as-cast Al-6.5% Mg and Al-6.5%Mg-1.5%Si alloys. Referring to the binary phase diagram of the aluminum-magnesium system, [15, 16] the microstructure reveals the presence of two phases. The first phase is a solid solution of aluminum, commonly referred to as α aluminum (α-Al), which appears white in the micrographs. The second phase is an intermetallic compound of aluminum and magnesium, known as the β phase or Al_3Mg_2, which appears as a dark black color. The formation of the β phase occurs through a eutectic reaction, as depicted in Figures 1(a) and 1(b).

In the case of Al-6.5%Mg-1.5%Si alloy, it is important to note that magnesium (Mg) has low solubility for silicon (Si). Consequently, the majority of silicon atoms react with magnesium atoms, leading to the precipitation of an intermetallic compound called Mg_2Si. The precipitate Mg_2Si is typically observed at the periphery of pi phase particles. These particles manifest as black Chinese script-like formations, [17] as illustrated in Figure 1 (c) and 1(d). Additionally, the precipitate can be identified at the boundary of primary silicon. The presence of Mg_2Si precipitates alters the microstructure compared to the Al-6.5% Mg alloy, highlighting the influence of silicon addition on the alloy's phase distribution and morphology.

Hardness Test

Figure 2 illustrates the hardness values of pure aluminum and the developed alloys. There is a significant increase in hardness with the addition of magnesium and silicon to aluminum. In the case of the Al-6.5%Mg composition, the hardness is notably enhanced due to the formation of the Al_3Mg_2 phase, also known as the Sampson or beta phase. [18] This specific phase exhibits higher hardness compared to pure aluminum, thus contributing to the overall hardness of the material.

In contrast, for the Al-6.5%Mg-1.5%Si composition, the increased hardness is attributed to the formation of the Mg_2Si phase. This phase plays a significant role in elevating the hardness of the alloy. It is interesting to observe how the addition of silicon, in addition to magnesium, influences the hardness properties of the material, showcasing the complex interplay of alloying elements in determining material characteristics.

Corrosion Behavior

Figures 3 and 4 depict the corrosion rates and images of the Al, Al-6.5Mg, and Al-6.5Mg-1.5Si alloys over a span of 7 weeks. In the case of pure aluminum, the corrosion rate remains relatively stable due to the formation of a passive layer. The addition of 6.5% Mg to the alloy resulted in a slight increase in corrosion rate compared to the Pure Al composition. However, upon further addition of 1.5% Si to the Al-6.5% Mg alloy, the corrosion rate experiences a significant increase, peaking in the sixth week and gradually declining by the seventh week.

The formation of intermetallic compounds, such as the β phase (Al_3Mg_2) in Al-6.5Mg alloys and Mg_2Si in the case of Al-6.5Mg-1.5Si alloy, can lead to galvanic corrosion. These phases, along with the aluminum solid solution (α-Al matrix), possess different electrode potentials. The β phase and Mg_2Si act as anodes, while the α-Al matrix serves as a cathode in a galvanic cell. This potential difference generates a driving force for galvanic corrosion, causing dissolution of the β phase and Mg_2Si, which subsequently form cavities or pits. These phases serve as initiation sites for corrosion, leading to localized corrosion or de-alloying. Images of the pits after six weeks are shown in figure 4.

CONCLUSIONS

- The presence of the Al_3Mg_2 phase in the Al-6.5Mg alloy contributes to its enhanced hardness, while the Mg_2Si phase in the Al-6.5Mg-1.5%Si alloy is responsible for its increased hardness.

- The microstructure of pure aluminum consists of α-Al, while the Al-6.5Mg alloy exhibits the presence of β phases. The addition of silicon in the Al-6.5%Mg-1.5%Si alloy leads to the formation of the Mg_2Si intermetallic compound.

- The corrosion rate in pure aluminum is relatively stable due to the formation of a passive layer. However, the addition of magnesium increases the corrosion rate, and the further addition of silicon significantly increases it. The formation of β-phase (Al_3Mg_2) and Mg_2Si creates a galvanic corrosion scenario, with the β-phase and Mg_2Si acting as anodes and the α-Al matrix as a cathode. This leads to dissolution and the formation of cavities or pits in the material.

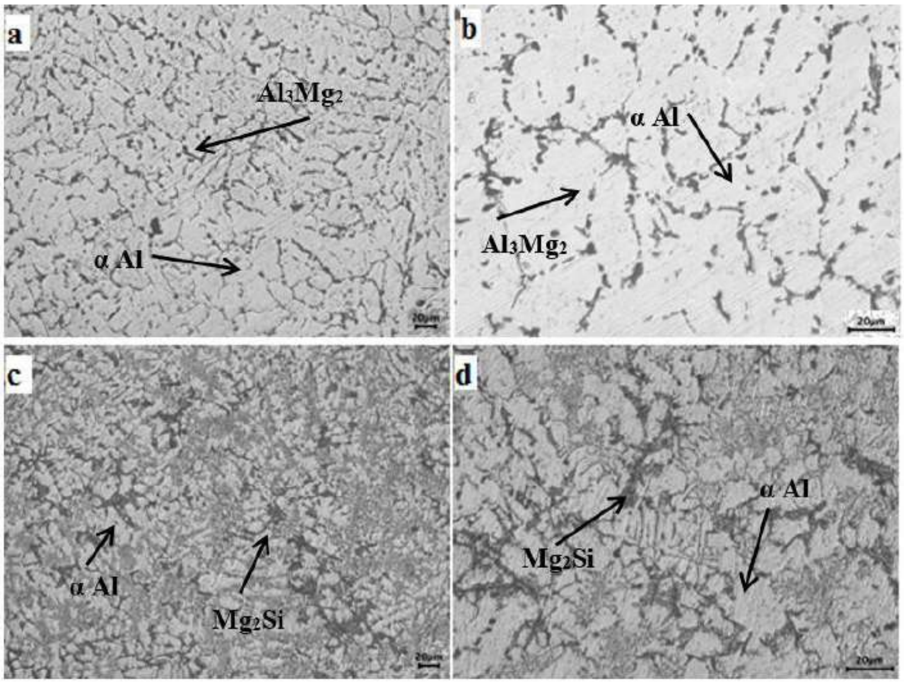

Figure 1. Microstructure of Al-6.5%Mg (a) at 200X, b) at 500X and Al-6.5%Mg-1.5%Si (c) at 200X, (d) at 500X

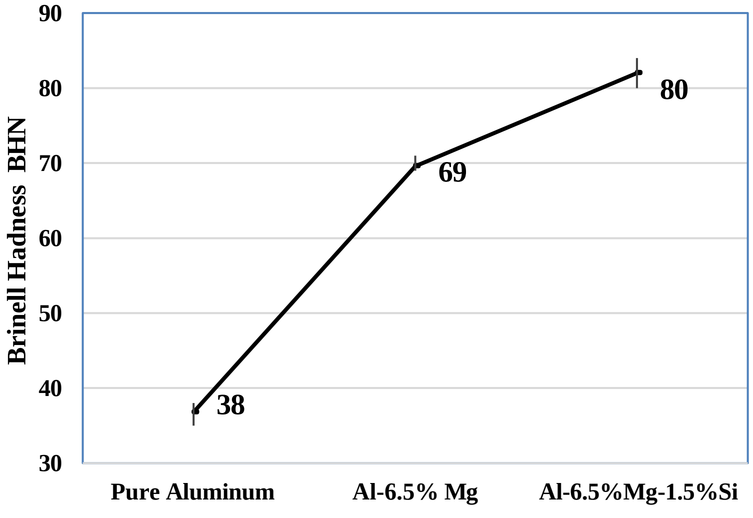

Figure 2: Brinell hardness of Al, Al-6.5%Mg and Al-6.5%Mg-1.5%Si

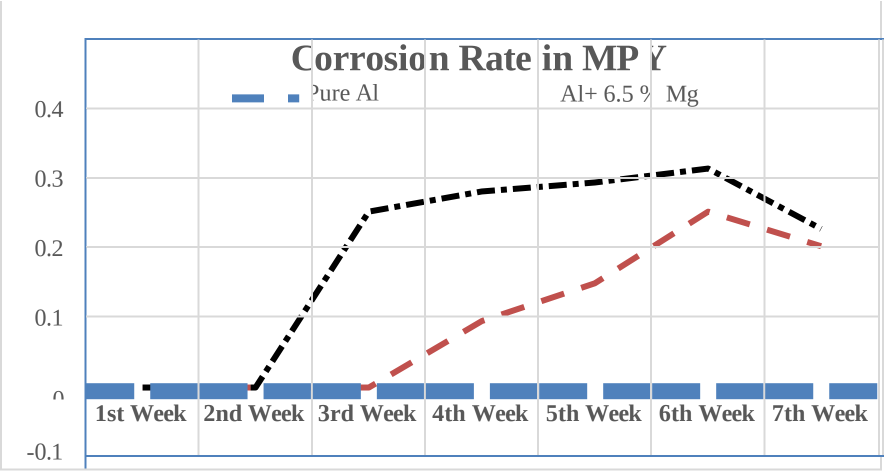

Figure 3. Corrosion rate in Mpy for Al, Al-6.5%Mg and Al-6.5%Mg-1.5%Si

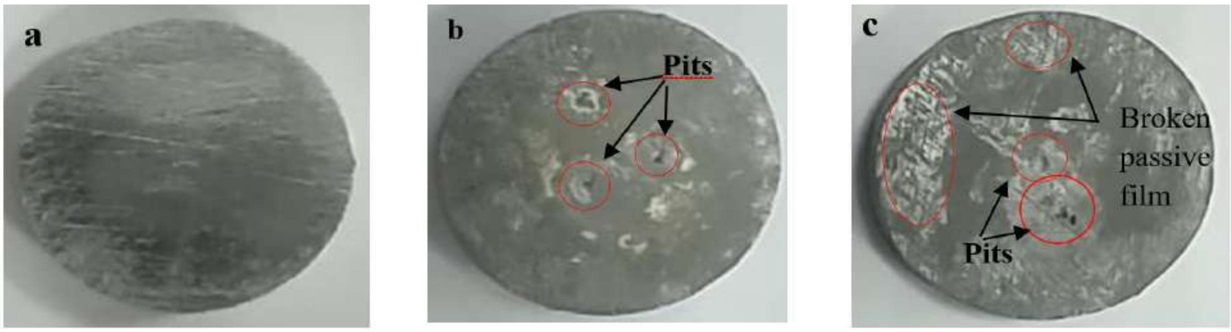

Figure 4. Image of samples after six week of corrosion test a) Pure Al, b) Al-6.5%Mg c) Al-6.5%Mg-1.5% Si Alloy.

REFERENCES

1. Idusuyi N, Oluwole OO (2012) Aluminium anode activation research-a review
2. Asmara YP, Siregar JP, Tezara C, Ann CT (2016) Improving Efficiency of Aluminium Sacrificial Anode Using Cold Work Process. IOP Conf Ser Mater Sci Eng 114:. https://doi.org/10.1088/1757- 899X/114/1/012045
3. Sperandio GF, Santos CML, Galdino AGS (2021) Influence of silicon on the corrosion behavior of Al– Zn–In sacrificial anode. J Mater Res Technol 15:614–622. https://doi.org/10.1016/j.jmrt.2021.08.033
4. Hariyanti, El-Mahdy GA, Nishikata A, Tsuru T (2012) Effect of scratching of coating surface on the electrochemical behavior of PVD Al-Mg-Si coated steel. Electrochemistry 80:214–217. https://doi.org/10.5796/electrochemistry.80.214
5. Campos MDRS, Blawert C, Scharnagl N, et al (2022) Cathodic Protection of Mild Steel Using Aluminium-Based Alloys. Materials (Basel) 15:. https://doi.org/10.3390/ma15041301
6. Vidhi A Mistry, Minal S Dani IBD (2022) A Review on Effect of Alloying Element on Aluminium Anode. GIT-Journal Eng Technol 1:1–9
7. Enokida M, Kyo Y, El-Mahdy GA, et al Effect of Mg and Si Content on the Electrochemical Behavior of Al-Mg-Si Alloy
8. Zeng FL, Wei ZL, Li JF, et al (2011) Corrosion mechanism associated with Mg 2Si and Si particles in Al-Mg-Si alloys. Trans Nonferrous Met Soc China (English Ed 21:2559–2567. https://doi.org/10.1016/S1003-6326(11)61092-3
9. Kruehong C, EL-Mahdy GA, Nishikata A, Tsuru T (2010) Influence of second phases on the electrochemical behavior of hot dipped Al-Mg-Si coated steel. Corros Sci 52:2379–2386. https://doi.org/10.1016/j.corsci.2010.04.013
10. Muazu A, Yaro (2011) Effects of Zinc Addition on the Performance of Aluminium as Sacrificial Anode in Seawater
11. Zheng Y, Luo B, Bai Z, et al (2017) Study of the precipitation hardening behaviour and intergranular corrosion of Al-Mg-Si alloys with differing Si contents. Metals (Basel) 7:. https://doi.org/10.3390/met7100387
12. Standard A (2017) Standard Test Method for Analysis of Aluminum and Aluminum Alloys by Spark Atomic Emission Spectrometry. ASTM Int West Conshohocken, PA, USA
13. Vander Voort GF, Lampman SR, Sanders BR, et al (2004) ASM handbook. Metallogr Microstruct 9:40002–44073
14. Cor- E (2008) Standard Practice for Laboratory Immersion Corrosion Testing of Metals 1. 72:
15. (1990) Vol 03 - Alloy Phase Diagrams. ASM International
16. Zahi S, Daud AR (2010) Phase diagram, thermodynamics and microstructure of Al-Mg system. In: 2010 34th IEEE/CPMT International Electronic Manufacturing Technology Symposium (IEMT). IEEE, pp 1–7
17. Williams S. Ebhota T-CJ (2017) Intermetallics Formation and Their Effect on Mechanical Properties of Al-Si-X Alloys. In: Intechopen. pp 21–41
18. Steurer W (2007) The Samson phase, β-Mg_2Al_3, revisited. Zeitschrift für Krist 222:259–288

Journal of the Maharaja Sayajirao University of Baroda: Science & Technology
Vol. 58, 2024, pp. 49-54

Impact of calcium nitrate accelerator on zinc phosphating performance

Suraj dabhekar[1], Sunil kahar[2]

[1]PhD Scholar, The Maharaja Sayajirao University of Baroda, Vadodara, Gujarat, India
[2] Assistant Professor, The Maharaja Sayajirao University of Baroda, Vadodara, Gujarat, India
2120suraj@gmail.com

The sluggish nature of zinc phosphating reactions, attributed to the polarization induced by hydrogen evolution in the cathodic process, can be improved through diverse chemical, mechanical, and electrochemical means. This research focuses on exploring the impact of Calcium Nitrate (Ca (NO3)2.4H2O) as an accelerator on the corrosion resistance and coating compactness of zinc phosphate coatings. The study involved the successful development of zinc phosphate coatings on low carbon steel, both with and without the use of the accelerator. Calcium Nitrate was incorporated into the phosphating bath solution at concentrations of 6%, 12%, and 18%. Corrosion resistance was evaluated through potentiodynamic tests in 3.5% NaCl and 0.1 N H2SO4 solutions. Additionally, Electrochemical Impedance Spectroscopy (EIS) was employed to assess coating compactness in the same solutions. The findings indicated a notable enhancement in coating properties with the addition of Ca (NO3)2.4H2O as an accelerator.

.

Keywords: *Zinc phosphating, corrosion resistance, calcium nitrate, potentiodynamic test*

INTRODUCTION

Metals have long served as the foundation of civilization; however, metals extracted from their ores exhibit a pronounced inclination to revert to their oxide form, leading to significant economic losses due to corrosion [1-3]. The primary approach to corrosion protection involves surface modification. Common methods for surface modification typically entail creating a physical barrier to shield the metal from corrosive environments [4,5]. One widely utilized technique is phosphate coating (phosphating), which involves the formation of an insoluble crystalline metal-phosphate salt through a chemical or electrochemical reaction between the substrate metal and a phosphoric acid solution containing metal ions such as zinc, iron, or manganese [6].

Phosphating emerges as the predominant metal pretreatment process extensively employed for surface treatment and finishing across both ferrous and non-ferrous metals [7]. The resulting phosphate coating assumes a pivotal role in fortifying the paint film and hindering the initiation and propagation of corrosion [8]. The phosphating process operates by facilitating the formation of numerous crystals of varied sizes, originating from nucleation centers, subsequently spreading, merging, and ultimately covering the surface [9]. However, a notable challenge associated with phosphating baths is the imperative for elevated operating temperatures, typically ranging from 90 to 98°C [10-12]. This elevated temperature requirement often leads to bath overheating, giving rise to complications in the operation and maintenance of heating coils due to scale formation. Consequently, improper heating of the bath solution necessitates frequent replacements, adding a layer of complexity to the operational efficiency of the phosphating process [13-16].

RESEARCH SIGNIFICANCE

The challenges inherent in traditional phosphating processes can be alleviated by improving the phosphating rate [17]. In practical applications, the phosphating reaction often experiences sluggishness due to polarization caused by hydrogen evolution in the cathodic

---

* Corresponding author.
Email: 2120suraj@gmail.com

reaction [18]. To expedite the formation of coatings within a reasonable timeframe, some form of acceleration is essential [19]. Methods for accelerating the formation of phosphate coatings can be broadly categorized as chemical, mechanical, and electrochemical accelerators [20].

Chemical accelerators provide a means to enhance the chemical, metallurgical, and mechanical properties of phosphated surfaces [21]. Commonly used oxidizing accelerators include nitrites, chlorates, nitrates, peroxides, and organic nitro compounds, either individually or in various combinations. Typical combinations include nitrite-nitrate, nitrite-chlorate-nitrate, and chlorate-nitrobenzene sulfonic acid. These accelerators play a crucial role in expediting the deposition process through distinct mechanisms [22-23]. Oxidizing agents depolarize the cathode half-cell reaction, preventing hydrogen accumulation at cathodic sites. Simultaneously, noble metal ions facilitate metal dissolution by providing low over-potential cathode sites through their deposition. This multifaceted action contributes to the overall enhancement of the phosphating process and the resulting coated surfaces [24].

Of all accelerators, calcium stands out for its eco-friendly nature and widespread availability. The use of calcium as an accelerator notably improves the corrosion resistance and coating compactness of phosphate coatings. Additionally, literature suggests that calcium has the potential to enhance surface morphology and contribute to the development of a robust crystal structure [25,26].

Optimizing the zinc phosphating process on low carbon steel (1020) requires a precise determination of the necessary calcium concentration, a fact that currently remains unclear. In response to this knowledge gap, our study investigates the effects of varying amounts of calcium as an accelerator. The experimental design systematically explores the impact of different calcium concentrations on the zinc phosphating process of low carbon steel (1020) [27,28]. Through these investigations, our research aims to provide valuable insights into the optimal utilization of calcium as an accelerator, with a specific focus on enhancing the properties of phosphate coatings on low carbon steel.

MATERIALS AND METHODS

Process of the Coating

A steel specimen (C-20) measuring 40 x 30 x 3 mm served as the substrate material for the deposition of a zinc phosphate coating. The Zinc Phosphating process was carried out using an immersion method, encompassing a sequence of four baths: a degreasing bath, a pickling bath, an acid activation bath, and a zinc phosphating bath. The bath composition and corresponding immersion times are detailed as follows [29].

Table 1: Sequence of phosphating

Sequence of pretreatment	Details of Bath Composition	Time
1	Degreasing solution: NaOH= 10%	10 minutes
2	Water rising: distilled water	2 minutes
3	Pickling solution: HCl= 0.1 M	8 minutes
4	Water rising: distilled water	2 minutes
5	Acid Activation solution: H_2SO_4 = 10%	2 minutes

After pretreatment, sample were carried out to phosphating bath with and without addition of calcium nitrate as per following table.

Table 2: Details of phosphating bath composition

Exp No	Details of Bath Composition	Accelerator addition
1	Zinc Phosphating $NaNO_2$ = 5g/L, ZnO= 20g/L, H_3PO_4 = 15g/L	0%
2	Zinc Phosphating $NaNO_2$ = 5g/L, ZnO= 20g/L, H_3PO_4 = 15g/L	6% Ca (NO3)2.4H2O
3	Zinc Phosphating $NaNO_2$ = 5g/L, ZnO= 20g/L, H_3PO_4 = 15g/L	12% Ca (NO3)2.4H2O
4	Zinc Phosphating $NaNO_2$ = 5g/L, ZnO= 20g/L, H_3PO_4 = 15g/L	18% Ca (NO3)2.4H2O

(a)

(b)

(c)

(d)

Figure 1: Various stages of treatment
(a) Degreasing in NaOH
(b) Pickling in HCL
(c) Acid Activation in H_2SO_4
(d) phosphating in ZnO+NaNO2+H_3PO4

Corrosion Studies

The corrosion studies of phosphated samples were performed by dissolving analytical grade of 3.5 % NaCl salt in distilled water and 0.1N H_2SO_4 solution[30]. It was carried out by Gamry Reference 600 instrument using a three- electrode system where the phosphate sample acted as the working electrode, the graphite as the counter electrode, and the calomel electrode as the reference electrode. The DC potentiodynamic polarization test was performed by ASTM G 5 standard method in 3.5 % NaCl and 0.1N H_2SO_4 solution. The electrochemical impedance spectroscopy (EIS) of the samples were carried out from 100 kHz to 0.01 Hz with a 10-mV sinusoidal voltage by ISO 16773-:2016 method in 3.5 % NaCl and 0.1N H_2SO_4 solution[31-35].

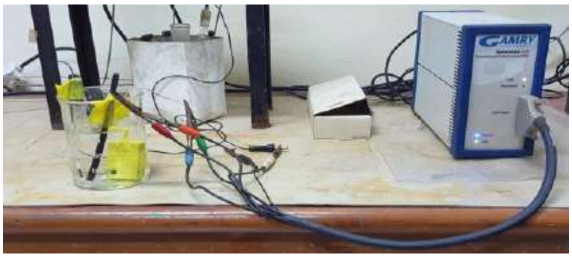

Figure 2: Experimental setup of Potentiodynamic and EIS test

Figure 3: Graphite and SCE electrode

RESULTS AND DISCUSSION

Potentiodynamic Test

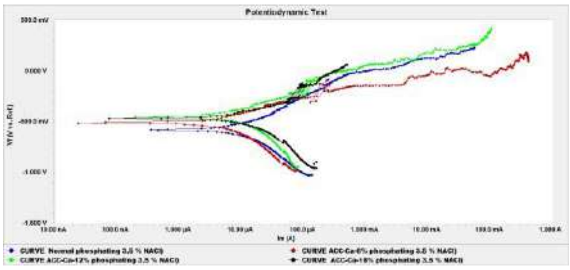

Figure 4: Comparison of corrosion behaviour of Zinc Phosphate coating with Calcium Nitrate addition in 3.5 % NaCl solution

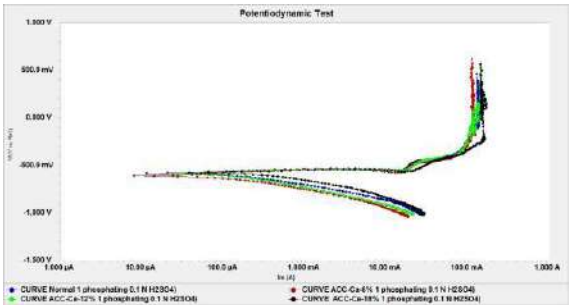

Figure 5: Comparison of corrosion behavior of Zinc Phosphate coating with Calcium Nitrate addition in 0.1N H2SO4 solution

Potentiodynamic testing serves as a widely employed electrochemical technique in corrosion research, offering valuable insights into the corrosion behavior of materials. To determine the corrosion rate from potentiodynamic testing, Tafel extrapolation methods were employed. The Tafel slopes derived from the polarization curve enabled the calculation of anodic and cathodic corrosion current densities [36,37]. The potentiodynamic test results in 3.5 % NaCl and 0.1N H2SO4 solution demonstrate a noteworthy reduction in the corrosion current (Icorr) values upon the introduction of a calcium accelerator into the zinc phosphating bath, indicating a concurrent decrease in the corrosion rate [38]. Comparative analysis reveals that the corrosion resistance of standard zinc phosphated samples is significantly surpassed by those treated with a calcium accelerator, signifying an enhancement in protective properties. Notably, the corrosion resistance values of phosphated samples exhibit an inverse relationship with the concentration of calcium accelerator, with 6% calcium addition yielding superior results compared to both 12% and 18%.

The corrosion rate is observed to be significantly elevated in 0.1N H2SO4 compared to the 3.5% NaCl solution, highlighting a higher susceptibility to corrosion in the acidic environment of sulfuric acid.

Table 3: Potentiodynamic test result value in 3.5% NaCl solution

Details of coating	Icorr (µA)	Ecorr (mV)	Corrosion Rate (mpy)
Zinc Phosphate Coating (without accelerators)	103.0	580.0	154.3
Zinc Phosphate Coating (with accelerators 6%)	**2.07**	**511.0**	**311.1e-3**
Zinc Phosphate Coating (with accelerators 12%)	3.340	449.0	5.030
Zinc Phosphate Coating (with accelerators 18%)	5.650	466.0	8.500

Table 4: Potentiodynamic test result value in 0.1N H2SO4 solution

Details of coating	Icorr (µA)	Ecorr (mV)	Corrosion Rate (mpy)
Zinc Phosphate Coating (without accelerators)	88.70	584.0	133.5
Zinc Phosphate Coating (with accelerators 6%)	49.20	590.0	74.02
Zinc Phosphate Coating (with accelerators 12%)	79.20	611.0	119.1
Zinc Phosphate Coating (with accelerators 18%)	84.0	579.0	126.2

Electrochemical Impedance Spectroscopy (EIS) test

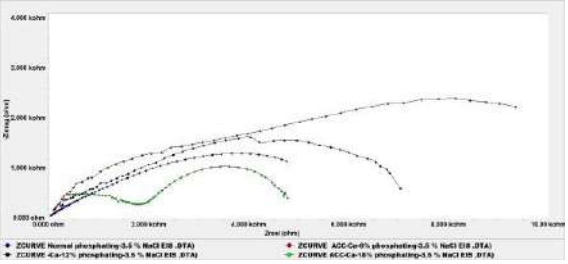

Figure 6: Comparison of compactness and uniformity of Zinc Phosphate coating with and without calcium nitrate in 3.5% NaCl solution by EIS Scan

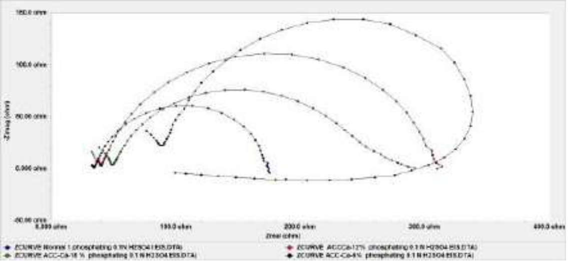

Figure 7: Comparison of compactness and uniformity of Zinc Phosphate coating with and without calcium nitrate in 0.1N H2SO4 solution by EIS Scan

The Electrochemical Impedance test results indicate a direct correlation between coating compactness and capacitance values, with higher capacitance values reflecting superior coating properties [39,40]. Notably, in the context of normal zinc phosphated and calcium nitrate addition zinc phosphating samples, the samples treated with a 6% accelerator demonstrate the highest capacitance values, signifying enhanced coating compactness in comparison to the 12% and 18% accelerator- treated samples.

Table 5: Electrochemical Impedance Spectroscopy (EIS) test result value in 3.5% NaCl

Zinc Phosphate coating (with & without acceletor)	**Capacitance Value**
Zinc Phosphate coating (without acceletor)	1299 kohm.
Zinc Phosphate coating (with 6 % Calcium Nitrate)	**2394 kohm.**
Zinc Phosphate coating (with 12 % Calcium Nitrate)	1631 Kohm
Zinc Phosphate coating (with 18 % Calcium Nitrate)	1031 Kohm

Table 6: Electrochemical Impedance Spectroscopy (EIS) test result value in 0.1N H2SO4

Zinc Phosphate coating (with & without acceletor)	**Capacitance Value**
Zinc Phosphate coating (without acceletor)	60.18 kohm.
Zinc Phosphate coating (with 6 % Calcium Nitrate)	**144.1 kohm.**
Zinc Phosphate coating (with 12 % Calcium Nitrate)	111.1 Kohm
Zinc Phosphate coating (with 18 % Calcium Nitrate)	75.83 Kohm

CONCLUSION

The incorporation of a calcium accelerator in zinc phosphating baths has demonstrated a substantial reduction in corrosion rates, as evidenced by potentiodynamic tests. Additionally, Electrochemical Impedance testing revealed that the capacitance values, indicative of coating compactness, were notably higher in samples treated with a 6% accelerator. This underscores the effectiveness of calcium nitrate addition in improving both corrosion resistance and coating properties. Furthermore, comparative studies between 3.5% NaCl and 0.1N H2SO4 highlighted the heightened corrosion susceptibility in the acidic environment of sulfuric acid. Overall, these findings contribute valuable insights into optimizing corrosion protection strategies in zinc phosphating processes.

REFERENCES

1. M.G. Fontana,*Corrosion Engineering*, 3rd Edition (McGraw-Hill Book Company, Singapore, 1987)
2. U.R. Evans, *An Introduction to Metallic Corrosion*, 3rd Edition (Edward Arnold Publishers Ltd., London, 1981)..
3. H.H. Uhlig, *Corrosion and Corrosion Control*, 2nd Edition (John Wiley & Sons, Inc., New York, 1971).
4. F.L. La Que, In: *Good Painting Practice*, ed. by John D. Keane, Vol. 1, 2nd Edition (Steel Structures Painting Council, Pittsburgh, 1973), Chap. 1.1, p. 3.
5. Henry Leidheiser, Jr., In: *Metals Handbook*, Vol. 13, 9th Edition (American Society of Metals, Ohio, 1987), p. 377.
6. Phosphate Conversion Coating – A Short Review." (June 2023). *Archives of Metallurgy and Materials*, 68(3), 1029-1034. DOI: 10.24425/amm.2023.145471.
7. Narayanan, T.S.N. Sankara. (2005). National Metallurgical Laboratory, Madras Centre CSIR, Complex, Taramani, Chennai-600 113, India. Received: April 22, 2005.
8. Freeman, D. B. (1986). *Phosphating and Metal Pretreatment - A Guide to Modern Processes and Practice*. New York: Industrial Press Inc.
9. T.S.N. Sankara Narayanan and M. Subbaiyan. "Trans. Inst. Met. Finish. 70(2) (1992) 81.
10. T.S.N. Sankara Narayanan and M. Panjatcharam and M. Subbaiyan. "Met. Finish. 91 (1993) 65.
11. T.S.N. Sankara Narayanan and M. Subbaiyan. "Trans. Inst. Met. Finish. 71 (1993) 52.
12. American Chemical Paint Co., British Patent, 501,739 (1939)
13. Societe Continentale Parker, French Patent, 849,856 (1939); Pyrene Company Ltd., British Patent 510,684 (1939).
14. B. Mayer, P. Kuhm, P. Balboni, M. Senner, H.D. Speckmann, J. Geke, J.W. Brouwer and A. Willer, U.S. Patent 6,379,474 (2002).
15. K.S. Rajagopalan, B. Dhandapani, and A. Jayaraman, In: Proceedings of the 3rd International Congress on Metallic Corrosion (1966) Vol. 1, p. 365.
16. K.S. Rajagopalan, C. Rajagopal, N. Krithivasan, M. Tajudeen, and M.E. Kochu Janaki // Werkstoffe und Korrosion 23 (1971) 347.
17. R. Murakami, Y. Mino, and K. Saito, European Patent 0,061,911 (1982); U.K. Patent Appl. 2,097,429 (1982)
18. Guy Lorin, Phosphating of Metals (Finishing Publications Ltd., London, 1974).
19. **C**. Rajagopal and K.I. Vasu, Conversion Coatings: A Reference for Phosphating, Chromating and Anodizing (Tata McGraw-Hill Publishing Company Ltd., New Delhi, 2000).
20. T.S.N. Sankara Narayanan, "Role of surfactants in phosphate conversion coatings," In: Surfactants in Polymers, Coatings, Inks and Adhesives, ed. by D.

Karsa (Blackwell Publishers, Oxford, 2003), Chapter 10, p. 227.

21. **G**. Bikulcius, V. Burokas, A. Martusiene, and E. Matulionis // Surf. Coat. Technol. 172 (2003) 139.
22. D.R. Gabe, K.A. Akanni, and C.P.S. Johal, In: Proceedings of the Interfinish'84, (Tel Aviv, Israel; 1984), p. 474
23. M. Arthanareeswari, P. Kamaraj, M. Tamilselvi, "Anticorrosive performance of zinc phosphate coatings on mild steel developed using galvanic coupling," Journal of Chemistry 673961 (2013).
24. D.P. Burduhos-Nergis, P. Vizureanu, A.V. Sandu, C. Bejinariu, "Evaluation of the corrosion resistance of phosphate coatings deposited on the surface of the carbon steel used for carabiners manufacturing," Applied Sciences 10 (8), 2753 (2020)
25. D.P. Burduhos-Nergiș, C. Nejneru, R. Cimpoeșu, A.M. Cazac, C. Baciu, D.C. Darabont, C. Bejinariu, "Analysis of chemically deposited phosphate layer on the carabiners steel surface used at personal protective equipments," Quality – Access to Success 20, 77-82 (2019).
26. **D.**P. Burduhos-Nergis, P. Vizureanu, A.V. Sandu, C. Bejinariu, "Phosphate Surface Treatment for Improving the Corrosion Resistance of the C45 Carbon Steel Used in Carabiners Manufacturing," Materials 13, 3410 (2020).
27. C. Bejinariu, D.P. Burduhos-Nergis, N. Cimpoesu, "Immersion Behavior of Carbon Steel, Phosphate Carbon Steel and Phosphate and Painted Carbon Steel in Saltwater," Materials 14, 188 (2021).
28. LeGeros RZ, Bleiwas CB, Retino M, Rohanizadeh R, LeGeros JP. Zinc effect on the in vitro formation of calcium phosphates: relevance to clinical inhibition of calculus formation. Am J Dent. 1999 Apr;12(2):65-71. PMID: 10477985.
29. Intorp, N. B., Kent, G. D., & Springstead, T. H. (1985). Zinc phosphate conversion coating composition. Google Patents.
30. Zurilla, R., & Hospadaruk, V. (1978). Quantitative test for zinc phosphate coating quality. SAE Technical Paper. Google Scholar.
31. Weng, D., Jokiel, P., Uebleis, A., & Boehni, H. (Year not provided). Corrosion and protection characteristics of zinc and manganese phosphate coatings.
32. Munir, S., Pelletier, M. H., & Walsh, W. R. (2016). Potentiodynamic Corrosion Testing. Journal of Visualized Experiments, 2016(115). DOI:10.3791/54351.
33. **S**. Jegannathan, T.S.N. Sankara Narayanan, K. Ravichandran, S. Rajeswari, "Progress Organic Coatings 57 (2006) 392.
34. K. Ravichandran, T.S.N. Sankara Narayanan, "Trans. Inst. Met. Finish. 79 (4) (2001) 143.
35. S. Jeganathan, T.S.N. Sankara Narayanan, K. Ravichandran, S. Rajeswari, "Surf. Coat. Technol. 200 (2006) 4117.
36. S. Jeganathan, T.S.N. Sankara Narayanan, K. Ravichandran, S. Rajeswari, "Surf. Coat. Technol. 200 (2006) 6014
37. Randviir, E. P., & Banks, C. E. (2013). Electrochemical impedance spectroscopy: An overview of bioanalytical applications. *Analytical Methods, 5*(5), 1098-1115. DOI: 10.1039/c3ay26476a.
38. Vadhva, P., Hu, J., Johnson, M. J., Stocker, R., Braglia, M., Brett, D. J. L., & Rettie, A. J. E. (2021). Electrochemical Impedance Spectroscopy for All-Solid-State Batteries: Theory, Methods and Future Outlook. *ChemElectroChem.* Advance online publication. https://doi.org/10.1002/celc.202100108.
39. Barsoukov, E., & Macdonald, J. R. (2005). *Impedance Spectroscopy: Theory, Experiment, and Applications.* Wiley.
40. Flis, J., Tobiyama, Y., Shiga, C., & Mochizuki, K. (2002). "J. Flis, Y. Tobiyama, C. Shiga and K. Mochizuki." *Journal of Applied Electrochemistry, 32*(2002), 401.

Journal of the Maharaja Sayajirao University of Baroda: Science & Technology
Vol. 58, 2024, pp. 55-62

Corrosion Inhibition Studies of Amino Acid – Aspartic Acid as Corrosion Inhibitor For Brass In Nitric Acid Environment

Shivani Kosada[1], Athira Moothandassery[1], A.A Patel2, M.B Mahida[1]

[1]Sir P.T Sarvajanik College of Science, Veer Narmad South Gujarat University, Surat-395007, Gujarat, INDIA

[2]Navyug Science College, Veer Narmad South Gujarat University,
Surat-395007, Gujarat, INDIA. shivani.kosada17@gmail.com

The detailed study of amino acid Aspartic acid as a corrosion inhibitor for brass in nitric acid solution has been performed through weight loss method, different temperature method, and polarization techniques. The experimental results show that Aspartic acid is a good corrosion inhibitor, and inhibition efficiency increases with the increase in inhibitor concentration, reaching a maximum value of 83.51% (in 0.5 M nitric acid concentration) at 20mM inhibitor concentration. The value of activation energy shows that aspartic acid is a good inhibitor for brass. The negative values of Q°ads support spontaneous adsorption of the inhibitor. Both the polarization technique and the weight-loss method yielded consistent results. The Tafel polarization study shows that it is a mixed type of inhibitor. The adsorption characteristic of the inhibitor on the brass surface obeys the Langmuir adsorption isotherm.

Keywords: *Corrosion inhibition, Amino acid, Aspartic acid, Metals, Corrosive media*

INTRODUCTION

Corrosion is a significant phenomenon that has a substantial impact on safety and economics, particularly for metals. A corrosion inhibitor is a chemical molecule that is adsorbed on the surface of a metallic substance to form a layer that isolates the metal's surface from reaction with the environment or inhibits the ions that attack the metal's surface. [1, 2]. When metals or alloys come into contact with hostile media, they oxidize, which can cause whole or partial surface damage. One of the best ways to prevent corrosion in metals and alloys is to employ inhibitors. An inhibitor is a substance that is added to a corrosive solution in modest amounts in order to slow down the rate of corrosion [3,4]. This resulted in the creation of a protective coherent layer on the metal surface, which was caused by the adsorption of inhibitor particles [5]. The organic molecules that contain heteroatoms (e.g., N, S, P, O) and multiple bonds along with some functional groups are thought to be the most effective corrosion inhibitors [6]. Additionally, it has been shown that organic molecules with the groups -OH, -COOH, -NH2, etc., are very effective at preventing corrosion, particularly in acidic conditions. Amino acids are among the chemicals that encouragers can utilize as safe corrosion inhibitors. They are biomolecules that have vital significance to all organism and they are the building blocks of proteins and many essential substances like neurotransmitters, hormones and nucleic acids. Amino acids are environmentally friendly compounds, completely soluble in aqueous media. As non-toxic chemical molecules, amino acids are easily synthesised at cheap cost and high purity and are biodegradable [7,8]. These Properties would support the use of them as inhibitors of corrosion.

RESEARCH SIGNIFINCANCE

Amino acids can be generally sorted into six main groups based on their structure and the chemical characteristics of their functional (R) groups: aliphatic, hydroxyl or sulfur-containing, cyclic, aromatic, basic, and acidic. Amino acids are molecules that must possess at least one carboxyl group and one amino group. Aspartic acid is an aliphatic. Aspartic acid is attractive due to the two carboxyl groups in their molecule. It can coordinate with metals, so it has been widely used as a corrosion inhibitor because it has the ability to control the corrosion of metal. Some related studies on the adsorption of Aspartic acid on metal surfaces were reported. The chemical structure of Aspartic acid is given in Fig(A)

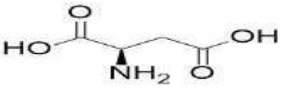

---

* Corresponding author.
Email: shivani.kosada17@gmail.com

Fig(A) Aspartic acid

MATERIALS AND METHODS

There are two very widely used methods to determine the corrosion rate: (1) weight loss and (2) polarization. The effects of temperature and concentration of the inhibitors were also studied. In this project, both of the methods of weight loss and polarization were employed. For the present investigation, brass with a composition of Cu- 69%, Zn-29%, and Sn less than 0.5% and traces of other impurities was chosen. A brass plate measuring 5.5 cm x 2.5 cm x 0.2 cm was cut from the sheet, and on the upper edge of the specimen, a small hole of 5 mm in diameter.

WEIGHT LOSS MEASUREMENT

Corrosion change is commonly assessed by weight loss; if metal is removed from the specimen by corrosion, the amount of metal can be determined by weighting the specimen before and after exposure. The corrosion rates may increase, decrease, or remain constant with time. The test time for exposure is invariably reported in each case. A more accurate method to get rate information in detail is suggested by Watcher and Treseder [9] known as the ‘Planned Interval Tests Technique', in which at least four identical specimens are exposed to the same environment under similar conditions and weight losses are measured at planned intervals. The post-exposure operation should be preceded by a visual inspection of the specimen for the formation of pits, deposits, etc. The corrosion products may be loose, strongly adherent, or tight. Passive films may be present on the surface. If the corrosion products are strongly adherent, true corrosion rates can be obtained by cleaning the metal surface. The corrosion rates can be expressed as variations in the weight per unit surface area per unit time or as penetration of the corrosive process into metal in unit time. The corrosion rate in mdd can be calculated using this expression.

$$\text{mdd} = 2400 \times \frac{w}{a} \times t \text{...................(1)}$$

Where ‘w’ is the weight loss (mg), ‘t’ the time(day) and ‘a’ the (surface area [cm2]), Corrosion rates are usually expressed in milligrams per square decimeter per day, i.e., mg/dm2/day (mdd). The inhibition efficiency (IE%) is calculated in percentage as follows:

$$\text{IE\%} = \frac{W_u - W_i}{W_u} \times 100 \text{............................. (2)}$$

Where W_u = weight loss of metal in uninhibited acid.

W_i = weight loss of metal in inhibited acid.

The coverage area of ‘θ’ of the metal surface was calculated from the equation

$$\theta = \frac{W_u - W_i}{W_u} \qquad \text{...... (3)}$$

W_u= weight loss of metal in uninhibited acid.

W_i= weight loss of metal in inhibited acid.

EFFECT OF TEMPERATURE

The value of the energy of activation (Ea) is calculated by the following equations [10]

$$\log \frac{\rho 1}{\rho 2} = \frac{Ea}{2.303\ R}\left(\frac{1}{T1} - \frac{1}{T2}\right) \qquad (4)$$

Where, ρ1 and ρ2 are the corrosion rates obtained by weight loss method at the temperaturesmT1 and T2 (K) respectively, and R is the gas constant.

Energy of activation (Ea) has been calculated from the slop of log ρ versus 1/T (ρ = corrosion rate, T= absolute temperature) with the help of Arrhenius equation [11]

Ea = 2.303 × R × slope........................ (5)

The almost similar values of Ea for all inhibitors suggest that the inhibitors were similar in their mechanisms of action.

The values of heat of adsorption (Q°ads) were calculated from the following equation [12]

$$Q^{\circ}_{ads} = 2.303\text{R}\{(\log \frac{\theta_2}{1-\theta_2} - \log \frac{\theta_1}{1-\theta_1}) . \frac{T_1\,T_2}{T_2 - T_1}\} (6)$$

Where $\theta 1$ and $\theta 2$ are the fractions of the metal surface covered by the inhibitor at temperatures T1 and T2 (K) respectively, and ‘R’ is the gas constant.

POLARIZATION MEASUREMENTS

When electrochemical corrosion occurs, the current that flows between anode and cathode causes a change in the electrode potential, this change is termed as polarization. Auxiliary platinum electrode was placed in a corrosive media through which external current was supplied from a regulated power supply. The electrochemical theory of corrosion had its origins of course, in more than one source.

The corrosion rate can be determined from the polarization data Using the Stern-Geary equation. The extrapolation of Tefal lines of anodic or cathodic curves to the value of ECorr in the Tafel intercept method is actually used in order to obtain the corrosion rate in terms or Icorr value.

$$\frac{\Delta E}{\Delta i_{app}} = \frac{\beta_a \beta_c}{2.3(I_{corr})(\beta_a + \beta_c)} \text{ .... (7)}$$

Where β_a and β_c are the Tefal slopes of the anodic and cathodic reaction respectively. The terms $\frac{\Delta E}{\Delta i_{app}}$ is given in ohms (milivolts/milliamperes).

This electrochemical technique of Tafel intercept has found wide use in evaluating the corrosion rates in the laboratory as well as in fields and the method is based on the equation very similar to that developed by Tafel. The basis of this technique which, the cathodic (β_c) and the anodic (β_a) Tafel slopes (lines) have been extrapolated to Ecorr in order to obtain the value of Icorr graphically. This figure also forms the basis of finding the cathodic exchange current density (loc) and the anodic exchange current density (Ioa) by further extrapolations of both the lines to the corresponding reversible potentials.

The value of IE% is calculated in percentage as

$$IE\% = \frac{I_{corr(w)} - I_{corr(inh)}}{I_{corr(w)}} \times 100 \text{.....................................} (8)$$

Where $I_{corr(w)}$ and $I_{corr(inh)}$ are the corrosion current densities without and with inhibitors, respectively.

RESULT AND DISCUSSION

Weight Loss Studies: The effect of acid concentration and exposure time on the corrosion loss of brass in nitric acid showed an increase in corrosion with time and more at higher acid concentrations. With a higher acid environment (2.0 M) strength, amino acids are found most effectively when inhibitor concentrations as high as 20 mM are maintained. At a higher concentration (2.0 M), Aspartic acid is found to be the most effective inhibitor. It can be said that to prevent corrosion reactions of brass in an acidic environment, derivatives of amino acids can be used safely as useful inhibitor.

Weight Loss at Different Temperatures: It was observed that the effect of temperature at 303K, 313K and 323K on corrosion and inhibition efficiency (IE%) of these amino acids was studied. The mdd values in table 4.4 increased from 836.87 at 303K to 941.71 at 323K in blank 2.0M (HNO3). Aspartic acid, when used as an inhibitor in an acid solution is found useful as an inhibitor. Aspartic acid employed in this acid environment is found to be a good eco-friendly inhibitor; however, at a 20 mM inhibitor concentration, there was 86.30% inhibition at 303K temperature and 80.90% inhibition at 323K temperature can be attained with the use of Aspartic acid.

Polarization Measurements: Potentiodynamic polarization studies were carried out in 2.0 M nitric acid with and without Aspartic acid. The values of Icorr were found to decrease in the presence of amino acids. The Icorr Value found for Aspartic acid inhibitor is mentioned in table 4.5. The decrease in Icorr values may be due to the adsorption of the inhibitor on the brass surface. This observation reveals that the inhibitor studied are effective inhibitor for the corrosion of brass in nitric acid.

CONCLUSIONS

Aspartic acid was found to be a good eco- friendly, non-toxic inhibitor for the corrosion control of brass in nitric acid solutions. The inhibition efficiency increases with an increase in amino acid concentration. It adsorbed on metal surfaces follow the Langmuir adsorption isotherm. The Tafel plot indicates aspartic acid acts as a mixed-type inhibitor. The two techniques give almost identical values of inhibition efficiency for brass in nitric acid. The values of activation energy are found to be higher in the presence of amino acid than in an uninhibited acid solution.

ACKNOWLEDGMENTS

The authors are thankful to the Chemistry Department, Sir P.T. Sarvajanik College of Science, Surat.

REFERENCES

1. El-Asri, A. Jmiai, Y. Lin, A. Taoufouq, M.M. Rguiti, H. Bourzi, and S. EI Issami, J. Corrs. Eng. Sci. Technol. (2022)
2. El Ibrahimi, A. Jmiai, L. Bazzi, and S. El Issami, Amino acids and their derivatives as corrosion inhibitors for metals and alloys, Arab. J. Chem. (2020)
3. S. Thomas, N. Birbilis, M.S. Venkatraman, and I.S. Cole, Corrosion (2012)
4. E. Yousif, Y. Win, A.H. Al-Hamadani, A.A. Al-Amiery, A.H. Kadhum, and A. Mohamad, Int. J. Electrochem. Science (2015)
5. H. Kumar, V. Yadav, A. Kumari, J. Phys. Chem. Solids, (2022)
6. A.S. Raja, S. Rajendran, J. Sathiyabama, and P. Angel, Int. J. Innov. Res. Sci. Eng. Technol. (2014)
7. B.E. Ibrahimi, A. Jmiai, L. Bazzi, S.E. Issami, Arab. J. Chem. (2017)
8. R. Loto, "Corrosion inhibition effect of a non-toxic α-amino acid compound on high carbon steel in a low molar concentration of hydrochloric acid", J. Mater. Res. Technol. (2019).
9. H. Ashassi-Sorkhabi, M. Majidi, and K. Seyyedi, Applied Surface Science (2004)
10. A. Watcher and R.S. Tresender, Chem. Engg. Progr. (1947)
11. N. Subramanian and K. Ramkrishna, Indian J.Tech. (1970)
12. S.A. Umrone, I.B. Obot, E.E. Ebsenso, N.O. Obi-Egbedi, Desalination (2009

TABLE-4.1: Effect of acid concentration on corrosion rate (mdd) and Inhibition Efficiency (IE%) of 70/30 Brass in HNO3 acid environment containing Amino acid. Effective Area of specimen: 31.5 cm2 (Temp. 303 ± 1K)

Inhibitor and its concentration (mM)		Acid Mixture Concentration (M)							
		0.5		1.0		1.5		2.0	
		CR (mdd)	I.E (%)	CR (mdd)	I.E (%)	CR (mdd)	I.E (%)	CR (mdd)	I.E (%)
I	mM	II	III	IV	V	VI	VII	VIII	IX
		83.65	-	240.38	-	672.07	-	849.98	-
Aspartic acid	1	27.12	67.75	115.2	52.07	255.10	62.03	381.86	55.07
	5	25.29	69.70	82.13	65.83	213.89	68.17	287.08	66.22
	10	16.70	80.15	74.36	69.06	115.96	76.79	165.48	80.53
	15	14.93	82.14	61.86	74.20	121.66	81.98	153.78	81.91
	20	13.79	83.51	60.64	74.77	70.17	89.55	49.39	85.97

TABLE-4.2: Weight Loss Data for Corrosion of 70/30 Brass in Nitric Acid Effect of Amino acid. Effective Area of Specimen: 31.5 cm2 , (Temp. 303±1K) , Immersion Time: 24 hr

Inhibitor and its concentration (mM)		Acid Mixture Concentration (M)							
		0.5				1.0			
		CR (mdd)	I.E (%)	Surface Coverageθ	$Log\ (\theta/1-\theta)$	CR (mdd)	I.E (%)	Surface Coverage θ	$Log\ (\theta/1-\theta)$
I	mM	II	III	IV	V	VI	VII	VIII	IX
		83.65	-	-	-	240.38	-	-	-
Aspartic acid	1	27.12	67.75	0.6775	0.3223	115.20	52.07	0.5207	0.0359
	5	25.29	69.76	0.6976	0.3630	82.13	65.83	0.6583	0.2847
	10	16.30	80.51	0.8051	0.6061	74.36	69.06	0.6906	0.3457
	15	14.93	82.14	0.8214	0.6626	61.86	74.26	0.7424	0.4595
	20	13.79	83.51	0.8351	0.7048	60.64	74.77	0.7477	0.4718

TABLE-4.3: Weight Loss Data for Corrosion of 70/30 Brass in Nitric Acid Effect of Amino acid. Effective Area of Specimen: 31.5 cm2, (Temp. 303±1K) , Immersion Time: 24 hrs.

Inhibitor and its concentration (mM)		Acid Mixture Concentration (M)							
		1.5				2.0			
		CR (mdd)	I.E (%)	Surface Coverageθ	$Log\ (\theta/1-\theta)$	CR (mdd)	I.E (%)	Surface Coverage θ	**$Log\ (\theta/1-\theta)$**
I	mM	II	III	IV	V	VI	VII	VIII	**IX**
		672.07	-	-	-	849.98	-	-	-
Aspartic acid	1	255.10	62.03	0.6203	0.2131	381.86	55.07	0.5507	0.0886
	5	213.86	68.17	0.6817	0.3307	287.68	66.22	0.6622	0.2923
	10	155.96	76.79	0.7679	0.5196	165.48	80.53	0.8053	0.6165
	15	121.06	81.98	0.8198	0.6579	153.75	81.91	0.8191	0.6558
	20	70.17	89.55	0.8955	0.9329	119.39	85.95	0.8595	0.7865

TABLE-4.4: Corrosion of 70/30 Brass in nitric Acid (HNO3) at Different Temperatures- Effect of Amino acid.
Area of Specimen 31.5 cm2, Immersion Time: 3 hrs, Acid Conc.: 2.0 M

Inhibitor and its concentration (mM)		Temperature (K)						gy of Activation-(Ea) (k.cal/mole)			
		303K CR (mdd)	I.E (%)	313K CR (mdd)	I.E (%)	323K CR (mdd)	I.E (%)	303-313K	313-323K	Mean Ea	Ea from Arrhenius plot
I	mM	II	III	IV	V	VI	VII	VIII	IX	X	XI
		836.87	-	905.14	-	941.71	-	1.4780	0.7957	1.1368	1.1440
Aspartic acid	1	375.46	55.31	507.73	48.31	647.31	31.20	5.6880	4.8798	5.2839	5.0471
	5	275.89	67.15	355.35	60.76	602.81	35.98	4.8388	10.6185	7.7286	7.7560
	10	161.52	80.69	22.47	75.43	408.99	56.56	6.0344	12.2330	9.1337	9.1521
	15	141.40	83.10	181.63	79.94	199.31	78.83	4.7191	1.8663	3.2927	3.2686
	20	114.5	86.30	149.33	83.51	179.80	80.90	5.0056	3.7308	4.3682	4.2900

TABLE 4.5: Tafel Parameters and Inhibition Efficiency (IE%) for Brass in 2.0M Nitric Acid Solution containing amino acid.Surface area of specimen: 31.5 cm2 Inhibitor Concentration: 20mM, Temperature: 25°C

Inhibitor	Open circuit Potential (mV)	Corrosion current density Icorr (μA/cm2)	Tafel slope (V / decade)		Inhibition efficiency(IE%) calculated from	
			Cathodic βc	Anodic βa	Polarization method	weight loss method
Blank	-112.0	12.40	113.70	74.50	-	-
Aspartic acid	-78.60	1.56	118.30	78.80	87.41	85.95

TABLE-4.6: Heat of absorption Q˚ads (kcal/mol) of 70/30 Brass in (2.0 M) Nitric Acid environment in presence of Amino acid.

Inhibitor	Temperature (K)	Inhibitor concentration (mM) and Heat of adsorption Q˚ads (kcal/mol)				
		1	5	10	15	20
Aspartic acid	303-313K	-10.796	-8.427	-5.811	-3.962	-4.909
	313-323K	-13.615	-20.305	-17.233	-1.364	-3.590

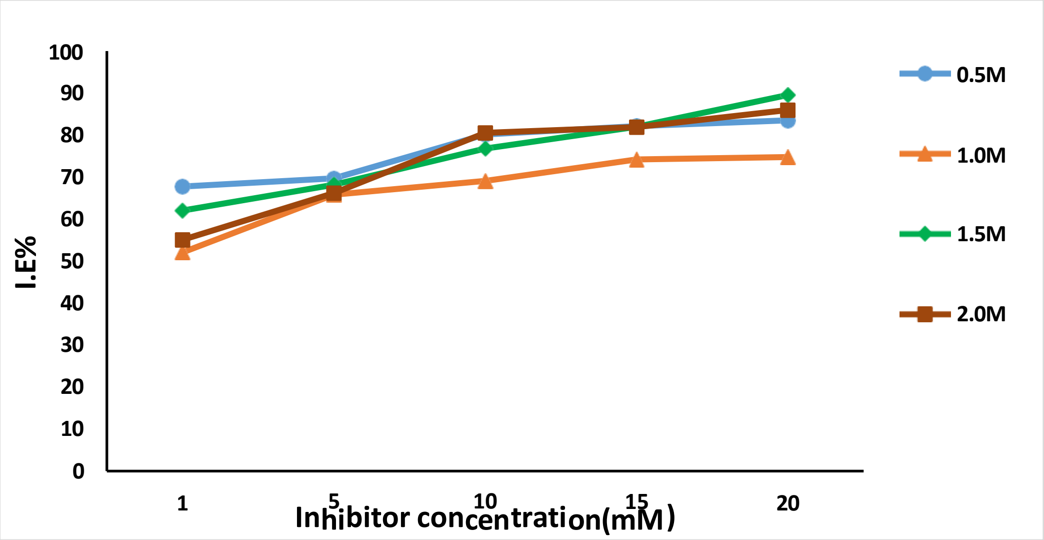

Figure 1: Effect of inhibitor concentration (mM) on I.E.% of Aspartic acid inhibitor for brass in nitric acid at 303±1K temperature for 24 h.

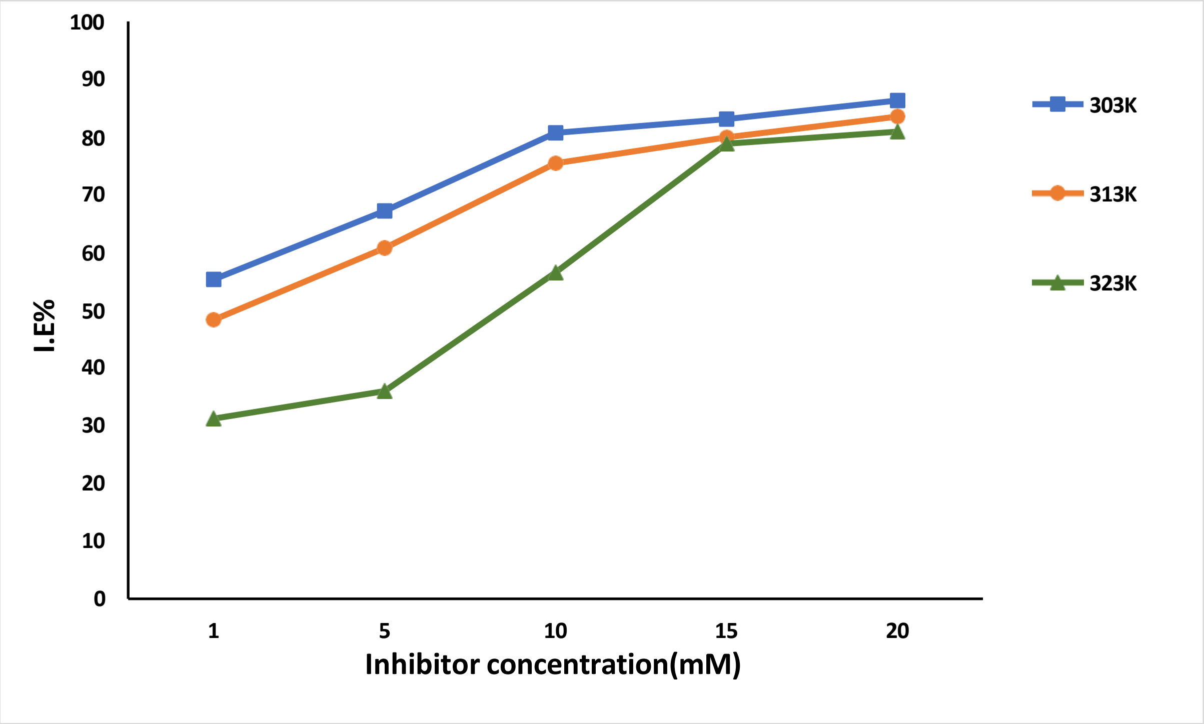

Figure 2: Effect of temperature on different inhibitor concentrations (mM) on the I.E% of Aspartic acid inhibitor for brass in nitric acid for 3 hrs. (Acid Conc.: 2.0 M)

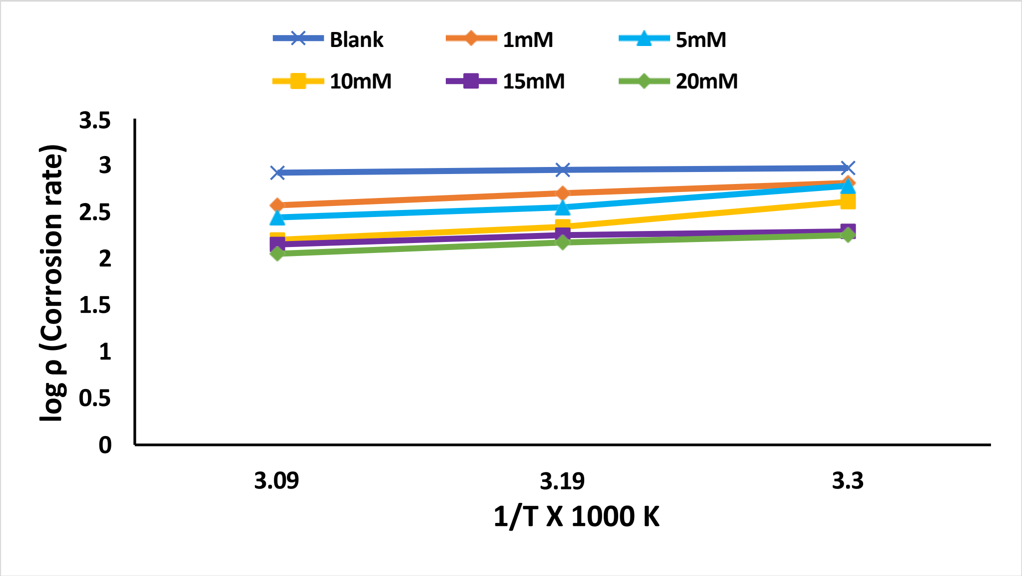

Figure 3: Arrhenius plot for corrosion of Brass in 2.0M Nitric acid solution in absence and presence of Aspartic acid.

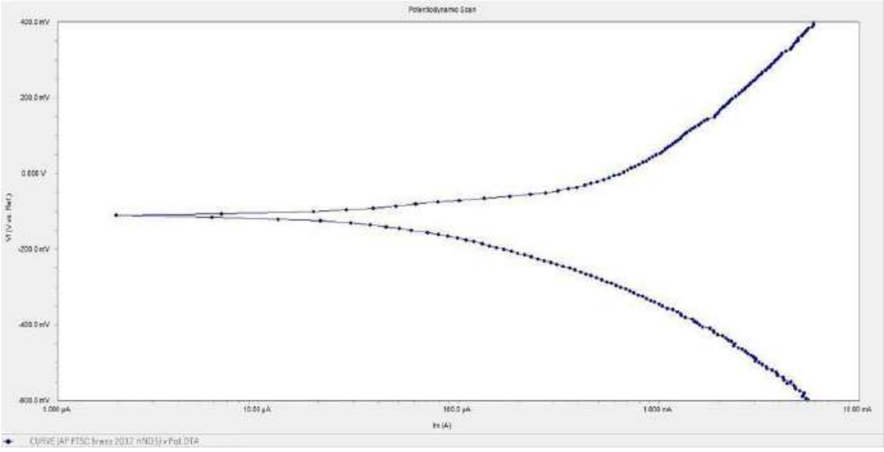

Figure 4: Polarization Curve for Corrosion of Brass in 2.0 M Nitric Acid Concentration for Blank.

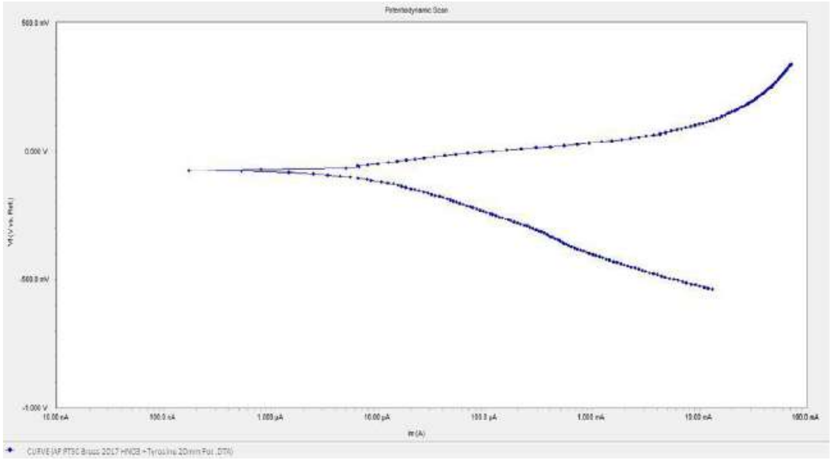

Figure 5: Polarization Curve for Corrosion of Brass in 2.0 M Nitric Acid Containing 20 mM Inhibitor Concentrations for Aspartic acid.

Journal of the Maharaja Sayajirao University of Baroda: Science & Technology
Vol. 58, 2024, pp. 63-69

Metallurgical Marvels: A Comprehensive Review Characterization & Corrosion Behaviour of Anodized Titanium Alloys

Nouman Kabutarwala, Faizan Ali Khan and Dr. Sunil Kahar

The Maharaja Sayajirao University of Baroda, Gujarat, India.

Anodizing is an electrolytic passivation process used to increase the thickness of the natural oxide layer on the surface of metal parts. Titanium is used as a biocompatible in different materials, in human implants, due to its excellent corrosion and wears resistance because of formation of very stable, continuous, highly adherent, and protective oxide films on metal surfaces. Anodizing of titanium generates an array of different colors without dyes, as the spectrum of different color formed is dependent on the thickness of the oxide, interference of light reflecting off the oxide surface and reflecting off the underlying metal surface. The anodized film of Titanium mainly consists of TiO2 and the mixtures of other titanium oxides, including TiO2, Ti2O3 etc.Using pure titanium plates as our canvases, we immersed ourselves in the enchanting realm of a Chromic Acid bath. Manipulating voltage ranges, we choreographed a symphony of colour, each hue indicative of diverse oxide compositions. Employing a methodology akin to a finely tuned ballet, our exploration unfolded through visual observation, SEM & EDAX analyses, Potentiodynamic studies, as revelations painted narratives of oxide variations, SEM & EDAX confirmed the artistic presence of TiO2 and Ti2O3. Potentiodynamic studies gracefully affirmed the corrosion resistance of our titanium masterpiece.

Keywords: Potentiodynamic Test, Anodizing Technologies, Metallurgical Excellence, Anodizing Technologies, Dynamic Resilience, Corrosion Resistance, Mechanical Prowess, Salt Spray Test (Fog Test), Process Optimization.

INTRODUCTION

Anodizing is an electrochemical process that converts the metal surface into a decorative, durable, corrosion-resistant, anodic oxide finish which can be used to increase the thickness of the natural oxide layer on the surface of metal parts. The process is called "anodizing" because the part to be treated is made anode in the electrolytic bath of acid solution. Anodizing increases corrosion resistance and wear resistance, and provides better adhesion for paint primers and glues than bare metal. Anodizing changes the microscopic texture of the surface and changes the crystal structure of the metal near the surface due to which it has got different spectrum of colors. Coatings are normally porous, which can be sealed to achieve better corrosion resistance. Titanium Anodizing is often used in the metal finishing of products, especially those used in the medical device, orthopedic implants, dental implants, and device components aerospace industries. The process provides the advantages of hardening and coloring the surface of titanium components without altering the mechanical properties of the metal. Imparting lasting color to a component's surface allows the easy identification of devices and parts. The benefits of this are essential in surgical applications and in the assembly of complex electronic or mechanical devices. Titanium is an extremely hard, durable metal used in a variety of applications. Anodizing titanium is a specialized capability which is not standard throughout the metal finishing industry. It is, however, essential to engineers and manufacturers who are relying more and more on the strength and applicability of titanium products in today's high-tech markets.

RESEARCH SIGNIFICANCE

This study carries substantial implications for both scientific understanding and practical applications, particularly in the field of anodized titanium and its pivotal role in biocompatible materials and medical implants. The findings are poised to address critical challenges faced by industries, especially those involved in medical device manufacturing. By unraveling the intricacies of oxide compositions formed during anodization, this research provides a foundational framework for optimizing anodizing technologies.

The societal and industrial importance of this work is underscored by its potential to revolutionize the way we approach surface modification of titanium. The comprehensive insights gained from this study can directly impact the development of medical implants, enhancing their corrosion resistance and wear durability.

---

* Corresponding author.
Email: sunil.d.kahar-metallurgy@msuaroda.ac.in

This, in turn, contributes to the longevity and reliability of implanted devices within the human body.

In Present review work the anodized film were microscopically analyzed by SEM & EDAX analysis, The anodized film of Titanium shows different spectrum of colors from Grey-Brown-Blue Yellow-Pink-Violet-Teal-Green due to different level of thickness of the oxide, interference of light reflecting off the oxide surface and reflecting off the underlying metal surface. SEM & EDAX analysis shows that the anodized film of Titanium is mainly made up of TiO_2 and Ti_2O_3 due to the inward diffusion of Oxygen ion & outward diffusion of Ti ion at Ti-electrolyte interface. Salt Spray Test and Potentiodynamic study reveals that the anodized film developed on Titanium using the bath of Chromic Acid exhibits good corrosion resistance. The A.C.Impedance study shows that the film having higher capacitance value as it is more compact, adherent and more uniform in case of bath in Chromic Acid bath.

The relevance of the research is emphasized by its role in closing existing knowledge gaps outlined in the introduction. While previous studies have acknowledged the biocompatibility and corrosion resistance of titanium, a comprehensive exploration of the diverse oxide compositions formed during anodization remains scarce. This work aims to fill this void, offering a more nuanced understanding of the oxide variations and their correlation with the mechanical and chemical properties of anodized titanium.

In essence, this study's broader impact is twofold: it addresses immediate challenges faced by industries relying on titanium for medical applications and contributes foundational knowledge that can guide future advancements in anodizing technologies. As the paper unfolds, the practical significance of these findings will become evident, opening avenues for improved materials engineering and surface modification techniques, with direct implications for both the scientific community and industries at large.

MATERIALS AND METHODS

In this section, the experimental procedures and methodologies employed in the research are detailed, ensuring a comprehensive understanding of the processes involved.

A. **Material Selection**

Pure titanium plates served as the substrates for the anodization process. The plates, sourced in compliance with ASTM standards, exhibited high purity, with a composition of 99.5% titanium. The decision to use pure titanium aimed to isolate the effects of the anodization process on the material without the influence of alloying elements.

B. **Anodization Process**

The anodization process was conducted in a controlled environment using a Chromic Acid bath. A series of pure titanium plates were immersed in the bath, and the voltage was systematically varied to orchestrate the desired array of oxide compositions. The anodization duration was precisely controlled to achieve uniform results across the experimental samples.

Chromic Acid Anodizing It produces coatings of exceptional corrosion and chemical resistance for its film thickness in an electrolyte, which is non-corrosive towards aluminum. These coatings are thin, and relatively soft and generally only used in specialized applications

C. Experimental Design

The experimental design encompassed a factorial arrangement, manipulating voltage levels and anodization durations as independent variables. This factorial design aimed to systematically explore the influence of these factors on the resulting oxide compositions. Multiple replicates were executed to ensure the robustness and repeatability of the findings.

E. **Experimental Setup**

Fig (1) experimental setup

In Anodizing, the cathode Ti or Graphite Rod and Anode (Test Sample) is arranged. By proper arrangement of Voltage and current different colors on Ti plate are obtained. We had selected baths of different concentration and voltage was varied from bath to bath and composition to composition. It was found that Coloring Effect on Titanium depends more on Voltage applied rather than other parameters. Moreover, no dyes were used in the process to obtain various colors. This is the unique feature of the process. Following Table gives Relation of Voltage, Time & Color appearance.

The voltage manipulation during anodization represented a departure from conventional techniques, providing a novel approach to induce specific oxide compositions. This unconventional method aimed to elucidate the direct impact of voltage variations on the resulting colours and oxide formations.

Table (1) Chromic Acid Bath

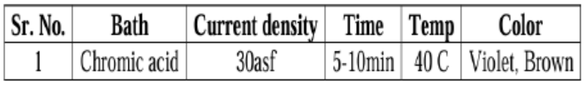

Sr. No.	Bath	Current density	Time	Temp	Color
1	Chromic acid	30asf	5-10min	40 C	Violet, Brown

A diagrammatic representation of the experimental setup is provided in the setup included a power supply for voltage manipulation, a controlled environment chamber for the anodization process, and a designated area for sample immersion and retrieval.

Material selected for anodizing was pure Titanium Metal of Commercial grade. 3.2 Sample Preparation The basic dimensions of the sample were 3x2x0.5 Cm which may vary by + or – (2-3 mm) due to human error. The sample were cut using Mechanical axe saw and Ti being a hard metal it took 15 minutes to cut one sample of required size. H.S.S blade was used in cutting and continuous water supply was fed as lot of heat was generated in cutting the sample.

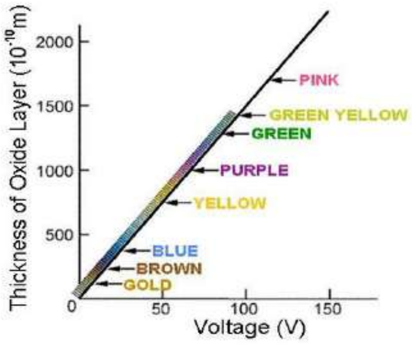

Fig [2]: Titanium Spectrum of voltage and Color

COLOURING EFFECT OF TITANIUM

The apparent color imparted to the metal is caused by interference between certain wavelengths of light reflecting off the metal and oxide coated surface. Light passing through the oxide layer, then reflecting off of the metal, must travel farther than light reflecting directly off the surface of the oxide. If one wave pattern is out of synch with the other, they will cancel each other out, making that particular color "darker" or not visible at all. If the thickness is such that a specific wavelength of light following one path closely synchronizes with that of the other path, then the wave strength (amplitude) will be increased, and that particular color would appear brighter. When the wave patterns cancel each other, it is called destructive interference, and when they match, it is constructive interference. It is possible that the thickness will create a combination of effects at the same time.

Table (2) Bath Composition for Chromic Acid

Sr. No	Bath Composition	Voltage	Time	Color
1	10 % Chromic acid	10 V	10 sec	Brown
2	10 % Chromic acid	50-55 V	10 sec	Violet
3	10 % Chromic acid	60-62 V	10 sec	Teal or peacock

Post Treatment 10 sec Green In post Treatment, after anodizing dipping of the sample into hot water or Hot water Sealing was done. In Hot water sealing, water is heated to 70 C and anodized Ti was kept in it for 3-4 minutes and then quickly dried using a dryer. This will improve the corrosion resistance of the metal and coloring effect will be shiny. If hot water sealing is not done the color of the film will become dull if kept in an Autoclave.

10% Chromic acid 100ml in 1 litre of distilled water.

No field investigation was conducted as the study primarily involved laboratory-based anodization processes.

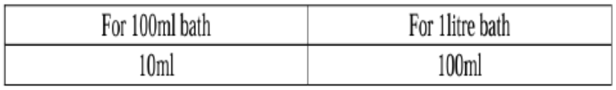

For 100ml bath	For 1litre bath
10ml	100ml

This detailed description of the materials, experimental design, and methodologies lays the foundation for the subsequent sections, presenting a clear framework for the systematic exploration of anodized titanium and its corrosion behaviour.

Corrosion Study For corrosion, studies of following tests were performed

Potentiodynamic Test →AC Impedance Test → Salt Spray Test → SEM & EDS. But before performing potentiodynamic test & AC Impedance test masking of the sample was done for both potentiodynamic test & AC Impedance Test. A 5*5 mm 1window was made on both sides of the sample and one window was sealed during one test to use a single sample for multiple tests. Insulating tape was used for masking of the sample

TESTS AND EVALUTAIONS

A scanning electron microscope (SEM)

SEM is a type of electron microscope that produces images of a sample by scanning it with a focused beam of electrons. The electrons interact with electrons in the sample, producing various signals that can be detected and that contain information about the sample's surface topography and composition. The electron beam is generally scanned in a raster scan pattern, and the beam's position is combined with the detected signal to produce an image. SEM can achieve resolution better than 1 nanometer. Specimens can be observed in high vacuum, low vacuum and in environmental SEM specimens can be observed in wet conditions.

Principles and Capacities: The types of signals produced by a SEM include secondary electrons (SE), back-scattered electrons (BSE), characteristic X-rays, light (cathodoluminescence) (CL), specimen current and transmitted electrons. Secondary electron detectors are standard equipment in all SEMs, but it is rare that a single machine would have detectors for all possible signals. The signals result from interactions of the electron beam with atoms at or near the surface of the sample. In the most common or standard detection mode, secondary electron imaging or SEI, the SEM can produce very high-resolution images of a sample surface, revealing details less than 1 nm in size. Due to the very narrow electron beam, SEM micrographs have a large depth of field yielding a characteristic three-dimensional appearance useful for understanding the surface structure of a sample. This is exemplified by the micrograph of pollen shown above. A wide range of magnifications is possible, from about 10 times (about equivalent to that of a powerful hand-lens) to more than 500,000 times, about 250 times the magnification limit of the best light microscopes. Back-scattered electrons (BSE) are beam electrons that are reflected from the sample by elastic scattering. BSE are often used in analytical SEM along with the spectra made from the characteristic X-rays, because the intensity of the BSE signal is strongly related to the atomic number (Z) of the specimen. BSE images can provide information about the distribution of different elements in the sample. For the same reason, BSE imaging can image colloidal gold immuno-labels of 5 or 10 nm diameters, which would otherwise be difficult or impossible to detect in secondary electron images in biological specimens. Characteristic X-rays are emitted when the electron beam removes an inner shell electron from the sample, causing a higher-energy electron to fill the shell and release energy. These characteristic X-rays are used to identify the composition and measure the abundance of elements in the sample.

Energy Dispersive X-ray Spectroscopy (EDAX):

Energy-dispersive X-ray spectroscopy (EDS, EDX, or XEDS) is an analytical technique used for the elemental analysis or chemical characterization of a sample. It relies on the investigation of an interaction of some source of X-ray excitation and a sample. Its characterization capabilities are due in large part to the fundamental principle that each element has a unique atomic structure allowing unique set of peaks on its X-ray spectrum. To stimulate the emission of characteristic X-rays from a specimen, a high energy beam of charged particles such as electrons or protons, or a beam of X-rays, is focused into the sample being studied. At rest, an atom within the sample contains ground state (or unexcited) electrons in discrete energy levels or electron shells bound to the nucleus. The incident beam may excite an electron in an inner shell, ejecting it from the shell while creating an electron hole where the electron was. An electron from an outer, higher-energy shell then fills the hole, and the difference in energy between the higher energy shell and the lower energy shell may be released in the form of an X-ray. The number and energy of the X-rays emitted from a specimen can be measured by an energy-dispersive spectrometer. As the energy of the X-rays is characteristic of the difference in energy between the two shells, and of the atomic structure of the element from which they were emitted, this allows the elemental composition of the specimen to be measured.

Salt Spray Test (Fog Test)

The salt spray test is a standardized test method used to check corrosion resistance of coated samples. Coatings provide corrosion resistance to metallic parts made of steel or brass. Since coatings can provide a high corrosion resistance through the intended life of the part in use, it is necessary to check corrosion resistance by other means. Salt spray test is an accelerated corrosion test that produces a corrosive attack to the coated samples in order to predict its suitability in use as a protective finish. The appearance of corrosion products (oxides) is evaluated after a period of time. Test duration depends on the corrosion resistance of the coating; the more corrosion resistant the coating is, the longer the period in testing without showing signs of corrosion. Salt spray testing is popular because it is cheap, quick, well standardized and reasonably repeatable. There is, however, only a weak correlation between the duration in salt spray test and the expected life of a coating, since corrosion is a very complicated process and can be influenced by many external factors. Nevertheless, salt spray test is widely used in the industrial sector for the evaluation of corrosion resistance of finished surfaces or parts.

Corrosion Study of Potentiodynamic Test

The procedure for sample preparation for the potentiodynamic and AC impedance test is same. The sample is covered with adhesive masking tape of water resistant quality. Then an exposed area of 0.25 cm2 is cut at one end and electrical connections are provided at other end the sample is exposed to two different corrosive environments. 3.5 % NaCl - Most naturally occurring highly corroding environment. 0.1N H2SO4 - Oxidizing Acid and same time very corrosive. Before this a continuity check is done where the continuity of the exposed area of the sample with the other end of the supply is checked by a digital multimeter. The cell is consisting of one counter electrode made up of graphite which is considered as inert. The cell also contains a standard electrode which is a standard calomel electrode (SCE). We introduce fresh solution for fibers coated in different baths. Both tests are carried out simultaneously without replacing the sample.

1. Potentiodynamic Test:-

Potentiodynamic – Done using potentiostat to study the corrosion rate and passivity behavior.

Model: EG&G PAR 273A & Gamry Potentiostat (reference 600)

Software: M273 & M398

Attachments: Computer system for data storage

Cell: 3 Electrodes

Working electrode: (Sample Specimen)

Reference electrode: (standard Calomel electrode)

Auxiliary electrode: (Graphite)

Principle: Works on the principle of Wheatstone bridge.

Procedure: The following flow sheet explains the working of software and working of potentiostat.

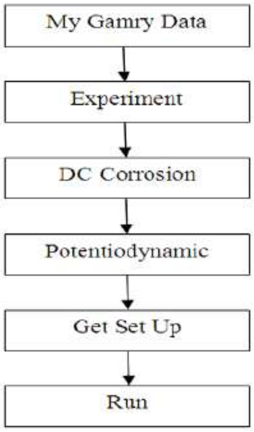

Analysis of different testing of titanium sample

In visual test, we observed different colors of anodized titanium plate. Here below is the list that we observed

Table (3) Anodizing of Titanium Plate

SR NO.	BATH	VOLTAGE(V)	TIME(SEC)	COLOUR
1	10% CHROMIC ACID	50-55	10	Violet
2	10% CHROMIC ACID	10-12	10	Brown
3	10% CHROMIC ACID	60-62	10	Teal or Peacock

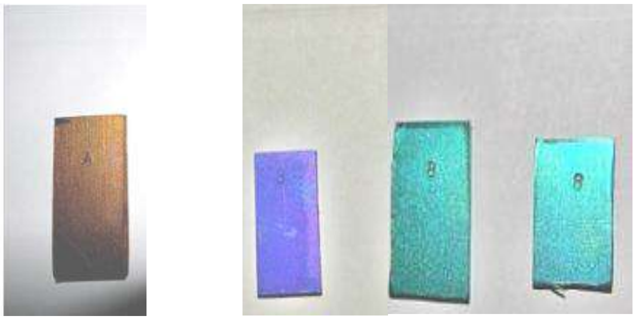

Fig 3 different type of colour Titanium Spectrum

The SEM & EDAX analysis shows that the anodized film developed on sample using bath (10% Chromic Acid) consists of TiO2 layer.

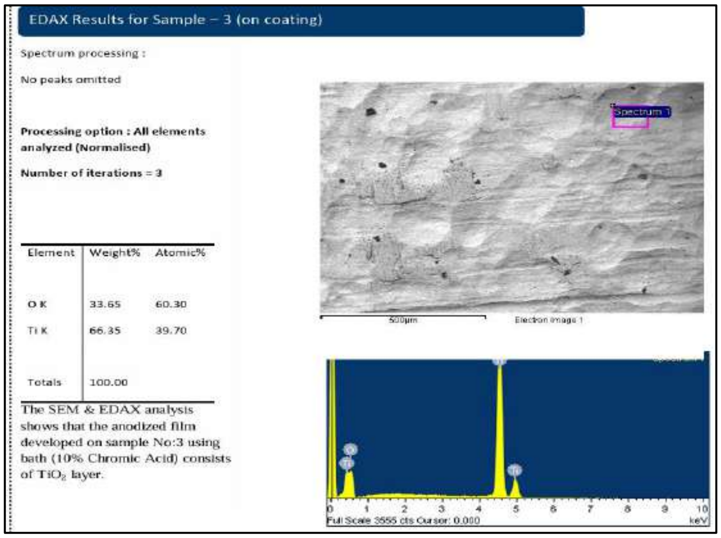

EDAX Results for Sample – 3 (on coating)

Spectrum processing :

No peaks omitted

Processing option : All elements analyzed (Normalised)

Number of iterations = 3

Element	Weight%	Atomic%
O K	33.65	60.30
Ti K	66.35	39.70
Totals	100.00	

The SEM & EDAX analysis shows that the anodized film developed on sample No:3 using bath (10% Chromic Acid) consists of TiO_2 layer.

Fig 4 : EDAX Study For Ti base Metal

Potentiodynamic study results for 0.1N H2SO4 For chromic acid bath

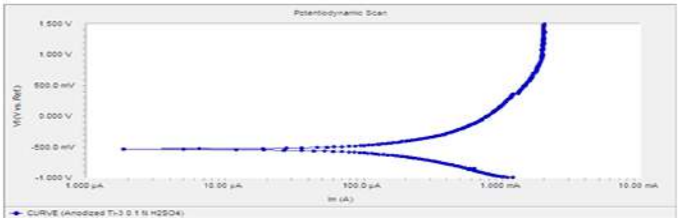

Fig : 6 Potentiodynamic Scan of Sample in H2SO4 solution

Table (4) Corrosion Rate in H_2SO_4 Solution

Ecorr.	Icorr.	Corr. Rate (mpy)
-532 mV	18.50 µA	25.80

shows active potential and having corrosion rate of 51.76 mpy in 0.1 N H2SO4 solution.

shows the potentiodynamic scan of Titanium anodized with Chromic Acid bath at different voltages in 0.1N H2SO4 solution. All samples exhibit active potential in given environment. Sample treated with bath of 10% Chromic Acid and 60-62 voltage range has best corrosion resistance among samples treated with Chromic Acid bath at different volts with Corrosion Rate of 25.8 mpy.

Results of Potentiodynamic test for 3.5% NaCl For chromic acid

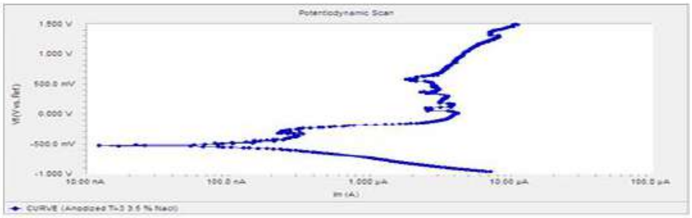

Fig : 7 Potentiodynamic Scan of Sample in NaCl solution

Table (5) Corrosion Rate in 3.5% NaCl

Ecorr.	Icorr.	Corr. Rate (mpy)
-528 mV	255 nA	0.3554

shows active potential and having corrosion rate of 0.3554 mpy in 3.5% NaCl solution.

shows the potentiodynamic scan of Titanium anodized with Chromic Acid bath at different voltages in 3.5% NaCl solution. All samples exhibit active potential in given environment. Sample treated with bath of 10% Chromic Acid at 50-55 voltage range has best corrosion resistance among all samples treated with Chromic Acid bath at different volts with Corrosion Rate of 0.3554 mpy.

CONCLUSION

From SEM & EDAX analysis, it can be concluded that the anodized film developed using different baths is consists mainly of TiO2 layer. From the potentiodynamic study of anodized film developed using different baths in 3.5% NaCl solution, it can be concluded that film developed with 10% Chromic Acid at 50-55 voltage range exhibits best corrosion resistance among all films

References:

1. http://en.wikipedia.org/wiki/Main_Page
2. http://www.electrohio.com/Finishing/TiAnodizing/TiAnodizing.htm
3. ASM Handbook - Volume 13A - Corrosion - Fundamentals, Testing, and Protection
4. http://www.valhallaarms.com/wyvern/titanium/anodizing.htm
5. SELF-COLOUR ANODIZING OF TITANIUM J.-L. DELPLANCKE, M. DEGREZ, A. FONTANA and R. WINAND Unwersitg Libre de Bruxelles -- CP 165, Department of Metallurgy and Electrochemistry, 50 avenue F. D. Roosevelt, B 1050 Brussels (Belgium)
6. Corrosion Engineering by Mars G. Fontana (3rd Edition)

7. Google Image Search
8. Anodizing titanium for space applications A. K. Sharma Thrrmul Systems Division, ISRO. (Received June 27. 1991; accepted August 29, 1991)
9. Electrometallurgy by Sharan & Narain.
10. J.-L. Delplancke,M. Degrez, A. Fontanaand R. Winand, Self colouring of Titanium, Surface (1982) pp 154 -158
11. Mr. Sunil D. Kahar, Arpit Macwan, Ms. Riddhi Oza, Vrund Oza, Smit Shah Characterization and Corrosion Study of Titanium Anodized Film Developed in KOH Bath, Int. Journal of Engineering Research and Application Vol. 3, Issue 5, Sep Oct2013, pp.441-442, www.ijera.com
12. A. K. Sharma, Anodizing Titanium for Space Applications, Thin Solid Films. (1992), P 48
13. A. Mazzarolo, M. Curioni, A. Vicenzo, P. Skeldon, G.E. Thompson, Anodic Growth of Titanium Oxide: Electrochemical Behaviour and Morphological Evolution, Electrochimica\ Acta 75 (2012) pp 289–291
14. Xuanyong Liua, Paul K. Chub, Chuanxian Dinga, Surface modification of titanium, titanium alloys, and related materials for biomedical applications, Materials Science and Engineering R 47 (2004) 49–121
15. Bangcheng Yang, Masaiki Uchida, Hyun-Min Kim, Xingdong Zhang, Tadashi Kokubo, Preparation of bioactive titanium metal via anodic oxidation treatment, Biomaterials 25 (2004) 1003–1010
16. M. Nakajima, Y. Miura, K. Fushimi, H. Habazaki, Corrosion Science 51 (2009) 1534 1539
17. Z. Liu, H. Liu, X. Zhong, T. Hashimoto, G.E. Thompson, P. Skeldon, Surface & Coatings Technology 258 (2014) 1025–1031
18. M. Manjaiah, Rudolph F Laubscher, Effect of anodizing on surface integrity of Grade 4 titanium for biomedical applications, Surface and Coatings Technology, Volume 310, 25 January 2017, Pages 263-272
19. Sunil D. Kahar, Corrosion Behaviour of Titanium Anodized Film in Different Corrosive Environments, Int. Journal of Engineering Research and Applications, Vol. 4, Issue 7(Version 6), July 2014, pp.17-2
20. Mr. Sunil D. Kahar, Characterization and Corrosion Study of Titanium Anodized Film Developed in KOH Bath, Int. Journal of Engineering Research and Applications, Vol. 3, Issue 5, Sep-Oct 2013, pp.441-445
21. Tiago Augusto Soares, HadiMozaffari, Holger Reinecke, Generation of microstructures on a Ti–6Al–4V substrate through anodization, Surface & Coatings Technology 278 (2015) 64–70
22. Naoya Masahashi, YoshiteruMizukoshi, Satoshi Semboshi, Kazuyo Ohmura, Shuji Hanada, Photo-induced properties of anodic oxide films on Ti6Al4V, Thin Solid Films 520 (2012) 4956–4964
23. Laís T. Duarte, Claudemiro Bolfarini, Sonia R. Biaggio, Romeu C. Rocha-Filho, Pedro A.P. Nascente, Materials Science and Engineering C 41 (2014) 343–348
24. M.V. Diamanti, M. Sebastiani, V. Mangione, B. Del Curto, M.P. Pedeferri, E. Bemporad, A. Cigada, F. Carassiti, Surface & Coatings Technology 227 (2013) 19–27

Journal of the Maharaja Sayajirao University of Baroda: Science & Technology
Vol. 58, 2024, pp. 70-73

Corrosion Prevention via Zn-Based Thermal Spray Coatings: Diverse Applications in NaCl Environments with Emphasis on the Oil and Gas Industry

Urvesh Vala[2], Vatsal Vala[1], Vinayak Joshi[1], I.B. Dave[3], Sunil D. Kahar[1]

[1]Dept. of Metallurgical and Materials Engg., The M.S. University of Baroda, India

[2] Research Scholer, Gujarat Technical University, Ahmedabad, Gujarat, India & L&T Energy Hydrocarbon Engineering Limited, L&T Knowledge City, Vadodara – 390019, urvesh.vala@larsentoubro.com

[3] Metallurgy Engineering, Government Engineering College, Sector-28, Gandhinagar -382028, Gujarat, India,

Surface coating is a reliable and cost-effective process which is widely used to obtain desired surface properties like corrosion, erosion and wear resistance for various components. Thermal Spraying is a type of surface coating which uses combination of thermal and kinetic energy leads to coating particles flattening and spreading on the substrate surface and creating full cover coating. Thermal Spraying have been widely used for many years throughout all the major engineering industry sectors like automotive power generation, aerospace, offshore marine environments, energy sectors for component protection and reclamation. Zinc thermal spraying is process where zinc or zinc alloys are melted and then sprayed onto a prepared substrate to create coating and is highly effective method for corrosion prevention, giving galvanic as well as barrier protection to iron and steel. Thermal spray process provides thickness range of 20 microns to several mm depending upon process and feedstock. Numerous coating materials are available like Zn, Al, Ni, Sn, Cu. The paper elucidates the multifaceted mechanisms underpinning corrosion processes, emphasizing the significance of Zn-based thermal spray coatings in mitigating degradation across various corrosive environments. Specifically, within the oil and gas domain, where equipment is constantly exposed to harsh conditions, the role of these coatings in safeguarding against corrosion is of paramount importance. Through meticulous examination, the review delineates the prowess of Zn-based thermal spray coatings in combatting corrosion in varied mediums such as acidic, saline, and atmospheric environments.

Keywords: Thermal Spray Coating, Zn Metal, Oil and Gas Environment

INTRODUCTION

Corrosion deteriorates materials inevitably by the chemical interaction with their environments. It is the returning of the materials to its original form (stable state) to the mother earth [1]. Corrosion, according to [2] is damaging to metals due to the attack by environmental reactions on material or metals, as well as by natural latent threats accompanied by oil and gas production and transportation. Corrosion represents an expensive problem for the industries of manufacture, chemical plants, oil industry and many more metal-using industries. Chemical leakage, oil pipelines breakdown and even fire can cause most corrosion problems: when exposed to electrical components and materials corroded. Different corrosion types include uniform corrosion, galvanic corrosion, corrosion of the crack, pitting, intergranular corrosion, and erosion. Cathodic and anodic chemical reactions between metals and their surroundings reduce corrosion of metals. The most important corrosion agents are water, air humidity, oppressive metal polishing, acids, oils, some solids, base salts, fluid chemicals, and even some Sulphur, ammonia and acidic-pH gaseous materials. Corrosion can also be defined as material collapse, usually air oxidation, and, sometimes, when it comes to water, acidic and alkaline mediums [3]. The

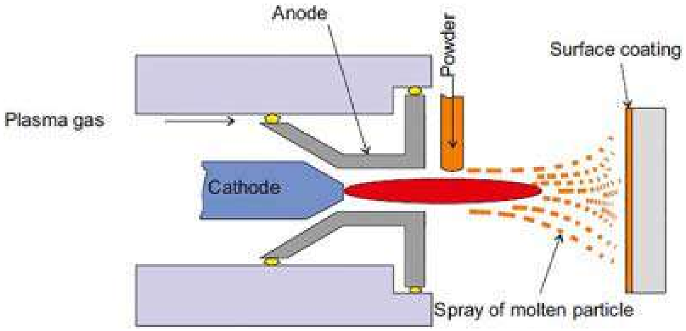

Fig. 1. Plasma Spraying Process

---

* Corresponding author.
Email: sunil.d.kahar-metallurgy@msuaroda.ac.in

most common form of corrosion is the corrosion of mild steel, especially in acid solution. This tends to limit its industrial applications on process safety and economics grounds coupled with environmental safety [4].

Thermal Spray Coating Techniques

Thermal spray coatings play a crucial role in contemporary industry, providing tailored surface properties for diverse industrial applications, including thermal barrier coatings for advanced turbine blades and erosion-resistant coatings for boiler tubes. Despite a significant surge in the adoption of thermal spray coatings, there is a noticeable delay in the development of methods to characterize and analyze these coatings [5]. The total coating thickness is usually generated in multiple passes of the coating device. The invention of the first thermal spray process is generally was attributed to in 1911 and was changes to being now known as flame spraying. Zinc thermal spraying is process where zinc or zinc alloys are melted and then sprayed onto a prepared substrate to create coating and is highly effective method for corrosion prevention, giving galvanic as well as barrier protection to iron and steel [6].

Electric Arc Wire Spray

Wire arc spraying is an inexpensive thermal spray deposition process in which the materials to be deposited are introduced into the plasma as wires in the form of consumable arc electrodes [7]. This leads to melting of substrate material. Compressed air atomizes and accelerates the material and sprays it onto work piece surface [8]. Spray rates are driven primarily by operating current and vary as a function of both melting point and conductivity. The process is energy efficient because all the input energy is used to melt the metal [9]. Arc spray coatings are normally denser and stronger than their equivalent combustion spray coatings. Low running costs, high spray rates and efficiency make it a good process for spraying large areas. Arc sprayed coatings also provide excellent resistance to atmospheric corrosion and are used on bridges and other infrastructure components. Most major aircraft engine manufacturers specify the use of the arc spray process for repairs of many aircraft engine components [7]. Electric arc spraying can also be carried out using inert gases or in a controlled-atmosphere chamber [8].

Plasma Spray Process

Plasma spraying involves the injection of powders into a direct current plasma jet, where they are melted and accelerated and directing the stream of molten particles onto a substrate, where they form a coating as they spread and solidify, as in Fig. 1. The adhesion of the particles to the substrate is mainly a mechanical bond. The high temperature (around 10,000 K) achieved in thermal plasmas allow the melting of any material, which does not decompose or vaporize excessively, within a very short time interval [9]. Because of low pressure, plasma becomes larger in diameter and length and has a higher gas speed. The absence of oxygen and the ability to operate with higher substrate temperatures produce denser, more adherent coating [10].

High Velocity Oxy-fuel Spray (HVOF)

In the HVOF process, fuel and oxygen are introduced to the combustion chamber together with the spray powder. The combustion of the gases produces a high temperature and high pressure in the chamber, which causes the supersonic flow of the gases through the nozzle. The powder particles melt or partially melt in the combustion chamber and during the flight through the nozzle. The flame temperature varies in the range of 2500 °C–3200 °C, depending on the fuel, the fuel gas/oxygen ratio and the gas pressure. In the HVOF process the particles melt completely or only partially, depending on the flame temperature, particle dwell time, material melting point and thermal conductivity [11].

Flame Spray Process

This process is the oldest of all thermal spraying processes. Flame spray uses combustible gases as a heat source to melt the coating material [12]. Flame spraying is a thermal spray coating process that produces high quality surface coatings using heat, from the combustion of a fuel gas with oxygen, to melt a spray coating material which is propelled onto a substrate. Flame spraying offers a cost-effective alternative for applying metallic and ceramic coatings in a less demanding environment. The utilization of the flame spraying surface treatment allows the spraying of a wide variety of metallic or ceramic coatings on to a large range of component materials where good wear resistance and excellent impact resistance are required [13].

MATERIALS AND METHODS

Protective coatings are unique method of corrosion control. They are used to give long term protection under a broad range of corrosive conditions, extending from atmospheric exposures to frill immersion in strongly corrosive solution. Protective solution provides little or no structural strength, yet they provide other material so that the strength and the integrity of a structure can be maintained. The function of protective coatings is to prevent highly corrosive industrial fumes, liquids, solids, or gases from contacting the reactive underlying substrate of the structure. This physical separation of two highly reactive materials, the atmosphere and the substrate, is extremely important [14]. In principle, any material that does not decompose as it is melted can be used as a thermal spray coating material [8]. Zinc is the most widely used metal for coating to gain protection against corrosion. The reasons behind the wide application of zinc for coating are as below:

- Zinc is much more abundant and affordable than any other metals used for coating.
- Because of attractive appearance helpful in decorative purpose.
- Zinc coating can be produced in wide range of textures and patterns.
- Zinc coatings are easy to apply and won't damage the substrate. Also, zinc can be used with a wide range of bath chemistries.
- If application involves painting, zinc can be an extremely effective undercoat due to its excellent adhesive properties [15].

Among these methods, the electric arc spraying process is environmentally friendly and can be used to effectively deposit surface coatings that have superior hardness and corrosion resistance. With equivalent combustion, coatings deposited by arc spraying are normally denser and stronger than those by other spraying technologies. Low running costs, high spray rates and efficiency make it a good process for spraying large areas [16]. Arc sprayed coatings can provide excellent resistance to atmospheric corrosion and are used on bridges and other infrastructure components. Hence, arc spraying can fully meet the requirements of the steel structure for long-term anticorrosion.

Although arc spraying has extensive application in the depositions of zinc coatings, it has some limitation. The zinc coating's density is low and it requires special installations. However, zinc-rich coatings are effective to overcome these disadvantages. They have been successfully used as anti-corrosion primers since the 1930s in a wide range of applications for protecting steels [17]. From the depositing process point of view, it does not require special installations and is quite available in the field. Furthermore, ZR coatings are suitable for heavier application such as in the marine environment [18].

Potentiodynamic Test of Electric Arc Spraying

A Potentiostat is an electrolyte device that is used to control the potential of a test electrode in an electrolyte. The magnitude of electrode potential changes (polarization) is determined by the amount of electrical current supplied by a potentiostat. Electrode potential is measured as the difference between itself a reference electrode.

Potentiodynamic Testing These studies were carried out to obtain potential (with respect to SCE) v/s log of current density plot which is known as polarization curve. The potential range was selected in a manner so the sample could be polarized both ways i.e. cathodically and anodically. It is used for:

1) Corrosion potential determination
2) Estimate corrosion current
3) Potential region for passivity

Potentiodynamic polarization test is mainly carried out to find the corrosion rate. Generation of polarization curves continuous to be important in aqueous corrosion research. Potentiostatic method is more time-consuming method. However, is has been replaced by potentiodynamic method, in which potential of the corroding metal is automatically varied with time. Potentiodynamic polarization test is most widely used electrochemical test to determine the potential region at which the alloy or metal is passive when exposed to particular environment. By using potentiodynamic method corrosion properties of passivating metals and alloys are identified. The method estimates the corrosion active region, the onset of passivation, the critical current density, the primary passivation potential, the current in the passive region, the voltage span of the passive region. This method can provide specific information regarding mechanism of corrosion, corrosion rate & susceptibility of particular materials to corrosion in specific environments.

Potentiodynamic test

A) Working Electrode (Test Specimen)

B) Counter or Auxilary Electrode

C) Reference electrode

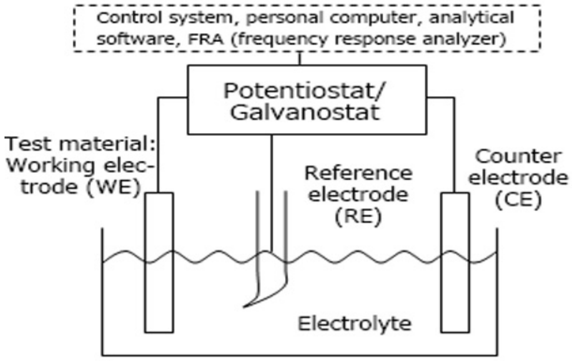

Fig. 2. Potentiodynamic Test Setup

Electrical current passing through a potentiostat can make change in a test electrode potential from its OCP is referred to as polarization. In order to maintain electronic equipment & Electrode electrical neutrality, current is supplied to a counter electrode. Difference between potentiostat & reference electrode is test electrode polarization. so it remains at its OCP and provides a 'fixed' reference point for corrosion measurement. The reference electrode provides feedback to the potentiostat so that test electrode potential can be monitored and adjusted to a desired level.

CONCLUSIONS

The major function of surface technology is to produce fictionally useful surfaces. Coating improves the life of the part and lowers the price of replacement. An extensive range of coatings can increase the corrosion, wear resistance and erosion of materials. From the study it is found that thermal spray coating is most important techniques of the surface modification.

In contrast to the absence of a passive region in the coating when exposed to a sodium chloride (NaCl) solution, a distinct passive region emerges in a methanol solution due to its considerably higher corrosion potential. Notably, observations from referenced sources indicate that in NaCl solutions, the arc-sprayed sample performs optimally at a concentration of 0.5%, surpassing the performance observed at 2%, 1%, and 4% NaCl solution concentrations.

Overall comparison of corrosion rate in NaCI solution, the arc spray is perform better compared to flame spray process while in the methanol solution the flame spray is better than the arc spray process. In this study the result shows in some environment the arc spray has good corrosion rate while, in some the flame spray has good. The high hardness, uniform coating thickness and continuous layer of coating can be obtained by using Flame spray process. Expect that wire arc spray also gaining importance now a days due to lower cost, high spray rate, and thicker coatings, and overall simplicity and flexibility.

REFERENCES

1. Bardal, E. (2003). Corrosion and Protection: Engineering Materials and Processes. Spinger: Verlag London Limited.
2. Gutti, B., Latinwo, G., Popoola, L., Balogun, A., & Grema, A. (2013). Corrosion problems during oil and gas production and its mitigation. International Journal of Industrial Chemistry, 4(1), 35.
3. Fayomi, O. S. I., Akande, I. G., Oluwole, O. O., & Daramola, D. (2018). Effect of water soluble chitosan on the electrochemical corrosion behaviour of mild steel. Chemical Data Collections, 17, 321-326
4. Aisha, M. A., Arab, T.S and Al-Reheli, A. A. (2010). Corrosion and Corrosion Inhibition of Mild Steel in H2SO4 solutions by Zizyphus spina-christi as Green Corrosion Inhibitor. International Journal of Chemistry.2(2)
5. https://www.sciencedirect.com/science/article/abs/pii/S1044580398000485
6. https://thermalsprayzinc.zinc.org/about-thermal-spray/
7. https://www.sciencedirect.com/science/article/abs/pii/S0924013605004243
8. “An Introduction to Thermal Spray” by SULZER INDUSTRIES
9. Sagar Amin, Hemant Panchal, (2016), “A Review on Thermal Spray Coating Processes”, International journal of current trends in engineering and research (IJCTER), ISSN: 2455-1392, Volume 2 Issue 4, pp. 556-563
10. https://www.sciencedirect.com/topics/materials-science/plasma-spraying#:~:text=Plasma%20spraying%20involves%20the%20injection,22.36.
11. Amardeep S.K., Singh, G. and Chawla, V. (2013), “Some Problems Associated with Thermal Spray Coating: A Review”, International journal of surface engineering and materials technology, volume 3, pp. 245-255
12. “Optimization and Characterization of High Velocity Oxy-fuel Sprayed Coatings: Techniques, Materials, and Applications”
13. Maria Oksa 1,*, Erja Turunen 1, Tomi Suhonen 1, Tommi Varis 1 and Simo-Pekka Hannula 2
14. Rakesh kumar, Santosh kumar , (2018), “Thermal Spray Coating : A study”, International journal of engineering science and research technology (IJESRT), ISSN : 2277-9655
15. https://www.bodycote.com/services/surface-technology/flame-spraying/
16. Sunil Kahar, Ashutosh Singh, Urvesh Vala, Aditya Desai, Smit Desai, International Research Journal of Engineering and Technology (IRJET) “Thermal Spray Coating Using Zinc: A Review”
17. I. Gedzevicius, A.V. Valiulis, J. Mater. Process. Technol. 175 (2006) 206–211.
18. R.A. Armas, C.A. Gervasi, A. di Sarli, S.G. Real, J.R. Vilche, Corrosion 48 (1992) 379.
19. H. Marchebois, S. Joiret, C. Savall, J. Bernard, S. Touzain, Surf. Coat. Technol. 157 (2002) 151–161.

Journal of the Maharaja Sayajirao University of Baroda: Science & Technology
Vol. 58, 2024, pp. 74-81

Bacopa Monnieri- A Novel Green Inhibitor for The Corrosion Inhibition Of Aluminium In Phosphoric Acid

K. N. Rathod[1], K. K. Patel[2] and R. T. Vashi[3]

[1]Department of Chemistry, M. B. Patel Science College, Anand, India
[2]Department of Chemistry, C. B. Patel Computer College & J. N. M Patel science College, Bharthana (Vesu), Surat, India
[3]Department of Chemistry, Navyug Science College,(Rander road) Surat, India
e-mail: khyatirathod43@gmail.com

The inhibition effect of bacopa Monnieri on the corrosion of aluminium in phosphoric acid was investigated by Weight loss method, Potentiodynamic Polarization and Electrochemical impedance measurement. It was conclude that inhibition efficiency increased with the increasing concentration of inhibitor. The investigation of adsorption isotherm indicate that the inhibitor fit Langmuir adsorption isotherm, fairly good. The phenomenon of physisorption is attributed to the values of Ea, Qads and ΔG0ads. The potentiodynamic polarization results reveal that the inhibitor acts as mixed type inhibitor. I.E. of inhibitor almost similar by weight loss method, polarization method as well as EIS methods.

Keyword: *Corrosion, Aluminium, Bacopa Monnieri, Phosphoric acid, Polarization, EIS.*

INTRODUCTION

Corrosion is a natural process, which converts refined metal to their more stable oxide. It is the gradual destruction of materials by chemical reaction with their environment [1]. the estimate of loss due to corrosion is approximately 2.5 billion dollers /annum all over the world. Hence it is necessary to understand the mechanism of corrosion studies of aluminium and its alloy are still of considerable interest because of their technological importance and industrial application, especially in automobile, aviation, household appliances, containers and electronic devices [2-5].

Aluminium is a silvery white, soft, ductile metal. Aluminium is the third most abundant element and the most abundant metal in the Earth's crust. It makes up about 8% by weight of the Earth's solid surface. Aluminium is remarkable for the metal's low density and for its ability to resist corrosion due to the phenomenon of passivation [6]. Corrosion resistance can be excellent due to a thin surface layer of aluminium oxide that forms when the metal is exposed to air, effectively preventing further oxidation.

Phosphoric acid (H3PO4) is widely used for acid cleaning and electro polishing of aluminium [7]. But it still strong corrosiveness on aluminium and its alloys. Therefore, it is necessary to seek inhibitors for the corrosion of aluminium in H3PO4 [8]. An extensive review of literature reveals that very little attention has been paid to inhibition studies on aluminium in phosphoric acid [3-5].The use of corrosion inhibitor is one of the most practical methods for protecting the corrosion of metal [9]. As a result, Corrosion inhibitors for hydrochloric acid, phosphoric acid and sulphuric acid have attracted increasing attention due to their extended applications. The protection of metals against corrosion by H3PO4 has been the subject of much study since it has been used in many industrial processes especially in fertilizer production.

RESEARCH SIGNIFICANCE

The main aim of this research work is to study the electrochemical behaviour of aluminium at different immersion time, temperature and concentration of Bacpoa monnieri (Brahmi) in H3PO4 solution using weight loss method and electrochemical techniques.

MATERIALS AND METHODS

To study the corrosion of aluminium in phosphoric acid several methods like weight loss, temperature effect, potential, polarization measurements and electrochemical impedance spectroscopy (EIS) have been used.

Aluminium sheets of the 2S type Aluminium (Al=99.54%, Si=0.090%, Fe=0.320%,Cu=0.0012%, Mn=0.0034%, Mg= 0.0014%, Cr= 0.0042%, Ni = 0.0046%, Zn = 0.0020%, Ti = 0.0079%, Pb = 0.0005% and Sn = 0.0026%) were used in this study. Rectangular specimens of aluminium having an area of 0.2797 dm2 were taken and cleaned by buffing and immersed in 0.10,

---

* Corresponding author.
Email: khyatirathod43@gmail.com

0.15, 0.20 and 0.25 M phosphoric acid concentration with and without inhibitor containing 230 ml test solution at 301± 1 K for 24 h immersion period. After the test, specimens were cleaned by chromic and nitric acid solution for a period of about 2 minutes [10]. After cleaning, test specimens were washed with distilled water followed by acetone and dried with air drier. The mean value of weight loss was reported as mg/dm2 shown in Table 1. All chemicals used were of AR grade. The corrosive solution was prepared in double distilled water.

Preparation of green inhibitors: Green inhibitor were prepared by following method as per chemical constitution of different leaves.

Bacopa Monnieri (Brhami) leaves extract

It was dried and blended to powder form, 10 gm powder was refluxed in 400 ml double distilled water for 5h. The refluxed solution was allowed to stand for 8h, filtered and stored. [26] The obtained filtrate was reduced to 10 ml. From the stock solution, a series of diluted solutions in 0.10, 0.15, 0.20 and 0.25 M H3PO4 were prepared with concentrations ranging from 1g/L to 4 g/L.

To study the effect of temperature on corrosion of aluminium in 0.1 M H3PO4, the specimens were immersed in 230 ml of corrosive solution and corrosion rate was determined at various temperatures like 313, 323 and 333 K for an immersion period of 2 h with and without inhibitor. From the data, I.E. (in %), energy of activation (Ea), heat of adsorption (Qads) and Gibbs free energy (ΔGa) were calculated and were shown in Table 2.

For polarization study, metal specimens were immersed in 230 ml corrosive solution without and with 4 g/L inhibitor concentration in 0.1 M H3PO4. The test cell includes the metal specimens as a working electrode, corrosive solution in which the specimen was to be tested and saturated calomel electrode (SCE) as a reference electrode as well as platinum electrode as an auxiliary electrode. The polarization study was made by using potentio-galvano-scan meter, polarization curves were plotted with potential against log current density (called Tafel plots). Cathodic and anodic polarization curves give cathodic and anodic Tafel lines correspondingly. The intersect point of cathodic and anodic Tafel lines gives the corrosion current (Icorr) and the corrosion potential (Ecorr) [11].

EIS measurement were carried out in the frequency range of 105 Hz to 0.1 Hz. The open circuit potential was measured after 30 minutes of immersion of electrode in test solution by applying amplitude of 0.005 V sine wave ac signal. EIS data were analysed using frequency response analyzer electrochemical set up. The charge transfer resistance (Rct), was obtained from the diameter of the semicircle of the Nyquist plot [12].

RESULTS AND DISCUSSION

The results are presented in Table 1 to 3 and in Figs. 1 to. To study the effect of corrosion of aluminium in phosphoric acid, bacopa monnieri was added as inhibitor.

I.E. has been calculated as follows:

$$\mathrm{IE}(\%) = \left\{\frac{(\mathrm{W_u} - \mathrm{W_i})}{\mathrm{W_u}}\right\} \mathrm{X}100 \qquad \dots(1)$$

Where, Wu is the weight loss of metal in uninhibited acid and Wi is the weight loss of metal in inhibited acid.

Energy of activation (Ea) has been calculated from the slop of log ρ versus 1/T (ρ= corrosion rate, T = absolute temperature) and also with the help of the Arrhenius equation [13].

$$\log\frac{\rho_2}{\rho_1} = \frac{\mathrm{E_a}}{2.303\mathrm{R}}\left(\frac{1}{\mathrm{T_1}} - \frac{1}{\mathrm{T_2}}\right) \qquad \dots(2)$$

Where ρ2 and ρ1 are the corrosion rate at temperature T1 and T2 respectively.

The value of heat of adsorption (Qads) were calculated by following equation [14].

$$\mathrm{Q_{ads}} = 2.303\mathrm{R}\left[\log\left(\frac{\theta_2}{1-\theta_2}\right) - \log\left(\frac{\theta_1}{1-\theta_1}\right)\right] \times \left[\frac{\mathrm{T_1 T_2}}{\mathrm{T_2 - T_1}}\right] \qquad \dots(3)$$

Where, $\theta_1$and θ_2 are the fractions of the metal surface covered by the inhibitors at temperature T1 and T2 respectively.

The value of ΔGoa from aqueous solution were calculated with the help of the equation [15],

$$\mathrm{K_{ads}} = \left(\frac{1}{55.5}\right)\exp\left(\frac{-\Delta \mathrm{G^0_{ads}}}{\mathrm{RT}}\right) \qquad \dots(4)$$

Where, $\mathrm{K_{ads}}$ can be calculated from following equation [16]:

$$\frac{\mathrm{C}}{\theta} = \frac{1}{\mathrm{K_{ads}}} + \mathrm{C} \qquad \dots(5)$$

Where, C = concentration of the inhibitor.

$\mathrm{K_{ads}}$ = equilibrium constant of the adsorption-desorption process.

The enthalpy of adsorption (ΔHoa) is calculated using the equation [17],

$$\Delta \mathrm{H^0_a} = \mathrm{E_a} - \mathrm{RT} \qquad \dots(6)$$

The entropy of adsorption (ΔSoa) is calculated using the equation [18],

$$\Delta \mathrm{S^0_a} = \frac{(\Delta \mathrm{H^0_a} - \Delta \mathrm{G^0_a})}{\mathrm{T}} \qquad \dots(7)$$

Corrosion in acid: The rate of corrosion increases with increase in acid concentration. The corrosion rate was found 389.7, 454.0, 486.2 and 525.6 mg/dm2 in 0.1, 0.15, 0.20 and 0.25 M H3PO4 concentrations respectively for a exposure period of 24 h at 301± 1 K as shown in Table 1.

Corrosion in presence of inhibitor: To assess their protective value bacopa monnieri was added in 1, 2, 3 and 4 g/Lit. concentrations in a solution of 0.1, 0.15, 0.20 and 0.25 M H3PO4 acid for 24 h duration period (Table 1).

Table 1: Corrosion rate (CR) and inhibition efficiency (I.E.) of aluminium in 0.10, 0.15, 0.20 and 0.25 M H3PO4 acid containing bacopa monnieri as an inhibitor for an immersion period of 24 h at 301± 1K.

Inhibitor	**Inhibitor concentration (g/L)**	**Acid concentration, M**							
		0.1		**0.15**		**0.20**		**0.25**	
		CR (mg dm^{-2}d^{-1})	**I.E. (%)**	**CR (mg dm^{-2}d^{-1})**	**I.E. (%)**	**CR (mg dm^{-2}d^{-1})**	**I.E. (%)**	**CR (mg dm^{-2}d^{-1})**	**I.E. (%)**
I	**II**	**III**	**IV**	**V**	**VI**	**VII**	**VIII**	**IX**	**X**
Blank	-	92.95	-	107.25	-	125.13	-	135.85	-
***BacopaMonnieri* (Brhami)**	1	64.35	30.77	78.66	26.66	92.96	25.71	107.26	21.05
	2	60.78	34.61	71.51	33.32	85.81	31.42	96.53	28.94
	3	53.63	42.30	67.93	36.66	82.23	34.28	92.96	31.57
	4	42.90	53.85	53.63	50.00	67.93	45.71	78.66	42.10

Table-2: Inhibition efficiency, corrosion rate and surface coverage of *Bacopa monnieri* extract on aluminium corrosion in 0.1 M phosphoric acid for an immersion period of 24h at 301 ± 1 K

Inhibitor	**Inhibitor concentration (g/L)**	**CR (ρ) (mg dm^{-2}d^{-1})**	**log ρ**	**I.E. (%)**	**surface coverage (θ)**	**1-θ**	**log (θ/1-θ)**
I	**II**	**III**	**IV**	**V**	**VI**	**VII**	**VIII**
Blank	**-**	92.95	1.9682	-	-	-	-
***BacopaMonnieri* (Brhami)**	1	64.35	1.8085	30.76	0.3076	0.6924	-0.3524
	2	53.63	1.7294	34.61	0.3461	0.6539	-0.2763
	3	42.9	1.6325	42.30	0.4230	0.5770	-0.1348
	4	64.35	1.8085	53.84	0.5384	0.4616	0.0668

Table-3: Temperature effect on corrosion loss (CL), activation energy (Ea) and heat of adsorption (Qads) for aluminium in 0.1 M H_3PO_4in absence and presence of Ficus religiosa extract for an immersion period of 2h.

Inhibitor	Inhibitor Concentration g/L	Temperature						Energy of activation (Ea)	Qads KJmol-1	
		313K		323K		333K		Mean	313-323K	323-333K
		CL mg dm-2	I.E. %	CL mg dm-2	I.E. %	CL mg dm-2	I.E. %			
I	II	III	IV	V	VI	VII	VIII	XI	XII	IV
Blank	-	50.05	-	132.28	-	271.71	-	73.04	-	-
Bacopa monnieri	1	39.33	21.42	107.26	18.92	228.82	15.79	76.06	-13.07	-26.47

	2	35.75	28.57	96.53	27.02	207.37	23.68	75.94	-6.49	-15.80
	3	32.18	35.71	89.38	32.43	182.34	32.89	74.83	-12.28	-1.87
	4	28.60	42.85	82.23	37.84	175.19	35.52	78.21	-17.51	-8.94

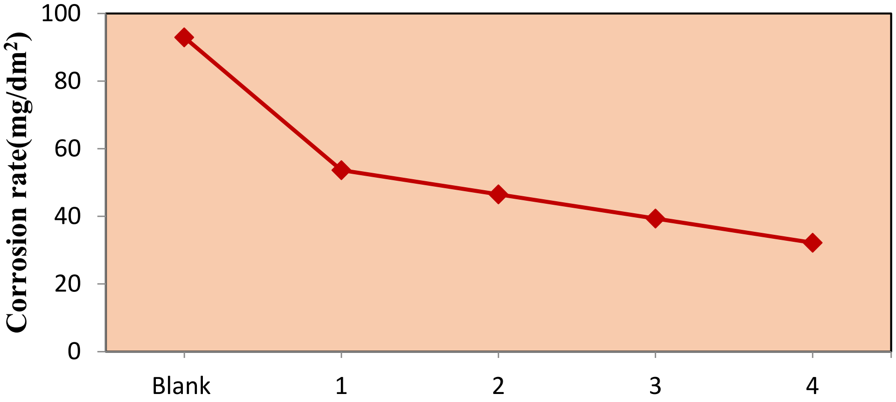

Figure 1.Inhibitor Concentratio(gm/lit)

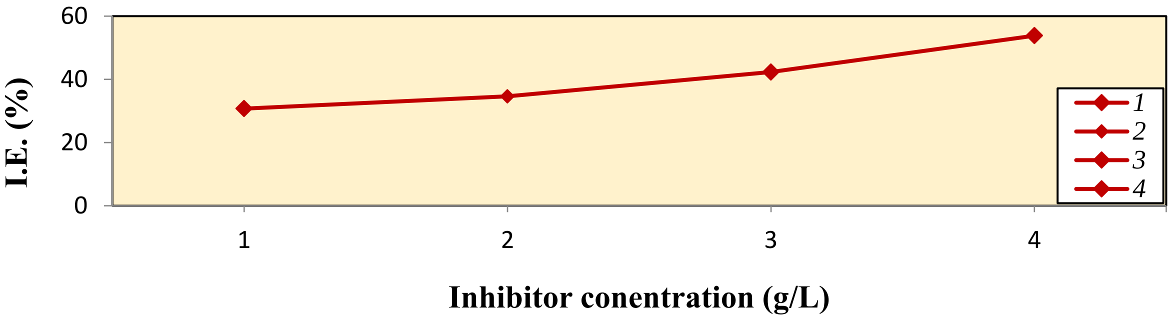

Fig. 2: Effect of inhibitor concentration on inhibition efficiency (I.E.) of green inhibitor for aluminium in **0.1 M** H_3PO_4 at 301 K. (immersion time 24 h)

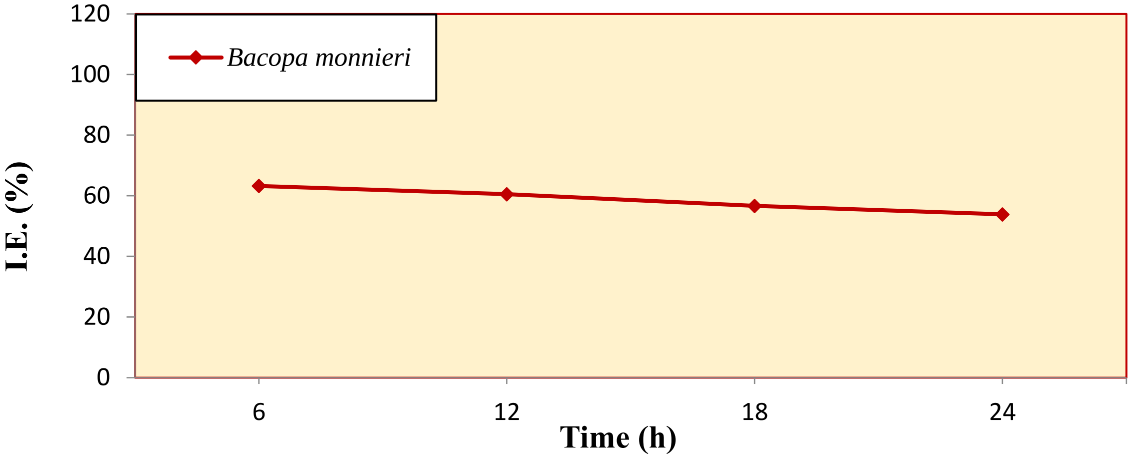

Fig. 3: Effect of immersion time on inhibition efficiency (I.E.) of aluminium in 0.1 M H_3PO_4 containing 4 g/L inhibitor concentration.

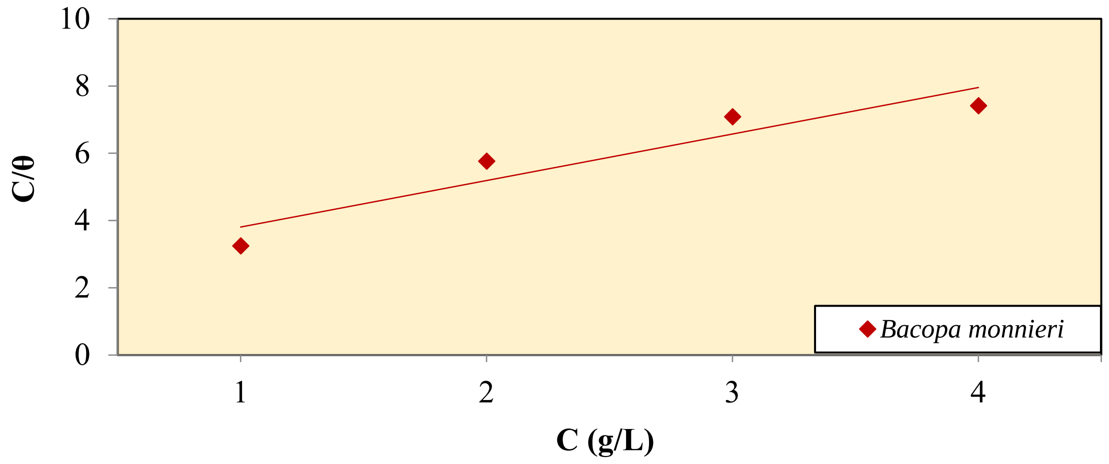

Fig. 4: Langmuir adsorption isotherm plot of C/θ versus 'C' for aluminium in **0.10 M** H_3PO_4 containing various green inhibitors at 301 K.

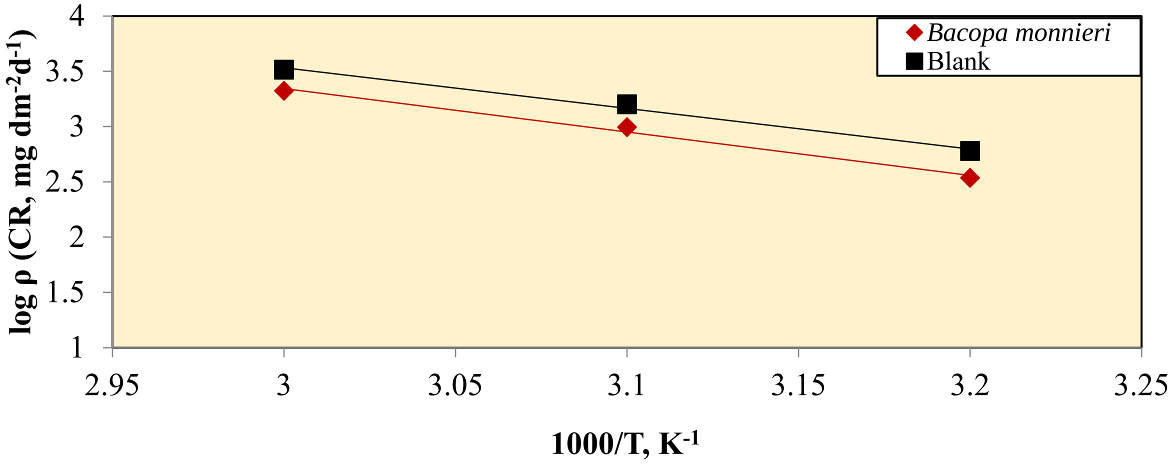

Fig. 5: Arrhenius plots of the corrosion rate of aluminium in 0.1 M H_3PO_4 in absence and in presence of **4 g/L** of various green inhibitor concentration.

Table-4: Potentiodynamic polarization parameters of Aluminium in in 0.1 M H_3PO_4 in absence and presence of *Bacopa monnieri* extract.

System	E_{corr}	CD	Tafel slope (V)		B	I.E.(%) from methods	
		I_{corr}	Anodic	Cathodic		By	By
	V	μA/cm^2	βa	βc	(V)	Weight loss	Polarization
Blank	-0.750	0.0009831	5.750	4.306	1.070	-	-
Bacopa monnieri	-0.622	0.0004839	7.075	3.943	1.100	53.84	50.77

Table -5: EIS parameters for Aluminium in 0.1 M H3PO4 in absence and presence of Bacopa Monnieri extract.

System	R_{ct} (ohm cm^2)	C_{dl} (μFcm^{-2})	From Weight loss (%)	From EIS (%)
Blank	291	4.241	-	-
Bacopa Monnieri	610	1.0441	53.84	52.29

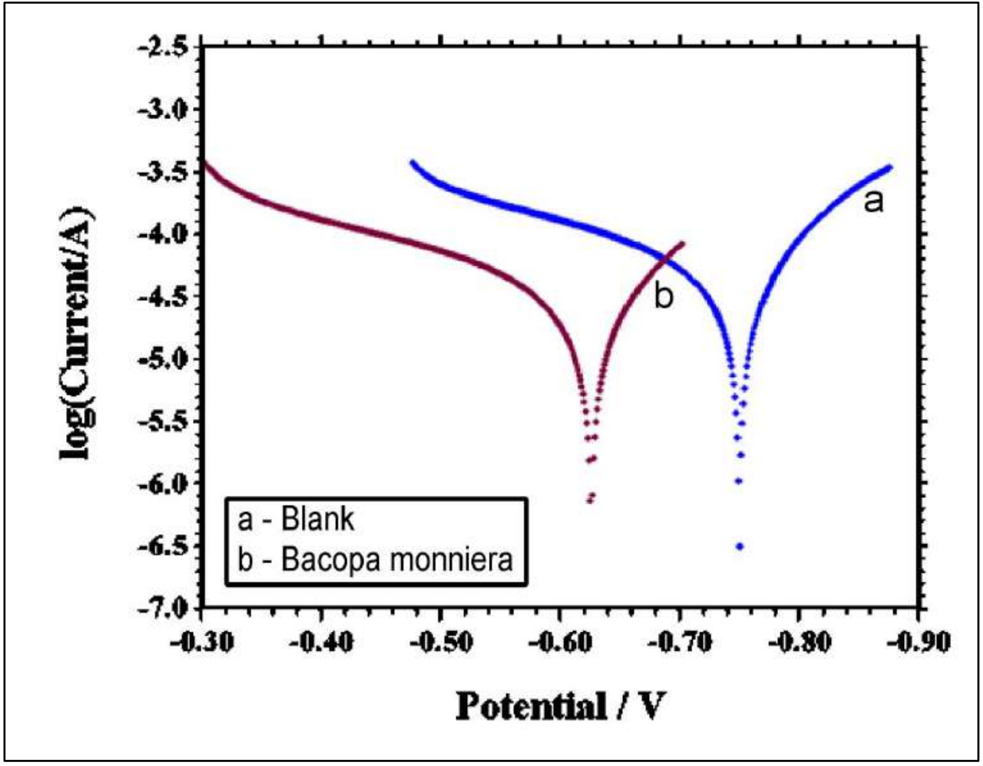

Figure 6. Potential Vs Current density

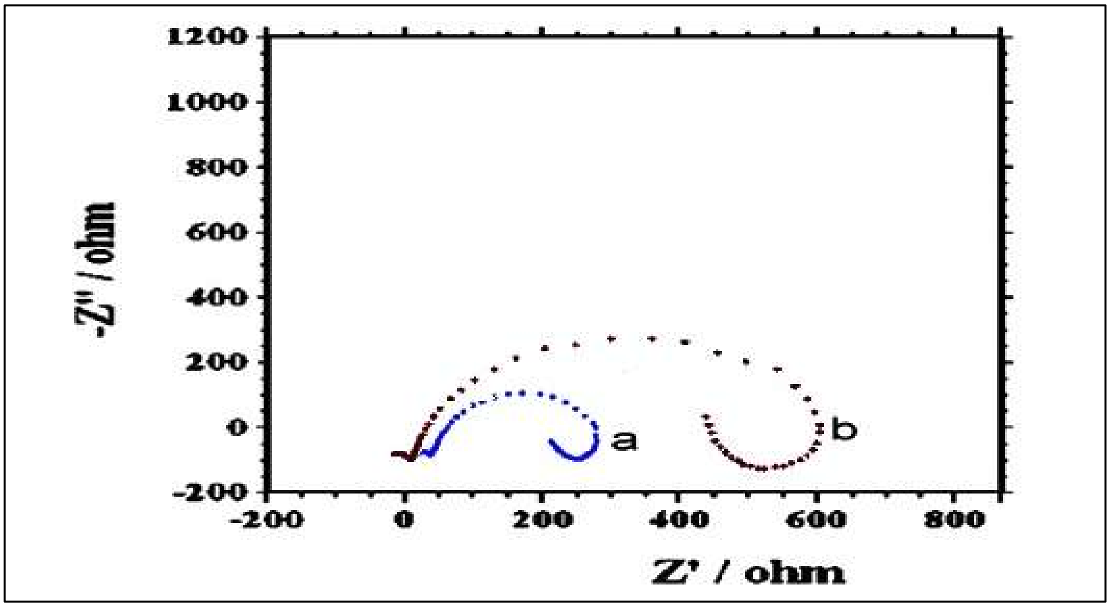

Fig. 7: Nyquist plot for aluminium in (a) 0.1 M H_3PO_4 and (b) 0.1 M H_3PO_4 in the presence of 4 g/L *Baccopa moneiri* extract.

Effect of inhibitor concentration: At constant acid concentration , the I.E. of the ammonium dichromate increases with the inhibitor concentration., In case of bacopa monnieri the I.E. was found to be 61.47, 70.64, 87.16 and 99.08 % with respect to 1, 2, 3 and 4mM inhibitor concentration respectively in 0.1 M H3PO4 (Table 1).

Effect of acid concentration: At constant inhibitor concentration, the I.E. decreases with the increase in acid concentration. At 4 mM inhibitor concentration, the I.E. of bacopa monnieri was found as 99.08, 94.49, 91.91 and 87.07 % with respect to 0.1, 0.15, 0.20 and 0.25 M acid concentration respectively (Table 1).

Effect of temperature: As the temperature increases, corrosion rate increases while percentage of I.E. decreases (Table 2). Mean 'Ea' values were calculated by using equation- 2 for aluminium in 0.1 M H3PO4 was 73.04 kJ mol-1 while in acid containing inhibitor, the mean Ea values were found to be higher than that of uninhibited system (Table 2). The higher values of mean Ea indicate physical adsorption of the inhibitors on metal surface. The values of Ea calculated from the slop of Arrhenius plot (Fig 2) and using equation 2 are almost similar. From Table 2, it is evident that in all cases, the Qads values are negative and ranging from -40.97 to -20.28 kJ mol-1. The mean ΔGa values are negative almost in all cases and lie in the range of -10.47 (1 mM) to -11.46 (4 mM). Thus suggest that they are strongly absorbed on the metal surface [19].The enthalpy changes (ΔHa0) are positive indicating the endothermic nature of the reaction and suggesting that higher temperature favours the corrosion process. The entropy (ΔSa0) values are positive confirming that the corrosion process is entropically favourable.

Polarization behaviour: Anodic and cathodic galvenostatic polarization data were shown in Table 3, which shows polarisation of both anodes as well as cathodes (Fig 3). In almost all the cases, the I.E. from Tafel plots agree well with the values obtained from weight loss data.

The electrochemical corrosion current density was evaluated using following equation.

$$\mathrm{I.E}(\%) = \frac{i_{corr(uninh)} - i_{corr(inh)}}{i_{corr(uninh)}} \qquad \dots(8)$$

u = uninhibited acid, i = inhibited acid.

Electrochemical Impedance Spectroscopy Measurements: The interfacial double layer capacitance (Cdl) values were obtained by determining the frequencies at which the imaginary component of the impedance is maximum f (-Z'max) using following equation:

$$\mathrm{C_{dl}} = \frac{1}{2\,\pi\, f_{max} \mathrm{R_{ct}}} \qquad \dots(9)$$

Where, Cdl= Double layer capacitance.

f (-Z'max) = The frequency at which the imaginary component of the impedance is maximum.

Rct = Charge-transfer resistance.

The percentage of I.E. was calculated from Rct values by using this equation 9:

$$\mathrm{I.E.}(\%) = \frac{\mathrm{R_{ct(inh)}} - \mathrm{R_{ct(uninh)}}}{\mathrm{R_{ct(inh)}}} \times 100 \qquad \dots(10)$$

$\mathrm{R_{ct(uninh)}}$= uninhibited acid and $\mathrm{R_{ct(inh)}}$= inhibited acid.

Impedance plots are semicircles both in the absence and in the presence of the inhibitor. The diameter of the capacitive loop increased with increase in the concentration of the inhibitor [20]. This indicates that the impedance of the inhibited substrate increases with the inhibitor concentration. Nyquist plots recorded for Al in 0.1M H3PO4 Solution without and with 4 gm/230ml concentration of Bacopa monnieri extract.

The results obtained suggest that the I.E. increases with increasing concentration of Bacopa monnieri leaves extract. The I.E. of Bacopa monnieri extract as obtained 53.85 % with 4 g/L inhibitor concentration in 0.1 M H3PO4 solution, which represented good inhibitive property. Adsorption of Bacopa monnieri stem extract can be explained on the basis that adsorption of the inhibitor was mainly via hetero atoms (viz.,N) present in different constituents of extract in addition to the availability of π electrons in the aromatic system [21]. The phytoconstituents of Bacopa monnieri stem includes Saponins, Monnierin, Hersaponin, Bacoside -A, Bacoside –B, Brahmine [22]. Some structure are given below:

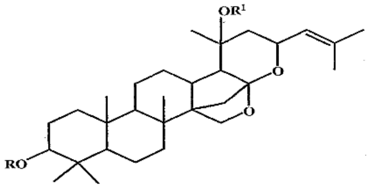

Bacoside – A

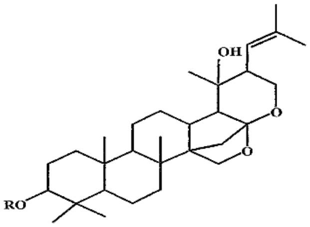

Bacoside – B

Structure of main constituents of Bacopa monnieri extract.

Bacopa monnieri extract as corrosion inhibitor was studied by various workers. The stem extract of Bacopa monnieri was investigated as a corrosion inhibitor for aluminum in 0.5 M sodium hydroxide solution by electrochemical and chemical methods [23]. Bacopa monnieri found as a mixed type inhibitor. These results were in good agreement with the work of Singh and Quraishi [24].

CONCLUSIONS

- As the acid concentration increases the corrosion rate increases.
- As the concentration of acid increases I.E. of inhibition decreases at all concentration of inhibitor.
- As the inhibitor concentration increases I.E. increases and corrosion rate decreases.
- As the temperature increases corrosion rate increases while I.E. of inhibitor decreases.
- Polarization measurements indicates that the inhibitor behave as a mixed type inhibitor.
- EIS spectra exhibit one capacitive loop which indicates that the corrosion reaction is controlled by charge transfer process.
- Extracts of Bacopa monnieri are found to be effective inhibitor in acid media giving up to 53.84 % efficiency and can be safely used without hydrogen damage, toxic effects and pollution.
- The importance of the study lies the fact that the naturally occurring plant products are environmentally compatible, non-polluting, easily available and biodegradable and cheaper corrosion inhibitors.

REFERENCES

1. Fontana M. G., Corrosion Engineering 3rd ed. MCgrew-Hill Book company, Singapore **(1910)**.
2. vargel C., corrosion of aluminium. Elsevier Ltd., New York, **(2004)**.
3. Kosting P. R.and Heins C. (1931) 'Corrosion of metals by phosphoric acid, *Ind. Eng. Chem.*, **23**, 140-150.
4. Badaway W. A., Alkharafi F. M. and El- Azab A. S.,(1994) Electrochemical behaviour and corrosion inhibition of Al., Al-6061 and Al-Cu in neutral aqueous solution., Corrosion Sci., 41, 709-727.
5. Desai P. S. and Kapopara S. M., (2009) Inhibiting effect of anisidines on corrosion of aluminium in hydrochloric acid., Ind. J. Chem. Tech., 16, 486-491.
6. Fonda A. S., Abdallah M., Ahmed I. S. and Eissa M., (2012) Corrosion inhibition of aluminium in 1M H3PO4 solutions by ethnolamines., Arabian J. of Chem., 5, 297- 307.
7. Vashi R. T. and Naik D. (2012), 4- aminoantipyrine as corrosion inhibitor for zinc in
8. phosphoric acid., Der pharma chemical., 4(14), 1471 -1476.
9. [8] Ameer M. A., Ghoneim A. A. and Fekry. (2012) A. M., Electrochemical corrosion inhibition of Al-Si alloy in phosphoric acid., Int. J. Electrochem. Sci., 7, 4418 – 4431.
10. [9] Uhlng's Corrosion Handbook, Second Edition, R. Winston Revie., Minister of Natural
11. resources., Canada, (1999).
12. [10] Vashi R. T. and Kadiya H. K., (2010) Asian J. of Chem., 22(2), 1151-1157 .
13. [11] Singh A., I. and Quraishi.M. A. (2012) Piper longum extract as green corrosion
14. inhibitor for aluminium in NaOH solution. Arabian J. of Chem.
15. [12] Ladha D. G., Naik U. J. and Shah N. K. (2013) Investigation of cumin (cuminium cyminum) extract as an eco – friendly green
16. corrosion inhibitor for pure aluminium in acid medium, J. Mater. Enviro. Sci., 4(5), 701-708.
17. [13] Vashi R. T., Bhajiwala H. M. and Desai.S. A. (2013) Hexamine as corrosion inhibitor for Zinc in (HNO3 + HCl) binary acid mixture, Multi Dsciplinary Edu Global Quest, 2(3).
18.
19. [14] Bataineh T. T., Al-Qudah,M. A., Nawafleh E. M. and Al Rawashdeh N. A. F. (2014) Sinapis alba extract as green corrosion inhibitor for aluminium in alkaline media. Int. J.
20. Electrochem.. Sci. 9, 3543-3557.
21. [15] T. H. Ibrahin, Y. Chehade and M. A. Zour, (2011) Int. J. Electrochem. Sci., 6, 6542-6556.
22. M. R. Singh, P. Gupta and K. Gupta (2015) Arabian J. Chem..
23. D. Agrawal, K. D. Gupta and K. K. (2003) Saxena,Trans. SAEST, 38, 111-114.
24. R. M. Issa, A. Z. El-Sonbati, A. A. El-Bindary and H. M. Kera (2002) Eur. Polym. J., 38 561.
25. Awad.M. I., (2006) Eco friendly corrosion inhibitors: inhibitive action of quinine for
26.
27. corrosion of low carbon steel in 1M HCl., J. of applied electrochem, 36,1163- 1168,.
28. Sherif E. M. and Park Su-Moon, (2006) Effects of 1,4 – naphthoquinone on aluminium
29. corrosion in 0.50M sodium chloride solutions., Electrochemica acta, 51, 1313 –
30. 1321,.
31. K. K. Lee, K.-B. Kim, (2001) Corros. Sci., 43 561.
32. T. Venu, D. Vishwanadham, P. R. Jayasree, P. R. Manish Kumar, Current Sci.,
33. 85, 10.
34. Singh, E. E. Ebenso and M. A. Quraishi, (2012) Int. J. Electrochem. Sci., 7,
35. 3409-3419.
36. Singh and M. A. Quraishi (2012) J. Chem. and Pharma Res., 4(1) 322-325.

Journal of the Maharaja Sayajirao University of Baroda: Science & Technology
Vol. 58, 2024, pp. 82-91

Eclipta Prostrata Leaf Extract as New Efficient And Ecologically Friendly Corrosion Inhibitor For Copper In Nitric Acid.

Athira Moothandassery[1], Shivani Kosada[1], M.B Mahida[1]*

[1]* Sir P.T Sarvajanik college of science,Surat-395007,Gujarat-INDIA

E-Mail : athiravijay1610@gmail.com

In this study, Eclipta prostrata' leaf extract, commonly known as Bhringraj was investigated as green eco friendly corrosion inhibitor of Copper in nitric acid solution using weight loss & polarization techniques. The study was also conducted at different temperature. The results reveal that the corrosion Inhibition efficiency (I.E) of Eclipta prostrata increases as the concentration of inhibitor increases and reached a maximum of 89.73% at 2000 ppm concentration, but the efficiency decreases with increase in temperature. The value of activation energy shows that Bhringraj is a good inhibitor of copper. Also, It obeys Langmuir's adsorption isotherm. The negative value of Qads portrays the spontaneous adsorption of the inhibitor on the copper surface. The Tafel Polarization states it as a mixed type of inhibitor. The results obtained from the weight loss and electrochemical techniques are studied and discussed in the paper.

Keywords: Copper, Inhibitor, Non-toxic, Corrosion, Green inhibitor

INTRODUCTION

Corrosion is not just an unavoidable natural phenomenon; it causes a deep impact on the economic aspects and jeopardize safety and hinder the efficiency. Hence, it becomes essential to prevent corrosion. According to the US National Association of Corrosion Engineers, the annual cost of corrosion is around USD 2.5 trillion[1]. Corrosion of metals is an important problem in industries causing great loss in total production, operation deficiencies, and high cost of maintenance. From previous reports, it is obvious that one of the best methods of protecting metals against corrosion entails the application of inhibitors which are additives that mitigate the rate of corrosion [2-7]. Discovery of various methods have been done since years to mitigate the rate of corrosion and overcome the losses due to corrosion. Use of inhibitors is one of the most common methods among them. Corrosion inhibitors are the chemical substances used to decrease the corrosion rate of the metals which are added in immensely low concentrations to the fluid[8]. A bad impact on environmental safety from the application of inorganic inhibitors made researchers turn their attention to organic compounds or natural products. The inhibition capability of these compounds corresponds to the availability of π electrons and functional groups such as –COOH, –COOR, –NR2, –NH2, –OH, –OR, and –SR [9-10]. Nevertheless, most commercial organic inhibitors are ineffective at high temperatures and the price is relatively expensive [11]. Besides, inhibitors from organic compounds must be synthesized and purified from natural sources. Consequently, more chemicals and energy are also required. This condition leads an increase in chemicals waste production. Now with the advent of green chemistry, Plant extracts and organic species have therefore become important as an environmentally acceptable, readily available, and renewable source for a wide range of inhibitors [12-17].

RESEARCH SIGNIFICANCE

Copper (Cu) finds its use in various applications because of its excellent electrical, good thermal conductivity and better mechanical properties. Its used mainly in making of sheets, wires and sheets. Copper also finds its use in cooling system of powerplants, automobile industries and various refineries. Copper and its alloys are generally resistant to corrosion however in aggressive medium its resistance lessens and it starts to corrode gradually.

The objective of this investigation is to find a cheaper and less harmful protection method to prevent the degradation of the metal.

---

* Corresponding author.
Email: athiravijay1610@gmail.com

MATERIALS AND METHODS

Eclipta prostrata, commonly known as false daisy, yerba de tago, guntagalagara aaku, Karisalankanni, and bhringraj, is a species of plant in the family Asteraceae. It is widespread across much of the world. This plant has cylindrical, grayish roots. Solid, circular, purplish stems with white fine hairs 0.8m. Leaves arranged in opposite pairs, hairy in two-sided, lanceolate, serrated 2–12.5 cm long, 5-35 mm wide. The solitary flower heads are 6–8 mm (0.24–0.31 in) in diameter, with white florets. The bumpy achenes are compressed and narrowly winged.

Fig: (A) Bhringraj plant

Fig: (B) Bhringraj leaf

Pharmacological action

It is harvested for its numerous therapeutic properties like an astringent, depurative, emetic, purgative, nervine tonic, catarrhal, febrifuge, ophthalmic, styptic, tonic, anti-nociceptive, anti-leprotic, anti-hemorrhagic, anti-myotoxic, anti-hyperlipidemic, anti-diabetic, hepatoprotective, diuretic, hypotensive, nootropic, anti-venom, ovicidal and spasmogenic. Bhringraj is a traditional plant, with plenty of ayurvedic uses. Bhringraj tastes tart, sharp, and bare. The Ayurvedic encyclopedia i.e. 'Raj Nighantu' explains the importance of this plant in great detail. The ancient use of Bhringraj in Raj Nighantu includes Kusthahara (Treat skin infections/diseases), Kesharanjaka (Hair protector/vitaliser), Raktapitta Shothahara (Treat blood disorders; Anti-inflammatory), Jantujit (Cure's worm trichinosis), Rasayana (Anti-ageing and Anti-cancerous), Pachana (Cures digestive problems), Kasahara (Cures cough and lung-related problems)

Many methods have been investigated for the study of corrosion inhibition process. Here in this study, two main methods are being focused (1)weight loss method & (2) Polarization study. The effect of temperature and inhibitor concentration are also studied and discussed in detail. The thermodynamic parameters for the process were computed and discussed.

Copper (Cu) metal sheet was brought and Purity assessment was performed. Copper here used consists of 93.17% Cu and 7.63% Zinc. Copper plate of 5.5 cm x 2.5 cm x 0.2 cm with a small hole of diameter about 5 mm on the upper edge of the specimen was cut from the sheet. The plates were buffed, cleaned properly with double distilled water and dried before using.

Here the medium used is HNO_3.Five different molar concentration of HNO_3 was prepared starting from 0.5M, 0.75M, 1.0M, 1.25M and 1.5M were used.

Preparation of Plant Extract

The alcoholic extract of roots of Eclipta prostra was brought and dried at 40°C and grinded into pure fine particles. The powder was reflexed with alcohol in 1:10 ratio respectively for 3 hours and filtered. The residue was removed and the filtrate was then followed up for fractional distillation from which alcohol was re-obtained and the thick slurry left behind was heated on sand bath and dried well. This solid extract was used to prepare the required concentration of green inhibitor.

Weight loss method

Weight loss is a very simple, cheap and helps in obtaining a quantitative data. It is necessary to run a blank experiment to find out the exact weight loss. After cleaning and weighing each specimen was suspended to the same depth below the surface of the liquid with help of glass hook. The volume of corrosive media was kept 200 ml and only one specimen was suspended in each vessel. This method approves only uniform corrosion and requires no complex equipment or procedures. A direct measurement is obtained with no theoretical assumptions or procedures. The only disadvantage of this method is that the corroding metal has a film of corrosion products and hence cleaning of specimens before and after exposure is critical to remove any contaminants that could affect the test results. Weight loss have been tested for the frequently expressed as loss in weight per unit area or loss in weight per unit area in per unit time. The Corrosion rate can be calculated by equation

$$\text{mdd} = 2400 \times \frac{w}{a} \times \text{t} \qquad \text{...... (1)}$$

Where 'w' is the weight loss (mg), 't' the time (day) and 'a' the surface area (cm2).

Corrosion rates are usually expressed in milligrams per square decimetre per day i.e. mg/dm2/day (mdd). Collection of corrosion data can be expressed either by conventional graphs or by ternary composition diagram having iso-corrosion lines for alloys. A less common way is to prepare a monographic chart to express approximate corrosion values. Conversion factors for interconversion of the units are also available. The inhibition efficiency (IE%) is calculated in percentage as,

$$\text{IE\%} = \frac{W_u - W_i}{W_u} \times 100 \qquad \text{.....(2)}$$

Where Wu= weight loss of metal in uninhibited acid.

Wi = weight loss of metal in inhibited acid.

The coverage area of 'θ' of the metal surface was calculated from the equation.

$$\theta = \frac{W_u - W_i}{W_u} \qquad \text{......(3)}$$

Wu= weight loss of metal in uninhibited acid.

Wi = weight loss of metal in inhibited acid.

Effect of temperature

During the investigation by weight loss measurements, it felt essential that the effect of temperature on the corrosion rate of the present system should be included and hence, the weight loss measurements are carried out at different temperature 303, 313 and 323 K using a constant temperature bath controlled automatically to the range of $\pm$2K of the desired temperature. Attention is paid to compensate the evaporation loss of electrolyte at different intervals of time to measure the corrosion rate accurately. The value of energy of activation (Ea) is calculated by the following equations.

$$\log \frac{\rho 1}{\rho 2} = \frac{E_a}{2.303\,R} \left(\frac{1}{T1} - \frac{1}{T2}\right) \qquad \text{........ (4)}$$

Where, ρ1 and ρ2 $a$re the corrosion rates obtained by weight loss method at the temperatures T1 and T2 (K) respectively and R is the gas constant.

The Ea value was also calculated from the slope of the plot of log ρ (corrosion rate/mg/dm2) versus $1/_T$ × 10-3.

Energy of activation (Ea) has been calculated from the slop of log ρ versus 1/T ($\rho =$ corrosion rate, T= absolute temperature) using Arrhenius equation.

$$\text{Ea} = 2.303 \times \text{R} \times \text{slope} \qquad \text{.......(5)}$$

The values of heat of adsorption (Q°ads) were calculated from the following equation:

$$Q^{\circ}_{ads} = 2.303\,\text{R} \left\{ \left(\log \frac{\theta_2}{1-\theta_2} - \log \frac{\theta_1}{1-\theta_1} \right) . \frac{T_1\,T_2}{T_2 - T_1} \right\} \quad \text{..(6)}$$

where θ1 and θ2 are the fractions of the metal surface covered by the inhibitor at temperatures T1 and T2 (K) respectively and 'R' is the gas constant.

Polarization Measurements

When electrochemical corrosion occurs, the current that flows between anode and cathode causes a change in the electrode potential, this change is termed as polarization. Auxiliary platinum electrode was placed in a corrosive media through which external current was supplied from a regulated power supply. The electrochemical theory of corrosion had its origins of course, in more than one source.

The corrosion rate can be determined from the polarization data Using the Stern-Geary equation. The extrapolation of Tefal lines of anodic or cathodic curves to the value of ECorr in the Tafel intercept method is actually used in order to obtain the corrosion rate in terms or Icorr value.

$$\frac{\Delta E}{\Delta i_{app}} = \frac{\beta_a \beta_c}{2.3(I_{corr})(\beta_a + \beta_c)} \qquad \text{......... (7)}$$

Where β_a and β_c are the Tefal slopes of the anodic and cathodic reaction respectively. The terms $\frac{\Delta E}{\Delta i_{app}}$ is given in ohms (milivolts/milliamperes).

This electrochemical technique of Tafel intercept has found wide use in evaluating the corrosion rates in the laboratory as well as in fields and the method is based on the equation very similar to that developed by Tafel. The basis of this technique which, the cathodic (β_c) and the anodic (β_a) Tafel slopes (lines) have been extrapolated to Ecorr in order to obtain the value of Icorr graphically. This figure also forms the basis of finding the cathodic exchange current density (loc) and the anodic exchange current density (Ioa) by further extrapolations of both the lines to the corresponding reversible potentials.

The value of IE is calculated in percentage as

$$IE\% = \frac{I_{corr(w)} - I_{corr(inh)}}{I_{corr(w)}} \times 100 \qquad \text{... (8)}$$

Where $I_{corr(w)}$ and $I_{corr(inh)}$ are the corrosion current densities without and with inhibitor respectively.

RESULTS AND DISCUSSION

Weight loss studies: The values of inhibition efficiency (I.E %) and the corrosion rate (CR) obtained from the weight loss method at different concentrations of HNO3 given in (table-1 to table-5) . The effect of acid concentration and exposure time on the corrosion loss of Copper in HNO3 showed increase in corrosion with time and more in higher acid concentration.

Weight Loss at Different Temperature

The weight loss data were also obtained to investigate the influence of temperature on the corrosion at 303, 313 and 323 K and also to determine the value of 'Ea' in the presence and absence of inhibitor Bhringraj in nitric acid. It was observed that with rise in the temperature, corrosion rate increased in blank 0.75M (HNO3) from 677.79 to 819.80 mdd at 303 and 323 K. However, the effect of different green inhibitors at different temperature to inhibit corrosion remained almost same. The value of activation energy (Ea) was slightly higher, but not remarkably high, in the presence of the Eclipta prostrathen the values in the blank acid (1.1440k.ca/mole). The values are obtained from Arrhenius plot, energy of activation (Ea) are given in the (table-6). it is evident that in all the cases, the Q°ads values are negative. The plots of effect of temperature on corrosion rate as shown in figure. The plots of inhibitor concentration versus activation energy are illustrated in figure.

Potential measurement

In 0.75 M HNO3 the potential shifted to the negative direction from its initial value. On addition of 2400ppm of the inhibitor Eclipta prostra (Bhringraj)in 0.75 M HNO3 the initial value of the OCP (open circuit potential) increased (become less negative) and settled at about within 5 minutes.

Potentiodynamic polarization studies were carried out in 0.75 M nitric acid with and without green inhibitors. The various electrochemical parameters such as corrosion potential (Ecorr, Corrosion current density (Icorr) the value of Tafel parameters (βa, βc, and β) were calculated from Tafel plot, were given in (Table-7).

The values of Icorr were found to be decrease in the presence of inhibitors. The decrease in Icorr Values can be due to the adsorption of the component of given plant roots extract on the Copper surface. This observation reveals that all the green inhibitors studied are effective inhibitors for the corrosion of brass in nitric acid. The Icorr Value found for green inhibitors were lower than that for 0.75 M nitric acid which is (Table- 7).

CONCLUSIONS

Roots of Eclipta prostra (Bhringraj) was found as an excellent eco-friendly inhibitor for the corrosion control of Copper in HNO3 solution. The inhibition efficiency increases with increase in Bhringraj concentration and an inclined temperature shows decrease in the efficiency of Green inhibitor. It adsorbed on metal surface as it follows Langmuir adsorption isotherm. From the Polarization and weight loss method, the efficiency has come in agreement with each other and shows an excellent efficiency of 89.37% in 0.75M HNO3 concentration with 2000 ppm concentration of inhibitor. Tafel plot indicates Bhringraj acts as a mixed type inhibitor. The two techniques give almost identical values of inhibition efficiency for Copper in HNO3.

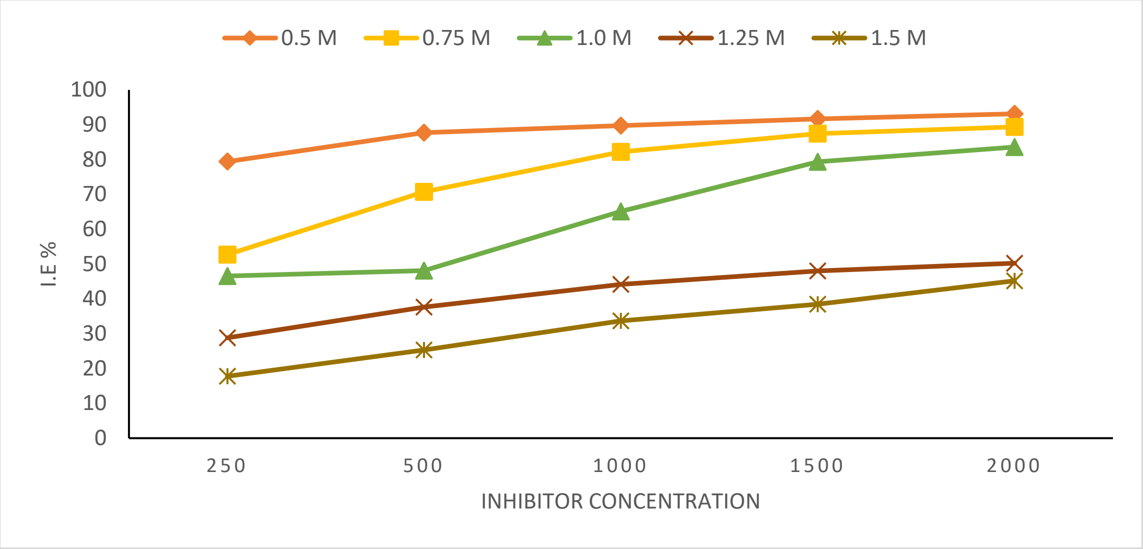

Figure 1: Effect of inhibitor concentration (ppm) on Corrosion Rate (mdd) of green inhibitor for Copper in nitric acid at 303±1K temperature for 24 h.

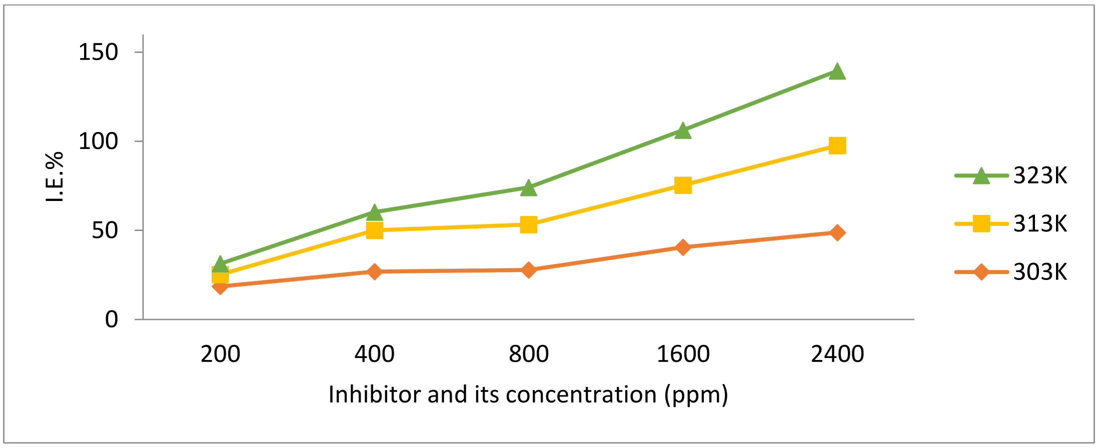

Figure 2: Effect of Temperature on I.E.% of green inhibitor for Copper in nitric acid

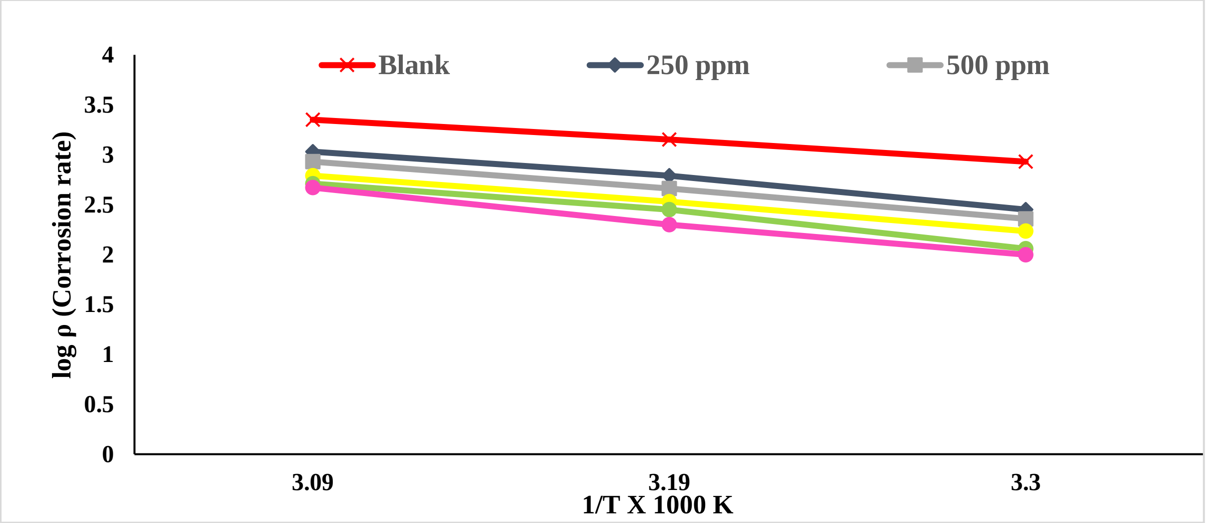

Figure 3 : Arrhenius plot for corrosion of copper in 1.0 M HNO3 solution in absence and presence of Bhringraj leafextract

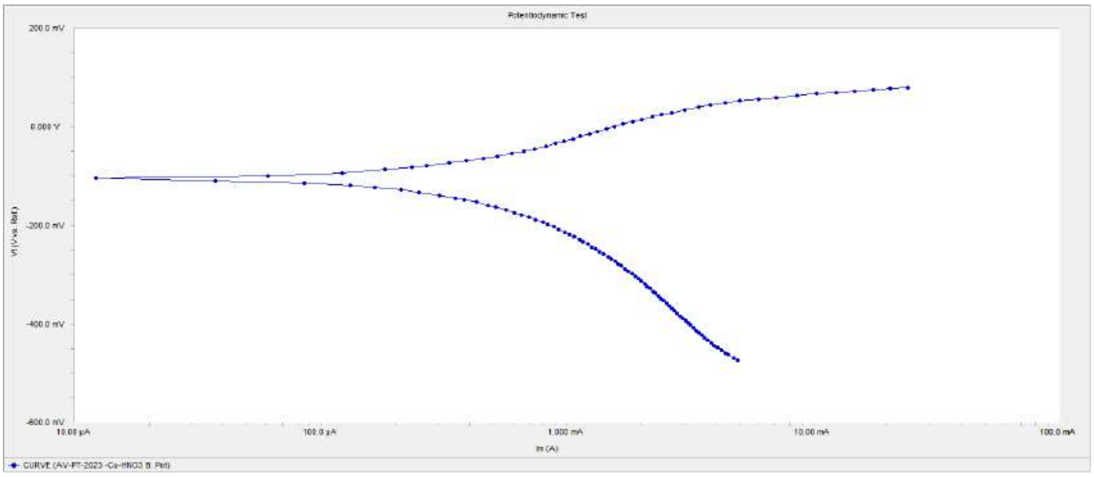

Figure : Blank

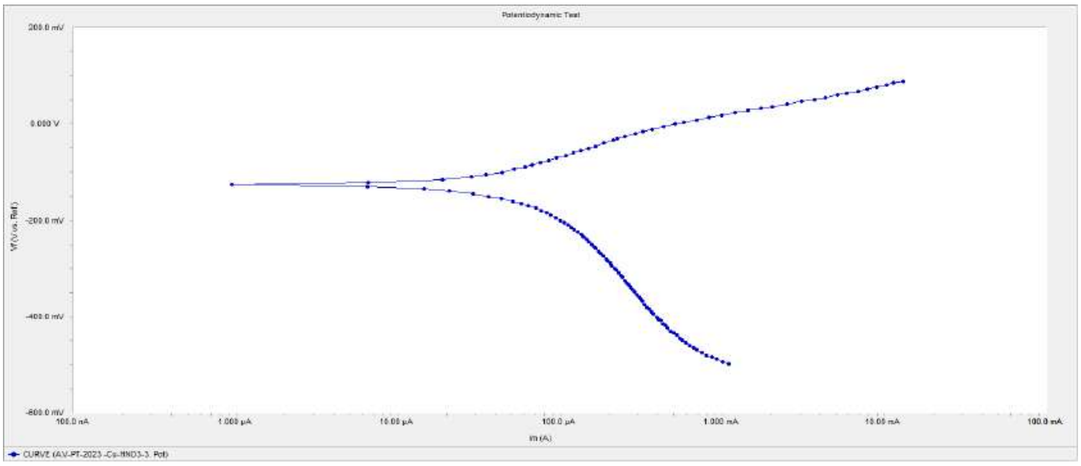

Figure : Bhringraj

Figure 4: Tafel Plot Effect of inhibitor concentration (ppm) on I.E.% of green inhibitor for Copper in nitric acid at different temperature for 3 h.

Table-1 : Effect of acid concentration on corrosion rate (mdd) and Inhibition Efficiency (I.E%) of Copper in nitric acid environment containing green inhibitor Bhringraj. Effective Area of specimen : 32.22 cm^2 (Temp. 303 ± 1K)

Inhibitor and its concentration (ppm)		Acid Mixture Concentration (M)									
		0.5* Corrosion rate and (mdd) II Inhibition Efficiency (IE %) III		0.75* Corrosion rate and (mdd) IV Inhibition Efficiency (IE%) V		1.0* Corrosion rate and (mdd) VI Inhibition Efficiency (IE%) VII		1.25* Corrosion rate and (mdd) VIII Inhibition Efficiency (IE%) IX		1.5* Corrosion rate and (mdd) X Inhibition Efficiency (IE%)	
I	ppm	II	III	IV	V	VI	VII	VIII	IX	X	XI
Blank	-	20.40	-	46.10	-	94.5	-	124.2	-	166.4	

BHRINGRAJ	250	4.20	79.41	21.88	52.71	50.54	46.56	88.40	28.82	136.8	17.78
	500	2.50	87.74	13.50	70.71	48.51	48.14	77.54	37.60	135.2	25.36
	1000	2.10	89.70	8.22	82.21	33.58	65.07	69.34	44.20	110.4	33.65
	1500	1.70	91.66	5.88	87.41	19.52	79.36	64.53	48.06	102.4	38.46
	2000	1.40	93.13	4.90	89.37	15.52	83.59	61.80	50.24	91.21	45.19

Table-2 : Weight Loss Data for Corrosion of Copper in Nitric Acid caused by Bhringraj. Effective Area of Specimen : 32.22 cm2 (Temp. 303±1K) Acid concentration: 0.5 M Immersion Time: 24 hrs.

Inhibitor and its concentration (ppm)		**Corrosion Rate (mdd)**	**Inhibition Efficiency (IE%)**	**Surface Coverage $\boldsymbol{\theta}$**	$\boldsymbol{Log}$ $(\boldsymbol{\theta}/\,\mathbf{1}-\,\boldsymbol{\theta})$
I	**ppm**	**II**	**III**	**IV**	$\boldsymbol{V}$
Blank		20.40	**-**	**-**	-
Bhringraj	250	4.20	79.41	0.7941	0.5862

<u>Table-3</u>: Weight Loss Data for Corrosion of Copper in Nitric Acid caused by Bhringraj.

Effective Area of Specimen : 32.22 cm2 (Temp. 303±1K) Acid concentration: 0.75 M Immersion Time: 24 hrs.

Inhibitor and its concentration (ppm)		Corrosion Rate (mdd)	Inhibition Efficiency (IE%)	Surface Coverage θ	Log $(\theta/\,1-\,\theta)$
I	ppm	II	III	IV	V
Blank		46.10	-	-	-
Bhringraj	250	21.88	52.71	0.5271	0.0471
	500	13.50	70.71	0.7071	0.3827
	1000	8.22	82.21	0.8221	0.6647
	1500	5.88	87.41	0.8741	0.8415
	2000	4.90	89.37	0.8937	0.9246

Table -4: Weight Loss Data for Corrosion of Copper in Nitric Acid caused by Bhringraj.

Effective Area of Specimen : 32.22 cm^2 (Temp. 303±1K)

Acid concentration: 1.0 M Immersion Time: 24 hrs.

Inhibitor and its concentration (ppm)		Corrosion Rate (mdd)	Inhibition Efficiency (IE%)	Surface Coverage θ	Log $(\theta/1-\theta)$
I	ppm	II	III	IV	V
Blank	-	94.5	-	-	-
Bhringraj	250	50.54	46.56	0.4656	-0.0598
	500	48.51	48.14	0.4814	-0.0323
	1000	33.58	65.07	0.6507	0.2701
	1500	19.52	79.36	0.7936	0.5848
	2000	15.52	83.59	0.8359	0.7070

Table-5: Weight Loss Data for Corrosion of Copper in Nitric Acid caused by Bhringraj.

Effective Area of Specimen : 32.22 cm^2 (Temp. 303±1K) Acid concentration: 1.25 M

Immersion Time: 24 hrs.

Inhibitor and its concentration (ppm)		Corrosion Rate (mdd)	Inhibition Efficiency (IE%)	Surface Coverage $\boldsymbol{\theta}$	$\boldsymbol{Log}$ $(\boldsymbol{\theta/1-\theta})$
I	ppm	II	III	IV	$\boldsymbol{V}$
Blank	-	124.2	-	-	--
Bhringraj	250	88.40	28.82	0.2882	-0.3926
	500	77.54	37.60	0.3760	-0.2199
	1000	69.34	44.20	0.4420	-0.1012
	1500	64.53	48.06	0.4806	-0.0337
	2000	61.80	50.24	0.5024	0.0041

TABLE-6: Weight Loss Data for Corrosion of Copper in Nitric Acid caused by Bhringraj

Effective Area of Specimen : 32.22 cm^2 (Temp. 303±1K) A cid concentration: 1.5 M Immersion Time: 24 hrs.

Inhibitor and its concentration (ppm)		Corrosion Rate (mdd)	Inhibition Efficiency (IE%)	Surface Coverage θ	Log $(\theta/1-\theta)$
I	ppm	II	III	IV	V
Blank	-	166.4	-	-	-
Bhringraj	250	136.8	17.78	0.1778	-0.6650
	500	135.2	25.36	0.2536	-0.4688
	1000	110.4	33.65	0.3365	-0.2948
	1500	102.4	38.46	0.3846	-0.2041
	2000	91.21	45.19	0.4519	-0.083

TABLE: 8 Effect of temperature: Heat of adsorption Q°ads of Copper in 1.0 M HNO3 in presence of Jethimadh inhibitor**.**

Inhibitor	Temperature (K)	Inhibitor's concentration (mM) and Heat of adsorption Q°_{ads} (kcal/mol)				
I	II	ppm				
=	=	250	500	1000	1500	2000
Bhringraj	303-313K	-38.01	-21.70	-19.65	-40.83	-20.45
	313-323K	-12.61	-21.75	-16.39	-13.38	-14.48

TABLE: 9 Tafel Parameters and Inhibition Efficiency (IE%) for Copper in 0.75 M Nitric acid solution containing green inhibitor.

Surface Area: 0.25cm2 Inhibitor conc.: 2000 ppm Temp: 28°C

Inhibitor	Open Circuit Potential (mV)	Corrosion Current density Icorr ($\mu A/cm^2$)	Tafel slope (V/Decade)		Inhibition efficiency I.E %	
			Cathodic βc	Anodic βa	Polarization Method	Weight loss Method
Blank	-106.0	2.250 X 10^{-3}	7.629	559.5	-	-
Bhringraj	-127.0	601.0	2.614	760.0	82.0%	89.97%

References

1. NACE Study "International Measures of Prevention, Application and Economics of Corrosion Technology". (accessed on 25 November 2022)
2. I.K Nwokolo, H.Shi, A.I Ikeuba, N.Gao, J.Li, S. Ahmed, F.Liu, Synthesis, Characterization and Investigation of Anticorrosion Properties of an Innovative Metal–Organic Framework, ZnMOF-BTA, on Carbon Steel in HCl Solution,Coatings 12 (9) (2022) 1288.
3. U.B Essien, M.E Ikpi, A.I Ikeuba, N.B Essien, Experimental and computational chemistry investigations of tartaric acid as a green inhibitor for API 5L X 52 Carbon Steel in 0.5 M HCl, Communications in Physics 7 (4) 2021, 482-193
4. I.N. Etim, D.I. Njoku, P.C. Uzoma, S.K. Kolawole, O.S. Olanrele, O.O. Ekarenem, B. O. Okonkwo, A.I. Ikeuba, I.I. Udoh, C.N. Njoku, W. Emori, Microbiologically Influenced Corrosion: a concern for oil and gas sector in Africa, Chemistry Africa 6 (2023) 779–804.
5. N.E Nya, A.I Ikeuba, P.C Okafor, B.U Ugi, V.M Bassey, A.I Obike, Mild Steel corrosion mitigation in sulphuric acid via benign isolated phytochemicals from viscum album, J.Mater.Sci.Chem.Eng.6 (2018) 132-146.
6. B.U Ugi, M.E Obeten, A.I Ikeuba, Inhibition efficiency of eco-friendly green inhibitors (ocimum tenuiflorum phytocompounds) on corrosion of high carbon steel in HCl environment using thermometric and electrochemical methods, Journal of Advanced electrochemistry 4(1) (2018) 158-16.
7. G.Karthik, M. Sundaravadivelu, Studies on the inhibition of mild steel corrosion in hydrochloric acid solution by atenolol drug, Egyptian journal of petroleum (2016) 183-191.
8. Pahuja, P., Dahiya, S., and Lata, S., 2018, Review on herbal drugs as corrosion inhibitor for low alloy steel, BMIET J. Sci. Technol. Manage., 2 (1), 7–19.
9. Agrawal, Y.K., Talati, J.D., Shah, M.D., Desai, M.N., and Shah, N.K., 2004, Schiff bases of ethylenediamine as corrosion inhibitors of zinc in sulphuric acid, Corros. Sci., 46 (3), 633–651.
10. Ashassi-Sorkhabi, H., Shaabani, B., and Seifzadeh, D., 2005, Effect of some pyrimidinic Shciff bases on the corrosion of mild steel in hydrochloric acid solution, Electrochim. Acta, 50 (16-17), 3446–3452.
11. Tamalmani, K., and Husin, H., 2020, Review on corrosion inhibitors for oil and gas corrosion issues, Appl. Sci., 10 (10), 3389
12. Rajendran, S., Amalraj, A.J., Joice, M.J., Anthony, N., Trivedi, D.C., Sundaravadivelu, M. Corrosion Rev. 2004, 22, 233248.
13. Mesbah, A., Juers, C., Lacouture, F., Mathieu, S., Rocca, E., Franc¸ois, M., Steinmetz, J. Solid State Sci. 2007, 9, 322328.
14. Okafor, P.C., Osabor, V.I., Ebenso, E.E. Pigment and Resin Technol. 2007, 36, 299305.
15. Lebrini, M., Traisnel, M., Lagrene´e, M., Mernari, B., Bentiss, F. Corrosion Sci. 2008, 50, 473479.
16. RadojC˘ic´, I., Berkovic´, K., KovaC˘, S., Vorkapic´-FuraC˘, J. Corrosion Sci. 2008, 50, 14981504.
17. Refaey, S.A.M., Abd El Malak, A.M., Taha, F., Abdel-Fatah, H.T.M. Int. J. Electrochem. Sci. 2008, 3, 167176.

Journal of the Maharaja Sayajirao University of Baroda: Science & Technology
Vol. 58, 2024, pp. 92-100

Analysing Hydrogen Embrittlement Challenge for Hydrogen Storage & Its Utilization in Industries

Daulat Kumar Sharma, Sarvesh Gurram, Rahul Yadav, Chirayu Pande

Metallurgy Department, Government Engineering College, Gandhinagar, Gujarat, India

The extensive study of hydrogen as an energy transition tool highlights its potential in de- carbonization. Its role as an energy carrier, heat source, and chemical reactant in industrial processes makes it a promising option. Efficient storage could significantly contribute to de- carbonizing industries, but understanding and controlling its impact on infrastructure are crucial. Investigating the retrofitting of existing industrial infrastructure is essential for the economic feasibility of hydrogen technology. The lack of comprehensive knowledge on alloys and components' performance in long-term hydrogen-containing environments poses a challenge, especially in high-temperature, high-pressure industrial conditions. Developing characterization techniques for hydrogen-metal interactions under these conditions is crucial for successful implementation. As we acknowledge, "Hydrogen embrittlement" refers to the irreversible loss of ductility in a metal or alloy brought on by hydrogen combined with either residual internal or external stress. Three parameters are required to cause failure: the presence of hydrogen, the tensile stress, and the susceptibility of the material but the root cause is the susceptibility of the material. The report also discusses the impact and use of Hydro- gen in large scale industrial processes and the detrimental effect of Hydrogen Embrittlement in steels.

Key words*:* Hydrogen Embrittlement, Hydrogen Utilization, Mechanical properties, Hydrogen Storage

1. *INTRODUCTION:*

Embrittlement also occurs as a result of expo- sure of charged alloy to a hydrogen environment. This form of hydrogen embrittlement, called external hydrogen, was first recognized by Van Ness and Dodge (1955) and described in detail by Hofmann and Rauls (1961). Be- tween 1961 and 1965 there were scattered re- ports on the effect of a hydrogen environment on the ductility of steel. External hydrogen storage gained prominence in June 1965 when the National Aeronautics and Space Administration found that a hydrogen storage vessel designed to operate at 5000 psi was not cost-effective. This vessel, welded from fabricated from ASTM A-517-F(T-1) steel under quenched and tempered conditions, failed catastrophically at 3900 psi (McPherson, 1969). Since then, it has be- come increasingly clear that external hydrogen gassing, which occurs not only in gaseous hydrogen environments but in all hydrogen environments, is a common form of gassing affecting most mechanical alloys [1].

Hydrogen embrittlement can be a complex process, as many factors can affect both its severity and form. For example, the decomposition process does not involve a single hydrogen- metal interaction mechanism but is the result of one or more of several mechanisms. The exact mechanism causing embrittlement depends on factors such as the rate of hydrogen transport and the amount and location of available hydro- gen both at its source and at the site of interaction. These factors are in turn influenced by other factors such as alloy composition including minor residual elements, microstructure, stress state, temperature, etc. [1].

It is a process resulting in a decrease in the ductility of metal due to the presence of atomic hydrogen [2].Hydrogen embrittlement is classified through these Hydrogen-metal interactions in three different categories:

- **Hydrogen Environmental Embrittlement (HEE)**

It represents the condition when the material is exposed to a high-pressure gaseous hydrogen environment.

- **Internal Hydrogen Embrittlement (IHE)**

In this, the material gets exposed to hydrogen from electrochemical processes such as electroplating, corrosion, and cathodic charging. The source of hydrogen also comes from moisture that enters during welding, casting, and solidification processes.

- **Hydrogen Reaction Embrittlement (HRE)**

In this irreversible Hydrogen damage occurs through a chemical reaction with hydrogen and that damage can occur without external applied stress [2].

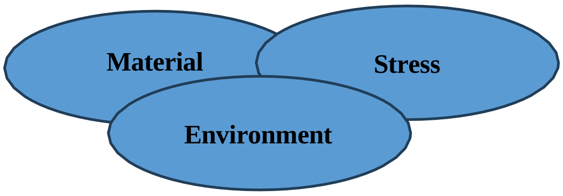

Figure 1: Main Factors for Hydrogen Embrittlement [3]

---

* Corresponding author.
Email: dksharma.met@gmail.com

The earliest theories of the mechanism of hydrogen embrittlement assumed that the reduction in toughness was due to a strain-hardening effect due to the formation of iron-hydrogen compounds. However, when the hydrogen con- tent is on the order of one atom per 100,000, embrittlement can occur [4]. This, together with the fact that iron does not form a hydride, suggests that the embrittlement effect is not due to hydrogen-containing compounds. Later, when solubility-pressure-temperature relationships were clarified, the effect was attributed to the very high pressures that hydrogen would experience if it were thrown out of solution (e.g. by cooling) and allowed to accumulate in the internal voids. Later some workers have argued that such pressures are sufficient to stress the surrounding lattice, while others suggest that embrittlement is due to the triaxiality of the internal stresses contained in the gas at such high pressures.

One of the characteristics of hydrogen embrittlement of steels is that, in the presence of hydrogen, the stress-strain curve breaks at a total strain smaller than that achieved without hydro- gen. This has been repeatedly observed in many types of steel. For example, Toh and Baldwin found that the elongation at break, Sf, of SAE 1020 steel was significantly reduced by hydrogen, independent of temperature, and Grant and Lunsford found a greater reduction in the sf of the same steel. but cold processed. and more as the amount of hydrogen in- creased. Hobson and Sykes found the same effect by increasing the hydrogen content to 6 f for a 3% Cr-Mo steel. Frohmberg et al observed a significant reduction due to hydrogen in 4340 steels with a yield of 1860 M N/m2 [5].

This paper presents a review of Hydrogen Embrittlement with a main focus on steels. The change in the parameters due to HE, Conventional material testing methods are used to evaluate the mechanical properties of hydrogen degradation, which occurs when a material is subjected to applied stress and exposed to hydrogen gas compared to air or helium. The effects of hydrogen gas on mechanical properties such as tensile strength, ductility, fracture, low and high cycle fatigue, crack growth rate, and creep rupture are analyzed. It is observed that the severity of HE effects is also influenced by hydrogen pressure, hydrogen purity, the effect of temperature, the effect of chemistry and microstructure and effect of surface conditions.

1.1 The creation, storage, use, and environmental effects of hydrogen:

A growing number of industries are realizing that dihydrogen (H2), also referred to as "hydrogen," is a clean and dependable energy vector for decarbonization and defossilization. By 2024, the amount of hydrogen needed globally is expected to rise from 70 million tons in 2019 to 120 million tons. The development of hydrogen should also help the world achieve its seventh sustainable energy goal, “affordable and clean energy." Here, we go over the life cycle analysis and production of hydrogen, as well as its geological storage and utilization. The processes of water electrolysis, coal gasification, steam methane reforming, and methane pyrolysis all yield hydrogen. Using life cycle analysis, we compare how different hydrogen manufacturing routes affect the environment [6].

The manufacture of ammonia and hydrocarbons, power systems, and the metal luminous industries all need hydrogen. In general, the utilization of hydrogen produced through electrolysis in conjunction with hydrogen storage in subterranean porous media, such as salt caverns and geological reservoirs, is an effective method for transferring surplus energy from off-peak hours to scheduled hours of use [7].

1.2 Materials with embedded hydrogen:

In general, high-strength materials that operate in hydrogen environments are highly susceptible to hydrogen embrittlement. High- strength steels, high Mn steel, aluminium alloys, titanium, magnesium, and magnesium alloys, among other materials, are highly susceptible to HE Steels that have a strength greater than 1000 MPa are highly susceptible to HE [8]. Several industries including the nuclear, aerospace, transportation, and automotive sectors, and even high-pressure hydrogen storage tanks, use these high-strength steels [3][4][5][6][7].

After a while, advances in high strength steel led to the creation of a new class of steels that are now widely used, including high manganese steel and martensitic advanced high strength steel (MS-AHSS). This high Mn steel offers many benefits, including great strength and ductility. However, this steel has an embrittlement issue, and high Mn steel's HE susceptibility is due to its chemical composition [9].

The strongest steel in the AHSS family is a new class of steel called MS-AHSS. Its strong strength-to-price ratio makes it useful in the automotive industry [10]. Its ductility, however, is marginally lower than that of other AHSS materials. The majority of MS-AHSS research has been conducted in controlled laboratory environments. The most effective way to use this lab result in real-world working or service conditions is still subject to argument. This will require research. Alloys made of aluminium are susceptible to simultaneous corrosion cracking and HE [11].

The following factors determine a material's sensitivity to HE: [8][10].

- The material's strength and residual stress.
- Exposure duration, temperature, and pressure.
- The material's surface state and the applied strain rate.
- Hydrogen concentration or amount and hydrogen trap amount.
- Particular precipitates and metallic coatings.
- The microstructure of a substance.
- Acidic solutions—solutions that react with metals.
- The process of heating a substance.

2. *CHARACTERISTICS OF HYDROGEN EMBRITTLEMENT:*

Three prerequisites need to be satisfied for the deterioration of mechanical characteristics brought on by hydrogen embrittlement.

a. A material with a UTS of more than 1000 MPa is vulnerable to hydrogen embrittlement.

b. Hydrogen that is already present in the atmosphere or the alloy.

c. Surface hardness and tensile stresses under service conditions ought to be higher than HRC 37.

Sensitivity to strain rate changes the potential for delayed failure are the primary features of hydrogen embrittlement. A slow stain rate is improved HE. The material is less sensitive to HE if a higher strain rate is applied. Likewise, the susceptibility to delayed failure has increased in HE components. It is also known that dislocation movement and hydrogen diffusion make hydrogen transit possible in steel and alloys. In high strength materials, hydrogen embrittlement is a well-known phenomenon [12].

Embrittlement causes a material to fail catastrophically below its intended stress or strength. Therefore, understanding how a crack may spread in a material as a result of hydrogen or corrosion response is necessary, as corrosion reaction can occasionally result in the production of hydrogen atoms. This requires an understanding of fracture mechanics. The material grew cracks as a result of dislocation emission or micro void coalescence (MVC), which was caused by the influence of hydrogen on the material.

According to the study, there are situations when a combination of dislocation emission and MVC can cause a crack to form, which in turn causes a material to fracture and fail below its allowable limit. Understanding the behavior of crack growth and crack growth rate in a material due to the action of hydrogen requires knowledge of fracture mechanics, and concurrent investigation of multiple crack growth mechanisms is needed. The subcritical crack propagation in a material is referred to as hydrogen assisted cracking (HAC).

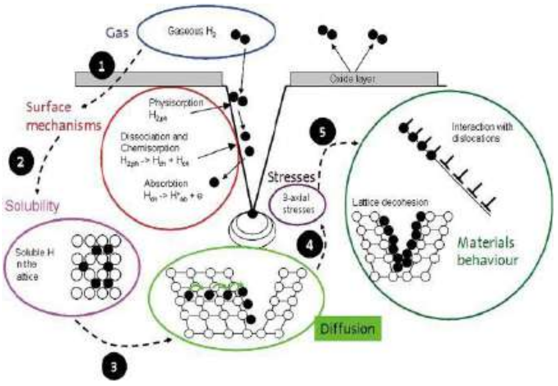

Figure 2: Schematic diagram of hydrogen atom evolution and HE failure [13].

3. *IMPORTANT FACTORS AFFECTING OF HYDROGEN GAS EMBRITTLEMENT:*

The effect of Hydrogen gas in the mechanical properties of the Carbon steel affected the different environment factors such as Hydrogen pressure, purity, temperature, and other environmental conditions, as well as material characteristics like chemistry and microstructure, which have a significant impact on the mechanical properties of carbon steels and the state of the surface. These crucial elements are covered in the sections that follows:

Effect of hydrogen Pressure: In general, it is thought that when hydrogen pressure rises, hydrogen gas embrittlement gets worse. It was evidently shown by Loginow and Phelps that as hydrogen pressure increased, the crack arrest stress intensity factor of high-strength steels (YS >590MPa) reduced [13]. Additionally, it has been demonstrated that the square root of the hydrogen pressure caused a corresponding de- crease in the tensile ductility of high-strength steels [8].

The fatigue fracture propagation rate of carbon steels is significantly influenced by hydrogen pressure as well. According to Walter and Chandler, the da/dN of Carbon steel increased by roughly a factor of 10 at DK = 22MPa−m when the hydrogen pressure increased from 6.9 to 103 MPa. That being said, DK also has a significant impact on the real pressure dependency. For instance, at DK = 33MPa−m, the same steel displayed comparable da/dN and the same increase in hydrogen pressure [8][14].

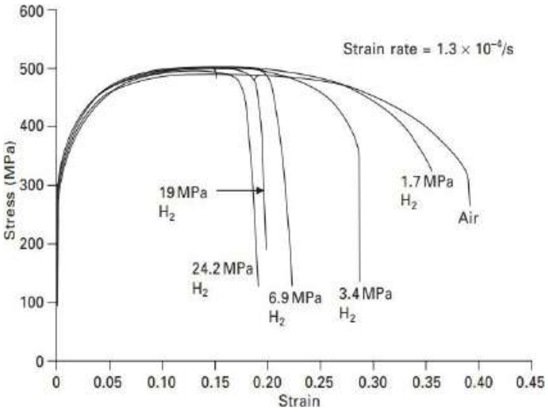

Figure 3: Tensile stress–strain curves of A-106 Grade B in air and H2 at different pressures [15].

Effect of hydrogen purity: It discusses how hydrogen embrittlement is affected by the purity of hydrogen gas. The surface chemistry of alloys can be significantly changed, the affinity of adsorbed hydrogen for steels can be de- creased, and hydrogen embrittlement can be avoided with very modest amounts of contaminants like oxygen and carbon monoxide in hydrogen gas [16].

Hofmann and Rauls showed that 1% oxygen could totally abolish tensile embrittlement and that the lowest oxygen content at which a reduction in embrittlement of a plain carbon steel in 10 MPa hydrogen occurred was roughly 1 ppmv [16]. Similar findings were recently published by Deimel et al., who demonstrated that the decline in tensile ductility of a normalized steel 15MnNi6 3 (YS ~ 320MPa, UTS ~ 510MPa) in 9MPa hydrogen may be greatly mitigated by as little as 19 ppmv O2. The ductility was recovered to an inert state at 143 ppmv O2 [17].

Impurity effects on hydrogen-enhanced fatigue fracture development rates were also noted. The impact of hydrogen gas impurities on the fatigue crack development of X42 was investigated by Holbrook et al [18]. It was discovered that lowering da/dN might be achieved with as little as 100 ppm of CO. The da/dN dropped as the CO concentration rose while maintaining a constant DK of 16.5MPam. It was also shown that a tiny concentration of COS, O2, SO2,and N2O [19]. was highly helpful in delaying the increased fatigue crack growth rates in hydrogen gas. However, it was discovered that the addition of CO2 and CH4 had little to no effect on the formation of fatigue cracks.[20] The preferential adsorption of the inhibitor species on the steel surface, which stops hydrogen from penetrating the steel, was thought to be the cause of the impurity's inhibitory effect. With fewer frequency and more pressure, impurities seemed to be losing their effectiveness.

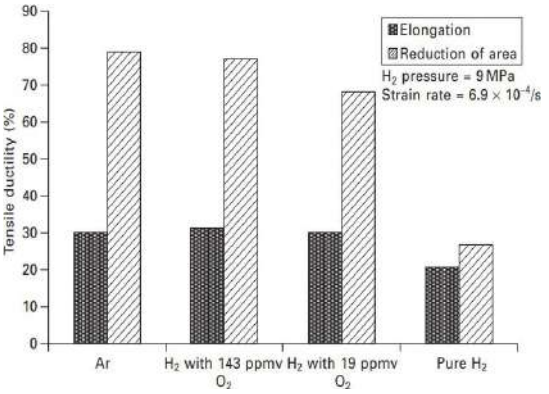

Figure 4: Effect of hydrogen impurities on tensile, ductility [17].

Effect of Temperature: A phenomenon that occurs close to room temperature is hydrogen embrittlement. When the temperature rises above 100 °C, hydrogen embrittlement steadily decreases. The majority of tests on hydrogen embrittlement were carried out at room temperature. Nonetheless sub-ambient settings are typically the most sensitive temperature for hydrogen embrittlement to occur. Hofmann and Raiuls examined the impact of temperature on hydrogen environment embrittlement on cold-drawn and normalized CK22, a low carbon steel with 0.22% C [16], at pressures of 15 MPa. Tensile strain occurred at a rate of 0.05/min. At any test temperature, there was no discernible impact on the ultimate tensile strength. Carbon steels undergo a deterioration process known as "hydrogen attack" at high temperatures and pressures. Atomic hydrogen combines with iron carbide to produce methane, which causes the steel to lose strength due to decarburization, create voids, and fracture. It is important to distinguish between hydrogen embrittlement, which happens at or close to room temperature, and hydrogen attack. API 941 outlines the upper limits for the use of carbon steels in high temperature hydrogen service.

Effect of chemistry and microstructure: It has been demonstrated that the concentrations of carbon and manganese in carbon steels make them more vulnerable to hydrogen embrittlement [8]. For hydrogen pipeline steels, the Compressed Gas Association (CGA) recommends a maximum carbon equivalent (CE) of 0.43. The carbon equivalent is computed as follows [8].

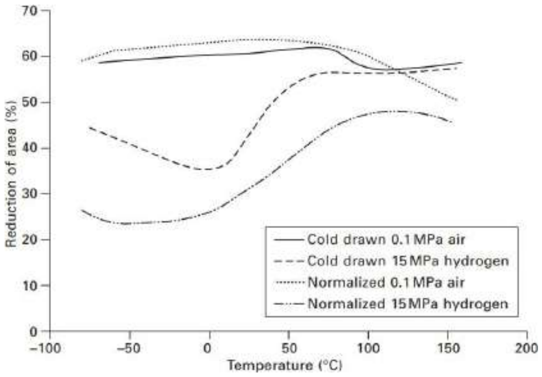

Figure 5: Effect of CO concentration in hydro- gen on fatigue crack growth rates of X42 steel [18].

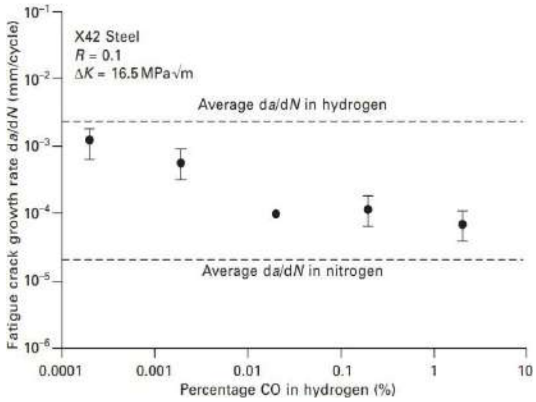

Figure 6: Effect of temperature on tensile reduction of area of cold drawn and normalized CK22 steel in air and 15 MPa hydrogen [16]

Other alloying elements have been discovered to have neutral or advantageous effects on hydrogen performance. By using thermomechanical methods, steels are strengthened and their fracture toughness is increased by the addition of micro alloyed elements like Nb, V, and Ti. In hydrogen settings, the micro alloyed steels showed some improved characteristics, particularly in the welds. It is yet unknown how well the micro- alloyed steels work with high pressure hydrogen.

Due to the combined effects of alloy chemistry, heat treatment, and strength, the relationship between microstructure and hydrogen embrittlement is highly complex. However, it is commonly accepted that the following microstructures rank higher in order of increasing vulnerability to hydrogen embrittlement at similar strength levels: martensite that has been quenched and tempered, spheroidized, normalized pearlite/ferrite, and untampered martensite [21].

Effect of surface conditions: The surface condition has a significant impact on the mechanical behavior of carbon steels in hydrogen. The results of notch tensile tests showed that, in a hydrogen atmosphere, carbon steels have a much higher notch sensitivity. In hydrogen tensile testing, the preferred sites for crack start were the machining marks. Murali et al. determined that a specimen subjected to ratchet tensile loading beyond the yield point and strain cycling to around 0.7% plastic strain each cycle till failure could have a substantial impact on the fatigue life [19].

4. *EFFECT OF HYDROGEN DURING STORAGE AND TRANSMISSION IN STEEL PIPELINES :*

In order to complete the internal hydrogen cycle, electrolytic water is also produced in tandem with the energy production from hydrogen gas. The use of hydrogen energy supports the achievement of the global zero carbon emission objective since it produces no greenhouse gases, such as carbon dioxide when compared to typical energy combustion methods[22] [23]. Currently, the primary method for long-distance transportation of hydrogen-blended natural gas is pipeline steels. Regrettably, its physical characteristics pose an engineering challenge for storage and delivery [24] [25]. It is impossible to prevent the permeation of H (valence electronic structure 1s1) with a covalent radius of 0.37 Å. Hydrogen embrittlement (HE) and hydrogen-induced cracks (HIC) are examples of the ensuing hydrogen effect (H-effect). The tensile strength, fatigue strength, and fracture toughness of pipeline steels can all be considerably reduced by these occurrences.

The following risks are predicated on how hydrogen moves through the steel pipes in the pipeline. The following four continuous processes are the main ways that H atoms get onto the surface of pipeline steels [26].

- Physical adsorption: Due to Vander Waals interactions and Brownian motion, hydrogen atoms are adsorbed onto the surface of metallic objects.
- Dissociation and chemical adsorption: Through chemical adsorption, hydrogen molecules separate and create adsorbed hydrogen atoms.
- Diffusion: dissolved hydrogen diffuses throughout the interstitial gaps;
- Dissolution: adsorbed hydrogen atoms create dissolved hydrogen atoms on the surface to enter interior material.

$H_2+M\rightarrow H_2\cdot M$… .... Eq.(1)

$H_2\cdot M + M\rightarrow 2H_{ads}\cdot M$… .... Eq.(2)

$H_{ads}\cdot M\rightarrow M\cdot H_{dis}$ .... Eq.(3)

$M\cdot H_{dis}\rightarrow M + H_{diff}$… .... Eq.(4)

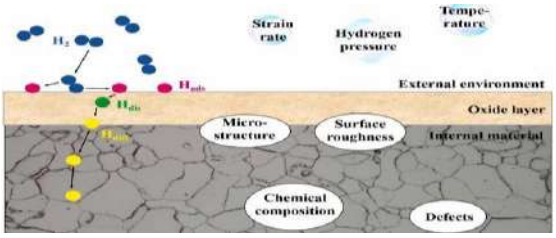

Figure 7: Schematic diagram of influencing factors of H-effect [32].

4.1 Need of Study:

After Analyses the patterns in the number of articles and keywords with the strongest citation bursts about hydrogen and natural gas in pipeline steels from the Web of Science Core Collection (WoSCC) database in 2001–2021 by year in order to directly visualize the development processes and hotspots. The quantity of paper publications has increased significantly over the previous 20 years [28][29]. One of the hotspots in the upcoming years is expected to be the use and storage of hydrogen and natural gas. The delivery of steel via pipelines and the associated precautions against hydrogen buildup will also become major concerns [30].

5. *HYDROGEN EMBRITTLEMENT PROBLEM IN DIFFERENT MATERIALS:*

5.1 Titanium Alloy:

5.1.1 Ti-6Al-4V:

Ti-6Al-4 V alloy is widely used, but it has low machinability due to poor thermal conductivity, high chemical reactivity to oxygen, and a tendency for strain hardening. Traditional methods for producing Ti-6Al-4 V parts result in significant material waste, expensive manufacturing costs, and long lead times. Additive manufacturing (AM) is a beneficial alternative for producing Ti-6Al-4 V components with complex shapes. However, the interaction of hydrogen with Ti-6Al-4 V manufactured by different AM methods varies. EBM Ti-6Al-4 V has a relatively slow cooling process and is characterized by prior β grains with a transformed α/β microstructure. SLM Ti- 6Al-4 V generally has an acicular α’-martensite phase due to fast cooling. Hydrogen-assisted cracking (HAC) has been observed in EBM Ti- 6Al-4 V with fine duplex α + β phases, but the amount of discontinuous β-phase is lower in EBM Ti-6Al-4 V than in conventional wrought alloys, making it more resistant to HAC in electrochemical and gaseous environments. SLM Ti-6Al-4 V has a higher trend of hydrogen absorption and hydride precipitation than EBM Ti-6Al-4 V due to its α’-martensite microstructure.

The activation energy in the SLM Ti-6Al-4 V was found to be 31 ± 5 kJ/mol, indicating a reversible trap assigned to dislocations. The second hydrogen trap was also reversible and assigned to GBs with an activation energy of approximately 50 kJ/mol. The third peak appeared at high temperatures and was characterized by an activation energy of 85 ± 9 kJ/mol, indicating a strong irreversible trap with Ti hydrides.

In contrast, the EBM sample had only two peaks associated with two hydrogen traps: a low activation energy of 53 ± 3 kJ/mol at low temperatures, corresponding to GB reversible trapping, and a high activation energy of 88 ± 5 kJ/mol at higher temperatures, indicating irreversible trapping by Ti hydrides. Based on the TDS spectra, the main trap was found to be irreversible in the SLM Ti-6Al-4 V, while in the EBM Ti–6Al–4 V, it was reversible.

However, Navi et al. reported that the HE susceptibility of EBM Ti-6Al-4 V was greater than that of the wrought alloy due to the increased amount of α/β interfaces and the discontinuous β-phase particles along the short-horizontal direction. Both factors promoted the formation of hydrides and micro voids, inducing HAC along the interphase boundaries. The time-of-flight secondary ion mass spectrometry image mapping of the total hydrogen intensity and the Ti-hydride intensity in wrought and EBM samples indicated that the hydrides were aligned parallel to the interphase boundaries, and the EBM alloy had a higher structural complexity with more Ti hydrides. In addition, the discontinuous β-phase also resulted in faster hydrogen desorption in the EBM Ti-6Al-4 V than the wrought alloy because the BCC β-phase was associated with the higher solute oxygen content. The contradictory conclusion between Metalninkov et al. and Navi et al. might be attributed to Metalninkov et al.'s underestimation of the influence of hydrides and micro void formation on HE susceptibility. It is necessary to conduct further studies to clarify the accuracy of these data and conclusions, especially since the TDS spectra in these two studies were different [31].

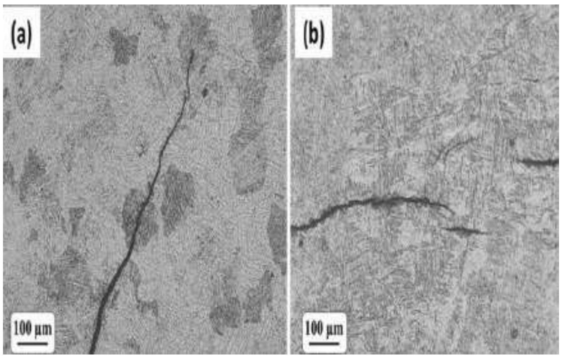

Figure 8: Micrographs of electrochemical hydrogen charged (a) SLM and (b) EBM Ti-6Al-4V [31].

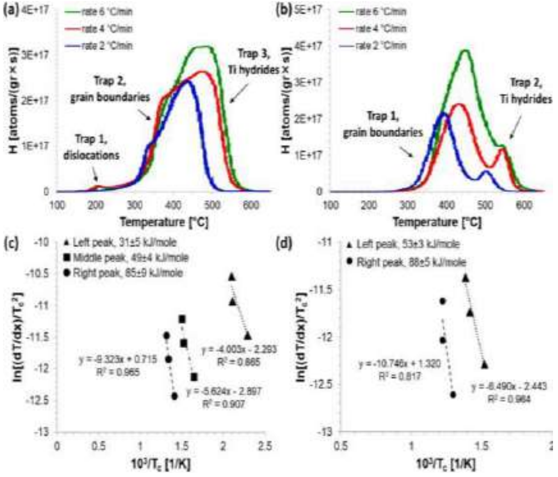

Figure 9: (a & b) TDS spectra of electrochemical hydrogen charged and (c & d) determination of the activation energies of each hydrogen desorption peaks (a & c) SLM and (b & d) EBM Ti–6Al–4 V [31].

5.2 Nickel Based Super alloy:

Nickel-based (Ni-based) super alloys are utilized when high creep and/or fatigue resistance is needed at temperatures above 500°C. These alloys usually contain up to 10 alloying elements, including light elements such as carbon or boron, aluminium, and heavy refractory elements such as tantalum, rhenium, or tungsten. Although the alloys were originally designed for turbine engine application, they are increasingly used in other sectors, such as ultra-supercritical power plants, nuclear power plants, fossil fuel-fired diesel engines, and fuel cells. The applications are most prevalent over 750°C because the characteristics of Ferritic steels deteriorate dramatically above this temperature. Due to the geometrical complexity of energy generation and aerospace components, AM (Additive Manufacturing) of Ni-based super alloys has attracted increasing interest from scientists and engineers. Different AM techniques, such as SLM (Selective Laser Melting), EBM (Electron Beam Melting), and DED (Direct Energy Deposition), have been used to process both solid solutions and precipitate-strengthened Ni-based super alloys. Comprehensive details of Ni-based super alloys processed by AM can be found in recently published review papers [31].

5.2.1 Inconel 718:

Inconel 718 (also called Ni-based 718 or IN 718) is the most studied alloy compared with others as it is the most widely used. Chemical, microstructure, and property inhomogeneities are major concerns in AM Ni-based super alloys. Such inhomogeneities result from the rapid and repeated thermal gyrations during AM, which are related to non-equilibrium phase formation, spatially dependent microstructure gradients, and multi-length scale microstructure inhomogeneities. Although super alloys have good high-temperature oxidation and creep resistance and good corrosion resistance at room temperature, these alloys are not immune to HE (Hydrogen Embrittlement) and/or water vapor effects in high-pressure hydrogen environments. It has been found that HE occurs over a much wider temperature range in many super alloys. More significant HE has been evidenced at substantially higher temperatures compared with lower temperatures. This is different from steels, which are more sensitive to HE at relatively lower temperatures ranging from -200°C to 200°C. Hence, HE is an important factor to consider for safe design in a hydrogen environment since most super alloys are often used at high temperatures. Thus, HE study of the Ni-based alloys, including fabricating by AM and conventional methods, is necessary [31].

5.3 Stainless Steel:

AISI 304 is the most common austenitic stainless steel (ASS) which has low cost, good corrosion resistance, high weldability, and mechanical properties similar to construction steel. However, the austenitic microstructure in 304L SS is susceptible to strain-induced transformation during service or forming due to its relatively low stacking fault energy. This transformation depends on microstructure, texture, and grain size. In comparison to the wrought counterpart, highly dense AM 304L SS exhibits similar tensile and fatigue performance in both ambient and severe hydrogen environments. However, internal hydrogen can cause tensile ductility loss in both PBF and DED-manufactured 304L SS. Moreover, micro segregation and defects in AM parts can promote microcrack coalescence, leading to a more severe reduction in ductility.

In 2017, Baek et al. reported that the DMT- processed 304L had higher hydrogen embrittlement (HE) resistance than the conventionally processed 304L. They found that the elongation to fracture of the DMT 304L was similar in air and with hydrogen, while the strain to failure of the rolled 304L was significantly reduced in hydrogen. The HELP and HEDE mechanisms can be used to explain HE in this material. According to the HELP model, a locally elevated hydrogen concentration augments dislocation activity, resulting in localized stress concentration and the initiation of failure at planar defects. The study concluded that AM technology could be more suitable for creating 304L SS products.

5.4 Maraging Steel:

Maraging steels are a type of steel that contains very little carbon but has a high content of other alloying elements, such as nickel, cobalt, and molybdenum. The strength of these steels is achieved through the precipitation of intermetallic compounds like Ni3Ti, Ni3Mo Fe2Mo, and Fe7Mo6, which form during aging after the steels are quenched to martensite. These steels are used in the aerospace sector because they combine ultrahigh strength with high toughness. The most common type of maraging steel is 18Ni, which can achieve tensile strength over 2000 MPa after proper heat treatment. Research has shown that SLM (Selective Laser Melting) processing can produce fully dense maraging steel with mechanical properties comparable to those produced using traditional manufacturing methods. However, maraging steels produced either using traditional routes, or using AM (Additive Manufacturing), are very susceptible to HE (Hydrogen Embrittlement), which causes a reduction in mechanical properties. In addition, the HE of maraging steel is increased by the presence of pores produced during SLM or casting because these defects can accumulate hydrogen and promote crack propagation and brittle fracture. Studies have investigated the HE behaviors of grade 300 maraging steel processed by SLM. The hydrogen-charged specimen suffered severe HE, as the strength and plasticity decreased significantly. The ductile to brittle fracture mode transition in the SLM maraging steel was induced by hydrogen charging. Microcracks released the localized stress fields in retained austenite and thus inhibited the further phase transformation from retained austenite to the newly formed martensite. These microcracks coalesced and propagated rapidly under the applied stress, leading to the brittle fracture of the hydrogen charged specimen.

Figure **10:** a) OM and (b) IPF micrographs of the studied AM grade 300 maraging steel, and (c) high energy XRD profiles of the hydrogen- free and hydrogen-charged specimens before deformation [31].

Metallurgical defects such as cracks, inclusions, and porosities are commonly introduced by AM processes. These defects can promote hydrogen absorption, leading to embrittlement . Moreover, micro-segregation and defects in AM components can cause microcrack coalescence, resulting in a more severe reduction in ductility. However, current research primarily focuses on evaluating the high-density samples' HE performance, with little attention to the impact of material defects on HE. Given the prevalence of defects in AM metals, it is essential to investigate their role in HE. It is also important to note the differences in hydrogen embrittlement susceptibility between metals produced using conventional methods and those produced using additive manufacturing techniques. Further research in this area will help in developing solutions to enhance the resistance of these materials to hydrogen embrittlement [31].

Table 1: The Dominant HE mechanism of metals by additive manufacturing [31].

Sr. No.	**Materials**	**AM**
1	Ti-6Al-4 V	HFC
2	IN 718	HELP+HEDE
3	AISI 304L	HELP+HEDE
4	AISI 316L	HELP
5	17-4 PH	HELP
6	18Ni 300	HELP
7	CoCrFeNiMn	HELP, HEDE
8	AlCoCrFeNi2	HELP+HEDE

6. *CONCLUSION:*

The probable behavior of these materials at high temperatures and pressures in an atmosphere containing hydrogen remains largely unknown, even after in-depth research on a variety of phenomena in metals and alloys that interact with hydrogen. This is especially true for advanced industrial processes. Despite extensive research and documentation on hydrogen embrittlement and attack processes, there are still considerable technical concerns associated with using hydrogen to decarbonize a given blend due to the action of these mechanisms at certain operating conditions and hydrogen content. It is still difficult to forecast how metals and materials will behave in the pipelines and reactors that make up today's industrial infrastructure, and methodologies to assess and characterize the resilience and potential lives of these systems for the introduction of hydrogen still require research and development. Applying current understanding of hydrogen evolution (HE), hydrogen attack, H2 reaction mechanisms, and intrinsic properties of metals and steels that interact with hydrogen (physisorption, dissociative chemisorption, absorption, diffusion, and interactions with dislocations) to extremely complex conditions such as different atmospheres, temperatures, pressures, and gradients of these can be difficult. We need to accurately evaluate materials in terms of their use in particular industries, forecast the lifespan of industrial components, and evaluate the compatibility of materials in industrial systems if modified in order to address these issues in industries where the switch from fossil fuel to hydrogen may occur. To achieve all of these objectives, current test protocols, processes, and techniques must be further developed.

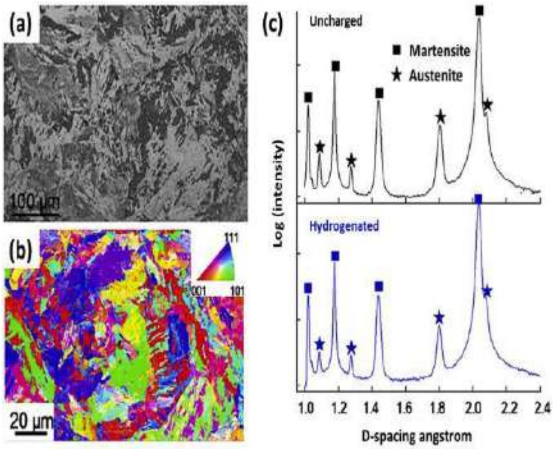

7. *CASE STUDY:*

A fresh study proposed to prevent bacteria from causing hydrogen embrittlement in nuclear waste containers.

‘A major issue that has always needed immediate attention for nuclear safety is the massive volume of radioactive waste generated with the use of nuclear energy. Currently, "deep geological disposal" is a workable technique that is widely acknowledged in numerous countries. Anaerobic conditions will be reached in the waste containers near the field environment when the oxygen content drops and hydrogen will seep into the interior materials over time. There may be a chance of hydrogen embrittlement due to hydrogen evolution corrosion. Hydrogen embrittlement causes significantly more harm to metal containers than does consistent, homogeneous corrosion. The influence of microorganisms on the corrosion behavior of container materials in the deep geological environment is a focus for investigation. Anaerobic and aerobic microbial corrosion are the two categories in which microbial corrosion occurs in deep geological settings. In the natural world, there is a particular kind of bacterium that consumes hydrogen and gets its energy from the oxidation of hydrogen. This gives us a fresh perspective on how to investigate lessening the vulnerability of nuclear waste container materials to hydrogen embrittlement. There is a chance of long-term HE in metal containers during nuclear waste disposal because, in this discussion, the cathodic reaction of corrosion has changed from oxygen absorption corrosion to hydrogen evolution corrosion due to the continual consumption of oxygen. Materials used in nuclear waste containment are frequently more severely impacted by unpredictable HE then by predictable uniform corrosion. In deep geological settings, there are bacteria that consume hydrogen and get their energy from hydrogen oxidation. If these microbes that eat hydrogen are able to do so atoms produced by the container material's natural corrosion process, which stops hydrogen from penetrating the inside and significantly lowers the risk of hydrogen explosion.

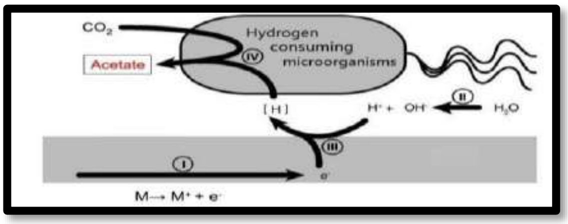

Figure 11: Schematic illustration of the mutual effects between hydrogen consuming organisms and metal surface [32].

Nevertheless, the majority of recent research has only taken into account the negative effects of microorganisms and has concentrated on the microbially accelerated corrosion rate of container materials in deep geological conditions. However, a novel method for researching the decrease in HE sensitivity for nuclear waste container materials is made possible by the existence of microorganisms that consume hydrogen [32].

8. *REFERENCES:*

1. H. G. Nelson, *Hydrogen Embrittlement.*, vol. 25, no. 1825. ACADEMIC PRESS, INC., 1983. doi: 10.1016/b978-0-12-341825-8.50014-3.
2. J. A. Lee, “NASA/TM-2016–218602 Hydrogen Embrittlement,” *Shreir’s Corros.*, no. April, pp. 1–62, 2016, [Online]. Available: https://ntrs.nasa.gov/api/citations/20160005654/downloads/20160005654.pdf
3. S. K. Dwivedi and M. Vishwakarma, “Hydrogen embrittlement in different materials: A review,” *Int. J. Hydrogen Energy*, vol. 43, no. 46, pp. 21603–21616, 2018, doi: 10.1016/j.ijhydene.2018.09.201.
4. Cotterill Peter, “The hydrogen embrittlement of metals,” *Prog. Mater. Sci.*, vol. 9, no. 4, pp. 205–301, 1961.
5. T. Shiraga, “Hydrogen embrittlement of steel,” *Zair. to Kankyo/ Corros. Eng.*, vol. 60, no. 5, pp. 236–240, 2011, doi: 10.3323/jcorr.60.236.
6. E. Anastasiou, K. O. Lorentz, G. J. Stein, and P. D. Mitchell, “Prehistoric schistosomiasis parasite found in the Middle East,” *Lancet Infect. Dis.*, vol. 14, no. 7, pp. 553–554, 2014, doi: 10.1016/S1473-3099(14)70794-7.
7. A. I. Osman *et al.*, *Hydrogen production, storage, utilisation and environmental impacts: a review*, vol. 20, no. 1. Springer International Publishing, 2022. doi: 10.1007/s10311-021-01322-8.
8. A. W. Thompson and I. M. Bernstein, “Selection of structural materials for hydrogen pipelines and storage vessels,” *Int. J. Hydrogen Energy*, vol. 2, no. 2, pp. 163–173, 1977, doi: 10.1016/0360-3199(77)90007-6.
9. M. Koyama, E. Akiyama, Y. K. Lee, D. Raabe, and K. Tsuzaki, “Overview of hydrogen embrittlement in high-Mn steels,” *Int. J. Hydrogen Energy*, vol. 42, no. 17, pp. 12706–12723, 2017, doi: 10.1016/j.ijhydene.2017.02.214.
10. J. Venezuela, Q. Liu, M. Zhang, Q. Zhou, and A. Atrens, “A review of hydrogen embrittlement of martensitic advanced high-strength steels,” *Corros. Rev.*, vol. 34, no. 3, pp. 153–186, 2016, doi: 10.1515/corrrev-2016-0006.
11. A. V. Bochkaryova, Y. V. Li, S. A. Barannikova, and L. B. Zuev, “The effect of hydrogen embrittlement on the mechanical properties of aluminum alloy,” *IOP Conf. Ser. Mater. Sci. Eng.*, vol. 71, no. 1, 2015, doi: 10.1088/1757-899X/71/1/012057.
12. M. Wang, E. Akiyama, and K. Tsuzaki, “Effect of hydrogen on the fracture behavior of high strength steel during slow strain rate test,” *Corros. Sci.*, vol. 49, no. 11, pp. 4081–4097, 2007, doi: 10.1016/j.corsci.2007.03.038.
13. T. Michler and J. Naumann, “Coatings to reduce hydrogen environment embrittlement of 304 austenitic stainless steel,” *Surf. Coatings Technol.*, vol. 203, no. 13, pp. 1819–1828, 2009, doi: 10.1016/j.surfcoat.2009.01.013.
14. A. W. Loginow and E. H. Phelps, “Steels for Seamless Hydrogen Pressure Vessels.,” *Corrosion*, vol. 31, no. 11. pp. 404–412, 1975. doi: 10.5006/0010-9312-31.11.404.
15. R. Abdi behnagh, M. K. Besharati Givi, and M. Akbari, “Mechanical properties, corrosion resistance, and microstructural changes during friction stir processing of 5083 aluminum rolled plates,” *Mater. Manuf. Process.*, vol. 27, no. 6, pp. 636–640, 2012, doi: 10.1080/10426914.2011.593243.
16. B. J. L. Carpenter, G. Mandel, and P. Mtanager, “Bibliography of Information on Mechanics of (Hydrogen Embrittlement, Protective Coatings, Composite Materials, NDE) Orlando Division National Aeronautics a nd Space Administration Aerospace Safety Research and Data Institute,” no. June, 1976.
17. P. Deimel, H. Leonhard, and E. Sattler, “Characterization of the influence of high-pressure hydrogen gas on the ductility of the steel 15 MnNi 6 3,” *Int. J. Hydrogen Energy*, vol. 18, no. 4, pp. 313–318, 1993, doi: 10.1016/0360-3199(93)90045-C.
18. E. J. D. J.H. Holbrook, E.W.Collings, H. J Cialone, “Hydrogen degradation of pipeline steels,” 1986.
19. J. D. Frandsen and H. L. Marcus, “Environmentally assisted fatigue crack propagation in steel,” *Metall. Trans. A*, vol. 8, no. 2, pp. 265–272, 1977, doi: 10.1007/BF02661639.
20. I. Nuclear, “50 + years of INIS,” no. 8320881, 1976.
21. T. H. E. Role, O. F. Traps, I. N. The, and M. Control, pp. 705–708, 2020, doi: 10.1126/science.aba7357.
22. H. Xing, C. Stuart, S. Spence, and H. Chen, “Alternative fuel options for low carbon maritime transportation: Pathways to 2050,” *J. Clean. Prod.*, vol. 297, no. April 2018, p. 126651, 2021, doi: 10.1016/j.jclepro.2021.126651.
23. T. Michler and J. Naumann, “Influence of high pressure hydrogen on the tensile and fatigue properties of a high strength Cu-Al-Ni-Fe alloy,” *Int. J. Hydrogen Energy*, vol. 35, no. 20, pp. 11373–11377, 2010, doi: 10.1016/j.ijhydene.2010.07.093.
24. Y. Q. Zhu *et al.*, “Advances in reducing hydrogen effect of pipeline steels on hydrogen-blended natural gas transportation: A systematic review of mitigation strategies,” *Renew. Sustain. Energy Rev.*, vol. 189, no. PA, p. 113950, 2024, doi: 10.1016/j.rser.2023.113950.
25. M. D. Mukelabai, U. K. G. Wijayantha, and R. E. Blanchard, “Renewable hydrogen economy outlook in Africa,” *Renew. Sustain. Energy Rev.*, vol. 167, no. January, p. 112705, 2022, doi: 10.1016/j.rser.2022.112705.
26. S. Pellegrino, A. Lanzini, and P. Leone, “Greening the gas network – The need for modelling the distributed injection of alternative fuels,” *Renew. Sustain. Energy Rev.*, vol. 70, no. November 2016, “EE/IhE/IEll/EEE”.
27. A. Al-Quraan, B. Al-Mhairat, A. M. A. Malkawi, A. Radaideh, and H. M. K. Al-Masri, “Optimal Prediction of Wind Energy Resources Based on WOA—A Case Study in Jordan,” *Sustain.*, vol. 15, no. 5, 2023, doi: 10.3390/su15053927.
28. D. Y. C. Leung, G. Caramanna, and M. M. Maroto- Valer, “An overview of current status of carbon dioxide capture and storage technologies,” *Renew. Sustain. Energy Rev.*, vol. 39, pp. 426–443, 2014, doi: 10.1016/j.rser.2014.07.093.
29. M. A. Clark *et al.*, “Global food system emissions could preclude achieving the 1.5° and 2°C climate change targets,” *Science (80-.).*, vol. 370, no. 6517, pp. 266–286, 2017, doi: 10.1016/j.rser.2016.11.243.
30. A. Ilyushechkin, L. Schoeman, L. Carter, and S. S. Hla, “Material Challenges and Hydrogen Embrittlement Assessment for Hydrogen Utilisation in Industrial Scale,” *Hydrogen*, vol. 4, no. 3, pp. 599–619, 2023, doi: 10.3390/hydrogen4030039.
31. J. Yao, Q. Tan, J. Venezuela, A. Atrens, and M. X. Zhang, “Recent research progress in hydrogen embrittlement of additively manufactured metals – A review,” *Curr. Opin. Solid State Mater. Sci.*, vol. 27, no. 5, p. 101106, 2023, doi: 10.1016/j.cossms.2023.101106.
32. Q. Zhang, Y. Jiang, X. Zhao, J. Duan, L. Chen, and Y. Xu, “A new research proposal to prevent hydrogen embrittlement for nuclear waste container by bacteria-a mini review,” *Front. Microbiol.*, vol. 14, no. November, pp. 1–5, 2023, doi: 10.3389/fmicb.2023.1304703.

Statement about the ownership and other particulars about newspapers

JOURNAL OF THE MAHARAJA SAYAJIRAO UNIVERSITY OF BARODA

(To be published in the first issue every year after the last day of February)

FORM IV

(See Rule 8)

1. Place of the Publication : The The Maharaja Sayajirao University of Baroda
M.S. University of Baroda, Vadodara - 390 002.

2. Periodicity of its Publication : Science & Technology
at any time during the year.

3. Printer's Name : Shri Jatin H. Somani
Nationality : Indian
Address : Manager, The M.S.University of Baroda Press,
(Sadhana Press), Vadodara - 390 001.

4. Publisher's Name : Prof. P. K. Jha
Nationality : Indian
Address : The M. S. University of Baroda,
Vadodara - 390 002.

5. Editor's Name : Prof. P. K. Jha
Nationality : Indian
Address : The M. S. University of Baroda,
Vadodara - 390 002.

6. Names & Addresses of Individuals who own the newspaper and partners or shareholders holding more than one percent of the total capital : The M. S. University of Broda,
Vadodara - 390 002.

I, P. K. Jha declare that the particulars given above are true to the best of my knowledge and belief.

Prof. P. K. Jha

JOURNAL OF THE MAHARAJA SAYAJIRAO UNIVERSITY OF BARODA

The Journal is mainly intended to publish original research papers contributed by the teachers and research scholars of the M.S. University of Baroda.

One volume of the Journal is issued every year in three parts. These parts are devoted respectively to topics relating to Humanities, Social Science, Science & Technology, Medicine. All manuscripts, books and publications for review should be addressed to :

The Editor (Science & Technology),
Journal of the M.S. University of Baroda,
A.I.C.S. Training Centre,
Baroda - 390 002.

email: editor.msujst@msubaroda.ac.in

Contributors are requested to submit manuscripts, by email attachment which should be typed with double spacing and on one side of the paper only. Authors are advised to retain a copy of the paper that they send for publication as the Editors cannot accept responsibility for any loss.

Authors of papers printed in the Journal are entitled to one copy of the issue free of charge.

ADVERTISEMENT

All advertising matters should be send so as to reach the office of the Journal a month before the publication of the Journal. Further information on rates and space can be had on writing to **editor.msujst@msubaroda.ac.in.**

सत्यं शिवं सुन्दरम्

Estd. 1949

"The full-blown lotus growing out of the lake symbolises the emergence of the mind and its triumph over matter. The flame rising from the center of the lotus is the flame of the human knowledge, spreading light and learning for the coming generations. The motto inscribed below the lotus defines the purpose and existence of life which is love of beauty, goodness and intellectual curiosity."

महाराजा सयाजीराव विश्वविद्यालय गीत

अमे वडोदराना विद्यापीठनां सपनां सारवनारा
अमे ज्योत जलावी सृष्टि नवली सहसा सर्जनहारा.

अमे गगनकुसुम कर धरनारा
अमे मगन मगन थई फरनारा
अगनबाथ अमे भरनारा
अमे दैन्यतिमिरने हरनारा.

श्री सयाजी विद्यापीठना ज्ञानदीपने धरनारा
सत्यं शिवं सुन्दरम् नो मंत्र अनंतर भणनारा.

Printed at: The Maharaja Sayajirao University of Baroda Press (Sadhana Press), Vadodara-390 001